Novel tools for characterizing photon correlations in parametric down-conversion

A thesis submitted
in Partial Fulfillment of the Requirements
for the Degree of

Doctor of Philosophy

by

Girish Kulkarni

DEPARTMENT OF PHYSICS
INDIAN INSTITUTE OF TECHNOLOGY KANPUR
March, 2019

Dedicated to my parents and teachers

CERTIFICATE

It is certified that the work contained in the thesis titled **Novel tools for characterizing photon correlations in parametric down-conversion**, by **Girish Kulkarni**, has been carried out under my supervision and that this work has not been submitted elsewhere for a degree.

01-MARCH-2019

Prof. Anand K. Jha
Department of Physics
IIT Kanpur

March, 2019

SYNOPSIS

Name of student: **Girish Kulkarni** Roll no: **14109264**

Degree for which submitted: **Doctor of Philosophy**

Department: **Physics**

Thesis title: **Novel tools for characterizing photon correlations in parametric down-conversion**

Name of thesis supervisor: **Prof. Anand K. Jha**

Month and year of thesis submission: **March, 2019**

Over the last two decades, numerous experimental studies have demonstrated that quantum systems are capable of performing information processing tasks – such as teleportation, superdense coding, secure communication, and efficient integer factorization – which are widely considered to be impossible with classical systems. These enhanced capabilities are believed to arise at least partly from the nonlocal correlations present in entangled quantum systems. While the intrinsic correlations that underlie interference effects are a general feature of both quantum and classical systems, the nonlocal correlations of entangled quantum systems have no known classical counterpart. In addition to being a vital resource for quantum applications, these nonlocal correlations also pose fundamental questions regarding the consistency and completeness of the quantum description of physical reality. Currently, the most important experimental source of entangled systems is parametric down-conversion – a second-order nonlinear optical process in which a single photon, referred to as pump, is annihilated in its interaction with a nonlinear medium to create a pair of entangled photons, referred to as signal and idler. The present thesis draws on concepts from optical coherence theory and quantum information theory, and develops tools and techniques for characterizing the correlations of the

signal-idler photons and their relationship to the intrinsic correlations of the pump photon in various degrees of freedom.

We first develop an experimental technique that can characterize the angular correlations of photons in a single-shot measurement. The orbital angular momentum (OAM) basis of photons – by being discrete and infinite-dimensional – provides a natural platform for preparing and manipulating high-dimensional quantum states. It is known that high-dimensional quantum states have certain advantages over conventional two-dimensional quantum states in information processing protocols. A problem that is encountered in several OAM-based protocols is the efficient measurement of photons whose state is described as an incoherent mixture of different OAM-carrying modes. The angular correlations of such photons are completely characterized by the distribution of the measurement probabilities corresponding to different OAM-carrying modes. This distribution is referred to as the OAM spectrum of the photons. The existing techniques for measuring the OAM spectrum suffer from issues such as poor scaling with spectral width, stringent stability requirements, and too much loss. Furthermore, most techniques measure only a post-selected part of the true spectrum. We demonstrate that a Mach-Zender interferometer with the simple-yet-crucial feature of having an odd and even number of mirrors in the two arms results in the OAM spectrum of the input photons being directly encoded in the output interferogram. By performing proof-of-concept demonstrations, we show that the interferometer provides a robust and efficient technique for measuring the true OAM spectrum of photons in a single-shot acquisition.

Next, we use the single-shot technique to experimentally characterize the angular correlations of signal-idler photons produced from PDC of a pump photon with zero OAM. Due to the conservation of OAM in PDC, the two-photon state is entangled in the OAM basis with measurements on the individual photons always yielding OAM values with opposite signs such that their sum is zero. The distribution of the measurement probabilities corresponding to different pairs of OAM values is referred to as the angular Schmidt spectrum of the two-photon state. The angular Schmidt

spectrum completely characterizes the angular correlations of the signal-idler photons. Until now, however, experimental measurements of the Schmidt spectrum measured only a post-selected part of the true spectrum or required coincidence detections with stringent alignment conditions or both. As the OAM spectrum of the individual photons is identical to the angular Schmidt spectrum of two-photon state, we employ the single-shot technique to experimentally measure the true angular Schmidt spectrum without the need for coincidence detections. Our measurements provide a complete characterization of the angular Schmidt spectrum of the signal-idler photons from collinear to non-collinear emission regimes with excellent agreement with theoretical predictions.

We then theoretically investigate the nonlocal correlations of the signal-idler photons and their relationship to the intrinsic correlations of the pump photon in the polarization and temporal degrees of freedom. In the polarization degree of freedom, we demonstrate that the degree of polarization of the pump photon predetermines the maximum achievable polarization entanglement of two-qubit signal-idler states. In the temporal degree of freedom, following up on previous studies that considered specific cases of a continuous-wave pump and a transform-limited pulsed pump, we theoretically demonstrate that even for a completely general pump, the temporal correlations of the pump photon are entirely transferred to the signal-idler photons. We further show that the energy-time entanglement of two-qubit signal-idler states is bounded by the degree of temporal coherence of the pump photon.

Lastly, we theoretically formulate a basis-invariant coherence measure for quantifying the intrinsic correlations of infinite-dimensional quantum states. For two-dimensional states, the degree of polarization is a well-established basis-invariant measure of coherence. Until recently, although some generalizations had been proposed, no analogous measure that possessed all the interpretations of the degree of polarization had been established for higher-dimensional states. As a result, it was not possible to characterize the intrinsic correlations of the pump and signal-idler states in infinite-dimensional representations such as OAM, photon number,

position, and momentum. Recently, a study demonstrated a measure analogous to the degree of polarization for finite-dimensional states which also possesses all its interpretations. Here, we generalize this measure to quantify the intrinsic coherence of infinite-dimensional states in the OAM, photon number, position and momentum representations. Our study will now enable a basis-invariant quantification of the intrinsic correlations of the pump and signal-idler photons in these representations.

Acknowledgments

I will first attempt the impossible task of adequately expressing in words my gratitude towards my advisor Prof. Anand Jha for the exemplary patience and care with which he has guided me in the past five years. His guidance always reflected a sharp perceptiveness to my difficulties and a strong commitment to my overall betterment. I am also deeply touched by the manner in which he stood by me through challenging times. His example inspires me to strive for the highest standards of honesty, simplicity, and detachment in research and other aspects of life.

I thank all the present and past members of our research group for the stimulating environment that they provided me in the laboratory. I am thankful to Prof. Harshawardhan Wanare, Prof. V. Subrahmanyam, Prof. Saikat Ghosh, Prof. Manoj Harbola and all the teachers and mentors in my life for the knowledge and encouragement that I have received from them.

I thank my friend Ishan for being a pillar of strength over these years. I am also thankful to Sumeet and Vinay for all the good times that we spent together. The numerous cycling trips, movie screenings, book recommendations, and conversations brought quality to my life.

I thank my best friend and wife Mugdha, my parents, my parents-in-law, and my brother Vivek for their constant love and support through all these years. Their faith in me was unwavering even at times when I was in doubt.

Finally, I submit my humble gratitude towards the people of India for the financial support they provide for research in the fundamental sciences.

Contents

List of Figures

List of Publications:

- **Intrinsic upper bound on two-qubit polarization entanglement predetermined by pump polarization correlations in parametric down-conversion**

  G. Kulkarni, V. Subrahmanyam, and A. K. Jha,

  Phys. Rev. A **93**, 063842 (2016).

- **Single-shot measurement of the orbital angular momentum spectrum of light**

  G. Kulkarni, R. Sahu, O. S. Magana-Loaiza, R. W. Boyd, and A. K. Jha,

  Nature Communications, **8**, 1054 (2017).

- **Transfer of temporal coherence in parametric down-conversion**

  G. Kulkarni, P. Kumar, and A. K. Jha,

  J. Opt. Soc. Am. B **34** (8), 1637-1643 (2017).

- **Angular Schmidt spectrum of entangled photons: derivation of an exact formula and experimental characterization for non-collinear phase matching**

  G. Kulkarni, L. Taneja, S. Aarav, and A. K. Jha,

  Phys. Rev. A **97**, 063846 (2018).

- **Intrinsic degree of coherence of finite-dimensional systems**

  A. S. M. Patoary, G. Kulkarni, and A. K. Jha,

  arXiv:1712.03475.

- **Intrinsic degree of coherence of infinite-dimensional systems**

  G. Kulkarni, A. S. M. Patoary, and A. K. Jha,

  (*to be submitted*)

Chapter 1

Background

1.1 Introduction

Correlations are ubiquitous in classical and quantum physics. In classical physics, the phase correlations of waves lead to the phenomenon of interference. In quantum physics, the wave-particle duality implies that all physical systems possess intrinsic correlations which potentially enable them to exhibit interference effects. The fundamental property that embodies these intrinsic correlations is known as coherence [1, 2, 3]. Historically, coherence has been extensively studied through interference experiments with light, and a rigorous framework called optical coherence theory has emerged for quantifying the coherence of light fields [2, 3, 4, 5, 6]. While the intrinsic correlations that constitute coherence are a general feature of both classical and quantum systems, there are certain correlations that are observed in quantum systems but have no known classical counterpart. In particular, multiparticle quantum systems can possess a curious property known as quantum entanglement [7, 8, 9], which refers to the inseparability of the physical state of a multiparticle system into independent physical states for the individual constituent particles. This inseparability results in strong correlations in measurements on the individual particles even when the particles are causally separated [10, 11]. The presence of such nonlocal correlations raises fundamental questions regarding the consistency and completeness of quantum theory [8, 9, 12]. In addition, the nonlocal correlations of entangled

states can be harnessed for several information processing tasks – such as superdense coding [13], teleportation [14], and efficient integer factorization [15] – that are widely believed to be impossible with classical systems [16]. As a result, the quantification of the correlations of general entangled quantum states is an active topic of research in quantum information theory with important implications for fundamental physics and quantum technologies [17, 18, 19, 20].

Presently, the most widely used experimental source of entangled states is parametric down-conversion (PDC) - a second-order nonlinear optical process in which a single photon, referred to as pump, gets annihilated in its interaction with a nonlinear medium to produce a pair of photons, referred to as signal and idler [21]. The constraints of energy, momentum, and orbital angular momentum (OAM) conservation render the signal and idler photons entangled in various degrees of freedom. It is fundamentally interesting to explore how the intrinsic correlations of the pump photon get transferred through the process to eventually manifest as the nonlocal correlations of the entangled signal-idler photons [22, 23, 24, 25, 26, 27, 28, 29, 30, 31, 32]. Moreover, the characterization and quantification of the correlations of these photons is also important for harnessing them effectively in quantum protocols [33, 34, 35, 36, 37]. In this thesis, we present experimental and theoretical studies on the characterization and quantification of the correlations of the signal-idler photons produced from PDC, and their relationship to the coherence properties of the pump photon in the angular, temporal, and polarization degrees of freedom.

This chapter is organized as follows: In Sections 1.2 and 1.3, we present a basic introduction to optical coherence in the context of the Michelson interference experiment, and derive the Wiener-Khintchine theorem for stationary light fields. In Sections 1.4, 1.5, and 1.6, we present a basic introduction to quantum entanglement, its implications for fundamental physics, and its role in quantum technologies. In Section 1.7, we describe the Schmidt decomposition for a bipartite pure quantum state. In Section 1.8, we describe some of the present coherence measures and entanglement measures, and discuss their limitations. In Sections 1.9 and 1.10, we

present a brief introduction to nonlinear optics and the process of PDC. In Section 1.11, we discuss the existing studies on the correlations of the signal-idler photons and their relationship to the coherence of the pump. In Section 1.12, we summarize and present an outline of the thesis.

1.2 Optical coherence

We present a brief introduction to the concept of coherence by analyzing the Michelson interference experiment in the framework of optical coherence theory [3]. We will first analyze the experiment in the formalism of classical coherence theory pioneered by Wolf [2], following which we will present the quantum treatment in the theory of quantum optical coherence due to Glauber and Sudarshan [4, 5, 6].

Consider a classical light field whose electric field amplitude at spatial location $\mathbf{r}$ and time t is denoted as $E(\mathbf{r}, t)$. In general, the field can be modeled as a random process (see Chapter 2 of Ref. [3] for an introduction to random processes). As depicted in Figure 1.1, the light field is incident onto a beam-splitter, where it is split into two paths with traversal times τ_1 and τ_2, and is then recombined before it is measured at detector D_A. The field $E_A(\mathbf{r}, t)$ at the detector is given by

$$E_A(\mathbf{r}, t) = k_1 E(\mathbf{r}, t - \tau_1) + k_2 E(\mathbf{r}, t - \tau_2), \tag{1.1}$$

where k_1 and k_2 are constants related to the splitting ratio of the beam-splitter. The detected intensity $I_A(\mathbf{r}, t) = \langle E_A^*(\mathbf{r}, t) E_A(\mathbf{r}, t) \rangle$ is given by

$$\begin{aligned} I_A(\mathbf{r}, t) = |k_1|^2 \langle E^*(\mathbf{r}, t - \tau_1) E(\mathbf{r}, t - \tau_1) \rangle + |k_2|^2 \langle E^*(\mathbf{r}, t - \tau_2) E(\mathbf{r}, t - \tau_2) \rangle \\ + k_1^* k_2 \langle E^*(\mathbf{r}, t - \tau_1) E(\mathbf{r}, t - \tau_2) \rangle + \text{c.c}, \end{aligned} \tag{1.2}$$

where $\langle \cdots \rangle$ represents an ensemble-average over many realizations of the field. The two-time cross-correlation function $\Gamma(t_1, t_2)$ of the input field is defined as $\Gamma(t_1, t_2) \equiv \langle E^*(\mathbf{r}, t_1) E(\mathbf{r}, t_2) \rangle$. The spatial co-ordinate argument has been suppressed in $\Gamma(t_1, t_2)$

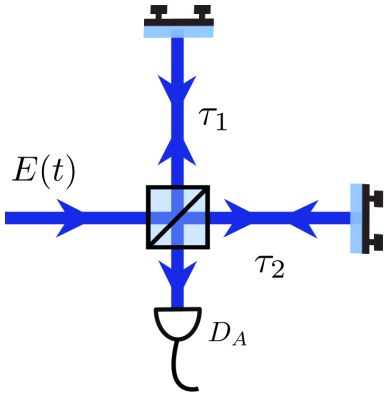

Figure 1.1: A classical light field with electric field amplitude $E(t)$ is split into two paths with source-to-detector traversal times τ_1 and τ_2, and is recombined and measured at detector D_A. The electric fields from the two paths superpose and lead to interference.

as we are focusing on the temporal coherence properties of the field. The measured intensity $I_A(\mathbf{r},t)$ of Equation (1.2) then takes the form

$$I_A(\mathbf{r},t) = |k_1|^2\Gamma(t-\tau_1,t-\tau_1)+|k_2|^2\Gamma(t-\tau_2,t-\tau_2)+k_1^*k_2\Gamma(t-\tau_1,t-\tau_2)+\text{c.c.} \quad (1.3)$$

This is the general expression for the intensity in a Michelson interference experiment. The degree of temporal coherence $\gamma(t-\tau_1,t-\tau_2)$ is defined as

$$\gamma(t-\tau_1,t-\tau_2) = \frac{\Gamma(t-\tau_1,t-\tau_2)}{\sqrt{\Gamma(t-\tau_1,t-\tau_1)\Gamma(t-\tau_2,t-\tau_2)}}. \quad (1.4)$$

Using Cauchy-Schwartz inequality, one can show that $0 \leq |\gamma(t-\tau_1,t-\tau_2)| \leq 1$. We denote $\gamma(t-\tau_1,t-\tau_2) = |\gamma(t-\tau_1,t-\tau_2)|e^{i\arg(\gamma)}$. Equation (1.3) can be written as

$$\begin{aligned} I_A(t) = {} & |k_1|^2 I(t-\tau_1) + |k_2|^2 I(t-\tau_2) \\ & + 2|k_1||k_2|\sqrt{I(t-\tau_1)I(t-\tau_2)}|\gamma(t-\tau_1,t-\tau_2)|\cos\{\arg(\gamma)+\phi\}, \end{aligned} \quad (1.5)$$

where we have defined $\phi \equiv \arg\{k_1^*k_2\}$ and $I(\mathbf{r},t) \equiv \Gamma(t,t)$. The first two terms correspond to the individual intensities from the two arms of the interferometer. The last term depends on both τ_1 and τ_2, and is responsible for interference. The coherence of the light field can be quantified in terms of the contrast or visibility V

of the interference fringes, which can be computed as

$$V = \frac{I_{\max} - I_{\min}}{I_{\max} + I_{\min}}. \tag{1.6}$$

Using equations (1.5) and (1.6), we obtain

$$V = \frac{2|k_1||k_2|\sqrt{I(t-\tau_1)I(t-\tau_2)}}{|k_1|^2 I(t-\tau_1) + |k_2|^2 I(t-\tau_2)} |\gamma(t-\tau_1, t-\tau_2)|. \tag{1.7}$$

We find that the visibility of the interference is directly proportional to the degree of temporal coherence $\gamma(t-\tau_1, t-\tau_2)$ of the superposing fields. For stationary fields such as a continuous-wave laser, when the time difference $\Delta\tau = \tau_2 - \tau_1$ is much smaller than the coherence time τ_{coh} of the laser, $\gamma(t-\tau_1, t-\tau_2)$ is close to unity which leads to interference with high contrast. In this situation, the fields from the two paths are highly coherent with respect to one another. When $\Delta\tau$ is much larger than τ_{coh}, the value of $\gamma(t-\tau_1, t-\tau_2)$ is close to zero, which results in the interference getting washed out. In this situation, one says that the fields from the two arms are incoherent with respect to one another. Thus, the degree of temporal coherence, which is the normalized cross-correlation function of the field, provides a way of quantifying the coherence of a light field. In Chapter 5, we will quantify the temporal coherence of the pump using its degree of temporal coherence.

In the quantum interpretation of the experiment, the interference is understood in terms of Dirac's famous statement, "... a single photon interferes with itself" [38]. As depicted in Figure 1.2, each photon of the input field has two alternative paths that it can take before it gets detected at D_A. When the two alternatives are indistinguishable, there is a quantum interference between the probability amplitudes corresponding to the alternatives. In terms of coherence, one says that interference occurs when the two alternatives are coherent with one another. We shall undertake the quantum analysis of the Michelson experiment, but before that we will briefly review the prerequisite concept of analytic field operators.

In the quantum theory of optical coherence [4], the quantized nature of the

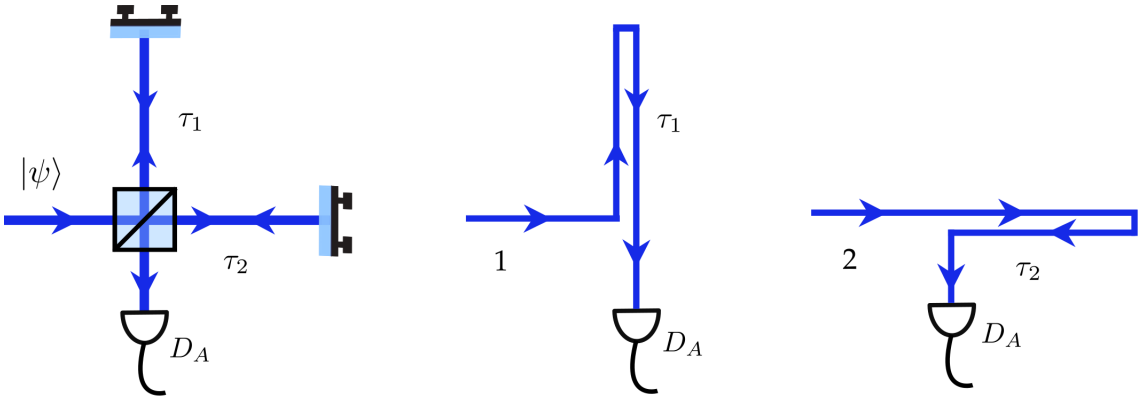

Figure 1.2: A quantum light field, described by the state $|\psi\rangle$, is split into two paths with source-to-detector light traversal times τ_1 and τ_2, and is recombined and measured at detector D_A. Each photon has two alternative paths 1 and 2 that it can take before getting detected at D_A. The probability amplitudes corresponding to the two paths superpose and lead to interference.

electromagnetic field is taken into account by promoting the electric field amplitude $E(\mathbf{r},t)$ to a Hermitian field operator $\hat{E}(\mathbf{r},t)$. This field operator can be written as

$$\begin{aligned}\hat{E}(\mathbf{r},t) &= \hat{E}^{(+)}(\mathbf{r},t) + \hat{E}^{(-)}(\mathbf{r},t) \\ &= \sum_{\mathbf{k}} i\left[\frac{\hbar\omega_k}{2\epsilon_0 L^3}\right]^{\frac{1}{2}} \hat{a}(\mathbf{k},t)e^{i(\mathbf{k}\cdot\mathbf{r}-\omega_k t)} - i\left[\frac{\hbar\omega_k}{2\epsilon_0 L^3}\right]^{\frac{1}{2}} \hat{a}^{\dagger}(\mathbf{k},t)e^{-i(\mathbf{k}\cdot\mathbf{r}-\omega_k t)}, \end{aligned} \tag{1.8}$$

where $\hat{E}^{(+)}(\mathbf{r},t)$ and $\hat{E}^{(-)}(\mathbf{r},t)$ are the positive and negative complex analytic field operators, respectively. The action of $\hat{E}^{(+)}(\mathbf{r},t)$ is to absorb a photon at $(\mathbf{r},t)$, whereas the action of $\hat{E}^{(-)}(\mathbf{r},t)$ is to emit a photon at $(\mathbf{r},t)$. These operators have then been expanded in the plane-wave mode annihilation and creation operators, $\hat{a}(\mathbf{k},t)$ and $\hat{a}^{\dagger}(\mathbf{k},t)$, respectively. The wave-vector and frequency of the plane-wave modes are denoted as $\mathbf{k}$ and ω_k, respectively, and the quantity L^3 refers to the quantization volume.

We now present the quantum treatment for the experiment. Consider an input light field, described by the state $|\psi\rangle$, that is incident into the beamsplitter of the Michelson setup depicted in Figure 1.2. The positive analytic field operator $\hat{E}_A^{(+)}(\mathbf{r},t)$ at detector D_A is given by

$$\hat{E}_A^{(+)}(\mathbf{r},t) = k_1 E^{(+)}(\mathbf{r},t-\tau_1) + k_2 E^{(+)}(\mathbf{r},t-\tau_2). \tag{1.9}$$

Here, $E^{(+)}(\mathbf{r}, t-\tau_1)$ and $E^{(+)}(\mathbf{r}, t-\tau_2)$ are the positive analytic field operators corresponding to the alternatives 1 and 2, respectively. The probability per unit time $p_A(t)$ that a photon is detected at D_A is calculated as

$$\begin{aligned} p_A(t) &= \langle\langle\psi|E_A^{(-)}(\mathbf{r},t)E_A^{(+)}(\mathbf{r},t)|\psi\rangle\rangle_e \\ &= |k_1|^2\langle\langle\psi|E^{(-)}(\mathbf{r},t-\tau_1)E^{(+)}(\mathbf{r},t-\tau_1)|\psi\rangle\rangle_e \\ &\quad + |k_2|^2\langle\langle\psi|E^{(-)}(\mathbf{r},t-\tau_2)E^{(+)}(\mathbf{r},t-\tau_2)|\psi\rangle\rangle_e \\ &\quad + k_1^*k_2\langle\langle\psi|E^{(-)}(\mathbf{r},t-\tau_1)E^{(+)}(\mathbf{r},t-\tau_1)|\psi\rangle\rangle_e + \text{c.c}, \end{aligned}$$

where $\langle\cdots\rangle_e$ represents an ensemble average over many realizations of the field. The first two terms represent the detection probabilities per unit time corresponding to the individual alternatives. The temporal autocorrelation function $G^{(1)}(t_1, t_2)$ is now defined as $G^{(1)}(t_1, t_2) \equiv \langle\langle\psi|E^{(-)}(\mathbf{r}, t_1)E^{(+)}(\mathbf{r}, t_2)|\psi\rangle\rangle_e$. The expression for $p_A(t)$ then takes the form

$$\begin{aligned} p_A(t) = |k_1|^2G^{(1)}(t-\tau_1, t-\tau_1) + |k_2|^2G^{(1)}(t-\tau_2, t-\tau_2) \\ + k_1^*k_2G^{(1)}(t-\tau_1, t-\tau_2) + \text{c.c} \end{aligned} \quad (1.10)$$

The above equation expresses the quantum description of Michelson's interference, and is analogous to Equation (1.3) which expresses the classical description. As in the classical treatment, the coherence of the light field can again be quantified in terms of the cross-correlation function of the field. The difference is that the cross-correlation function $G^{(1)}(t-\tau_1, t-\tau_2)$ now involves normally-ordered field operators, instead of field amplitudes. However, for most conventional light fields such as thermal fields, continuous-wave lasers among others, the classical and quantum treatments of Michelson interference lead to equivalent predictions [6].

The Michelson's interference involves the detection of one photon at a time, and is therefore an example of one-photon interference. In one-photon interference, the probability amplitudes for the alternatives available to a single photon super-

pose and lead to interference. As a result, the probability per unit time that a photon is detected exhibits interference fringes, and the visibility of these is quantified in terms of a first-order cross-correlation function such as $G^{(1)}(\mathbf{r}_1, t_1; \mathbf{r}_2, t_2) \equiv \langle\langle\psi|E^{(-)}(\mathbf{r}_1, t_1)E^{(+)}(\mathbf{r}_2, t_2)|\psi\rangle\rangle_e$ that has second powers of field. In contrast, there are interference experiments such as the ones by Hanbury Brown-Twiss [39, 40], Hong-Ou-Mandel [41], Franson [42] among others which involve coincidence detections of two photons at a time, and are therefore referred to as two-photon interference. In such situations, the probability amplitudes for the alternatives available to a two-photon system superpose and lead to interference. The interference fringes are then observed in the probability per unit (time)^2 that the two-photon is detected at a pair of detectors. The visibility of this interference can be quantified in terms of a second-order cross-correlation function such as $G^{(2)}(\mathbf{r}_1, t_1, \mathbf{r}_2, t_2; \mathbf{r}_3, t_3, \mathbf{r}_4, t_4) \equiv \langle\langle\psi|E^{(-)}(\mathbf{r}_1, t_1)E^{(-)}(\mathbf{r}_2, t_2)E^{(+)}(\mathbf{r}_3, t_3)E^{(+)}(\mathbf{r}_4, t_4)|\psi\rangle\rangle_e$ that has fourth powers of the field. In Chapter 5, we will use a second-order correlation function to quantify the temporal coherence of the signal-idler two-photon state produced from PDC.

1.3 Wiener-Khintchine theorem

We now derive the Wiener-Khintchine relation for temporally stationary classical light fields. Our treatment closely follows the analysis by Mandel and Wolf (see Section 2.4.1 of Ref. [3]). Consider a classical light field whose electric field is denoted as $E(\mathbf{r}, t)$. If the Fourier transform of $E(\mathbf{r}, t)$ with respect to the time variable exists, then we can write

$$E(\mathbf{r}, t) = \int_{-\infty}^{+\infty} \tilde{E}(\mathbf{r}, \omega)e^{-i\omega t}\,\mathrm{d}\omega, \tag{1.11a}$$

$$\tilde{E}(\mathbf{r}, \omega) = \frac{1}{2\pi}\int_{-\infty}^{+\infty} E(\mathbf{r}, t)e^{i\omega t}\,\mathrm{d}t. \tag{1.11b}$$

However, there are certain classes of fields (for eg. stationary fields) which are not absolutely integrable, i.e, the condition $\int_{-\infty}^{+\infty} |E(\mathbf{r}, t)|\mathrm{d}t < \infty$ is not satisfied. For such fields, the Fourier transform does not exist. Although this problem can be rigor-

ously addressed using Wiener's theory of generalized harmonic analysis [43], for our purposes it is sufficient that the cross-correlation function $\Gamma(t_1, t_2) = \langle E^*(t_1)E(t_2)\rangle$ be absolutely integrable. Here $\langle\cdots\rangle$ indicates an ensemble average over infinitely-many realizations of the field. Using Equations (1.11) heuristically, it follows that

$$\Gamma(t_1, t_2) = \frac{1}{(2\pi)^2}\int_{-\infty}^{+\infty}\int_{-\infty}^{+\infty} W(\omega_1, \omega_2)\, e^{i(\omega_1 t_1 - \omega_2 t_2)}\, \mathrm{d}\omega_1\, \mathrm{d}\omega_2, \tag{1.12}$$

where the cross-spectral density is defined as $W(\omega_1, \omega_2) \equiv \langle \tilde{E}^*(\mathbf{r}, \omega_1)\tilde{E}(\mathbf{r}, \omega_2)\rangle$. The above equation (1.12), which relates the cross-correlation function to the cross-spectral density by a two-dimensional Fourier transform, is referred to as the generalized Wiener-Khintchine theorem.

Now let us assume that the field $E(\mathbf{r}, t)$ is stationary in time (at least in the wide sense) [3]. This implies that its mean intensity $\Gamma(t, t)$ is time-independent, and that the cross-correlation function $\Gamma(t_1, t_2)$ depends only on the time difference $\tau = t_1 - t_2$, i.e, $\Gamma(t_1, t_2) = \Gamma(t_1 - t_2) = \Gamma(\tau)$. The autocorrelation function $\Gamma(\tau)$ is also referred to as the temporal coherence function. This condition when subsituted in Equation (1.12) implies that the cross-spectral density $W(\omega_1, \omega_2)$ for stationary fields takes the form

$$W(\omega_1, \omega_2) = S(\omega_1)\delta(\omega_1 - \omega_2), \tag{1.13}$$

where $S(\omega)$ is called the spectral density (or frequency spectrum) of the field. It refers to the weightage of the different monochromatic frequency components of the field. The Dirac delta condition implies that all the frequency components are completely uncorrelated with one another. An example of a field that is approximately stationary is the field from a continuous-wave laser.

Now we note that by substituting Equation (1.13) in Equation (1.12), it follows

that

$$\Gamma(\tau) = \int_{-\infty}^{+\infty} S(\omega) e^{-i\omega\tau} \, \mathrm{d}\omega, \tag{1.14a}$$

$$S(\omega) = \frac{1}{2\pi} \int_{-\infty}^{+\infty} \Gamma(\tau) e^{i\omega\tau} \, \mathrm{d}\tau. \tag{1.14b}$$

The above relations constitute the Wiener-Khintchine theorem, which states that the spectral density $S(\omega)$ and the autocorrelation function $\Gamma(\tau)$ of a stationary field are related to each other by a one-dimensional Fourier transform. In other words, the functions $S(\omega)$ and $\Gamma(\tau)$ are informationally equivalent. The Wiener-Khintchine theorem plays a crucial role in some techniques in frequency spectroscopy where the frequency spectral density $S(\omega)$ of an unknown field is measured by measuring the autocorrelation function $\Gamma(\tau)$, and then performing an inverse Fourier transform.

In Chapter 2, we will use an analog of the Wiener-Khintchine theorem for the OAM-angle degree of freedom. Like time and frequency, the OAM and angle variables also form a Fourier-conjugate pair [44, 45]. As a result, for a field whose different OAM components are completely uncorrelated, the corresponding OAM spectrum is related to the angular coherence function by a Fourier transform [46, 37, 47, 32]. In Chapter 2, we will describe an interferometric technique that measures the OAM spectrum of such a field by measuring its angular coherence function in a single-shot acquisition.

1.4 Quantum entanglement

Quantum entanglement is a physical phenomenon that arises when the principle of linear superposition is applied to multipartite quantum systems. The joint pure state $|\psi\rangle_{AB}$ of a composite system AB is said to be entangled if the composite state is not separable as a product of states $|\phi\rangle_A$ and $|\chi\rangle_B$ corresponding to the constituent systems A and B [16], i.e,

$$|\psi\rangle_{AB} \neq |\phi\rangle_A \otimes |\chi\rangle_B, \tag{1.15}$$

The most dramatic consequence of this inseparability is the observation of nonlocal correlations in measurements on systems A and B even when they are spatially separated with no possibility of any causal influence. We shall now briefly describe these nonlocal correlations in the context of a polarization-entangled two-photon system.

Consider a system of two photons A and B whose horizontal and vertical polarization basis vectors are labeled as $\{|H\rangle_A, |V\rangle_A\}$ and $\{|H\rangle_B, |V\rangle_B\}$, respectively. According to quantum theory, the Hilbert space of the composite two-photon system AB is the tensor product of the individual Hilbert spaces of the constituent photons A and B. Therefore, the polarization Hilbert space of AB is spanned by the set of basis vectors $\{|H\rangle_A|H\rangle_B, |H\rangle_A|V\rangle_B, |V\rangle_A|H\rangle_B, |V\rangle_A|V\rangle_B\}$. Now let the two photons A and B be described by a two-photon state of the form

$$|\psi\rangle_{AB} = \frac{1}{\sqrt{2}} \left(|H\rangle_A|V\rangle_B - |V\rangle_A|H\rangle_B\right). \tag{1.16}$$

The above state $|\psi\rangle_{AB}$ cannot be represented as a direct product of states for photons A and B, and is therefore an entangled state.

If we now perform polarization measurements on the individual photons A and B at spatially distant locations, we find that whenever photon A is measured to be horizontally-polarized, the photon B is measured to be vertically-polarized, and vice-versa. In other words, the polarization states of the two photons are perfectly anti-correlated. However, the presence of such correlations only in a single basis is not sufficient to ascertain entanglement. The quintessential feature of entanglement is that such correlations are observed no matter in what basis the measurements are performed. Therefore, even if we had chosen to measure the polarizations of A and B in the left-circular and right-circular polarization basis, or the $+45^\circ$ and -45° polarization basis, or any other orthonormal basis, we would have still found that the polarization states of photons A and B are perfectly anti-correlated. Moreover, these correlations are observed even if the photons are causally separated in spacetime with no possibility of a physical interaction. Thus, the simultaneous manifestation

of nonlocal correlations in measurement outcomes in different bases is the hallmark of quantum entanglement; and this phenomenon has no counterpart in classical physics. Schrodinger had already recognized the significance of entanglement in his 1935 paper [7], where he referred to entanglement as "... not *one* but rather *the* characteristic trait of quantum mechanics, the one that enforces its entire departure from classical lines of thought."

1.5 Fundamental implications of entanglement

The fundamental implications of the nonlocal correlations of entangled quantum states were first investigated by Einstein, Podolsky, and Rosen (EPR) in a seminal 1935 paper [8]. The authors stated that any physical theory must satisfy the principle of local realism, which comprises of two conditions: (i) locality, which demands that a measurement on one particle cannot instantaneously influence the state of another spatially separated particle, and (ii) realism, which states that if a physical property of a system can be predicted with certainty without measurement, then it is an element of reality of the particle. The authors showed that the existence of entangled states violates local realism, and therefore argued that quantum theory cannot be regarded as a complete physical description of nature.

In the context of our polarization-entangled two-photon state $|\psi\rangle_{AB}$ of Equation (1.16), the EPR argument can be stated as follows: If the polarization of photon A is measured in the horizontal-vertical basis with the outcome being horizontal, then photon B collapses into vertical polarization instantaneously. But if photon A had been measured in the left-right circular basis with the outcome left-circular, then photon B would have collapsed into the right-circular state instantaneously. Now if photon B is spatially separated from photon A with no possibility of any causal influence, then its physical state must be independent of the basis in which photon A was measured. This can only happen if the vertical and right-circular polarization states are the elements of reality of photon B at the same time, i.e, photon B is in the vertical polarization state and right-circular polarization state

at the same time – which is impossible. In this way, the authors argued that the quantum description of physical reality is incomplete, and contended that quantum mechanics must be a part of a more complete local realistic theory involving hidden variables.

The issues raised by EPR were famously debated by Einstein and Bohr among others for several years, but a consensus was never reached [9, 48]. In 1964, John Bell decided to mathematically formalize the notion of local realism, and was able to formulate certain inequality relations for the measurement correlations between parts of any composite physical system [12]. Bell showed that these inequalities would be obeyed by any local realistic theory involving hidden variables, but were violated by quantum theory. In essence, his inequalities provided a way to experimentally test the EPR assumption of local realism. Subsequently, there have been numerous experiments in which the correlations of entangled systems have been measured – and all these experiments have demonstrated a clear violation of Bell's inequalities [49, 10, 11, 50, 51, 52, 53]. While earlier tests were affected by certain experimental loopholes [49, 10, 11, 50, 51], technological advances have now led to loophole-free violations of Bell's inequalities [52, 53]. As a result, there is a widespread consensus today that the existence of local hidden variable theories has been conclusively ruled out. However, the fundamental concerns about the interpretations, consistency, and completeness of quantum theory raised by the EPR paper are not completely settled yet, and continue to be discussed and debated by researchers working on the foundations of quantum mechanics.

1.6 Role of entanglement in quantum technologies

While entanglement mostly remained only a matter of fundamental curiosity for physicists and philosophers for several decades after the EPR paper, it is now recognized to be a critical resource for several quantum information processing tasks

that are widely considered to be classically impossible. The field of quantum information can be regarded to have begun with the discovery of the no-cloning theorem [54, 55], which states that the linearity of quantum theory forbids the cloning of arbitrary quantum states. This theorem was initially crucial in proving that quantum theory does not allow communication of information at superluminal speeds [54, 55]. However, it was later realized that the impossibility of cloning quantum states also enables certain communication protocols that are guaranteed to be secure [56, 57, 58]. These initial discoveries sparked a surge of interest among researchers in the information processing capabilities of quantum systems. Subsequently, quantum systems have been theoretically and experimentally demonstrated to perform a number of tasks such as superdense coding [13, 59], teleportation [14, 60, 61, 62], entanglement swapping [63, 64], integer factorization [15, 65], metrology beyond the standard quantum limit [66, 67] among others.

The precise underlying factors responsible for such enhanced information processing capabilities are still not well-understood. While there are certain tasks such as superdense coding [13], teleportation [14], integer factorization [15] among others for which entanglement is essential, there are also some protocols such as B92 key distribution [57], DQC1 model of computation [68, 69], quantum search [70], quantum secret sharing [71] among others which utilize superpositions but do not need entanglement. At present, the role of different kinds of correlations in quantum information processing tasks is still a topic of research [72, 73, 74, 75, 76].

1.7 Schmidt decomposition

We will now review the concept of Schmidt decomposition of entangled bipartite (two-party) pure states. Consider a bipartite pure state $|\psi\rangle_{AB}$ of a composite system of two particles A and B whose Hilbert spaces have dimensionality m and n,

respectively. In general, the state $|\psi\rangle_{AB}$ has the form

$$|\psi\rangle_{AB} = \sum_{i=1}^{m}\sum_{j=1}^{n} c_{ij}|i\rangle_A|j\rangle_B, \tag{1.17}$$

where c_{ij} are complex coefficients that satisfy $\sum_{i,j}|c_{ij}|^2 = 1$. The kets $|i\rangle_A$'s for $i = 1, 2, .., m$ and $|j\rangle_B$'s for $j = 1, 2, .., n$ are orthonormal basis vectors in the Hilbert spaces of A and B, respectively. Without any loss of generality, let us assume that $m \geq n$, i.e, the dimensionality of A is greater than or equal to that of B. We can then rewrite Equation (1.17) as

$$|\psi\rangle_{AB} = \sum_{i=1}^{m}\sum_{j=1}^{n}\sum_{k=1}^{n} u_{ik}d_{kk}v_{kj}|i\rangle_A|j\rangle_B, \tag{1.18}$$

where we have performed a singular value decomposition of the complex matrix of coefficients c_{ij} into a product of an $m\times m$ unitary matrix formed by complex elements u_{ik}, an $m \times n$ rectangular diagonal matrix formed by n real diagonal elements d_{kk}, and the $n \times n$ unitary matrix formed by complex elements v_{kj}. We can further simplify Equation (1.18) to get

$$|\psi\rangle_{AB} = \sum_{k=1}^{n} d_{kk}|k\rangle_A|\tilde{k}\rangle_B, \tag{1.19}$$

where we have denoted $|k\rangle_A = \sum_{i=1}^{m} u_{ik}|i\rangle_A$ and $|\tilde{k}\rangle_B = \sum_{j=1}^{n} v_{kj}|j\rangle_B$. The above equation (1.19) is called the Schmidt decomposition of the state $|\psi\rangle_{AB}$. The probabilities $|d_{kk}|^2$ for $k = 1, ..., n$ are collectively referred to as the Schmidt spectrum of the state. As the state $|\psi\rangle_{AB}$ is normalized, the Schmidt spectrum is also normalized such that $\sum_k |d_{kk}|^2 = 1$. The correlations between the particles A and B of the entangled system AB are completely characterized by the Schmidt spectrum of the state. The effective dimensionality of the spectrum can be quantified using the Schmidt number K, defined as $K = 1/\sum_k d_{kk}^4$.

It is known that the high-dimensional OAM-entangled states produced from PDC of a Gaussian pump have a Schmidt-decomposed form in the OAM product

basis of the signal and idler photons [36, 77]. In Chapter 3, we will experimentally and theoretically characterize the Schmidt spectrum of these entangled two-photon states from PDC.

1.8 Quantifying coherence and entanglement

As discussed in Section 1.2, in optical coherence theory, coherence is quantified in terms of the visibility of the interference, which is typically proportional to a correlation function involving the fields at different spacetime points or polarization directions. While such correlation functions are extremely useful in quantitatively explaining a variety of interference effects of classical and non-classical fields, they are manifestly basis-dependent and therefore, quantify coherence only in an restricted sense [2, 78, 3]. The necessity of a basis-independent quantification of coherence was already emphasized by Glauber in his seminal 1963 paper where, concerning a set of conditions for full coherence, he stated that, "It is clear, however, that these conditions do not constitute an adequate definition of coherence, since they are not, in general, invariant under the rotation of coordinate axes." [4]. Such a basis-invariant quantification of coherence is possible for the two-dimensional polarization states of light in terms of a measure called the degree of polarization [78, 3]. As the 2×2 coherency matrix [2] that describes the polarization state of a light field is formally identical to the 2×2 density matrix [16] that describes an arbitrary two-dimensional quantum state, the degree of polarization can also be used to quantify the intrinsic coherence of two-dimensional quantum states. Over the last decades, some studies have attempted to generalize the degree of polarization and its known interpretations to higher-dimensional states [79, 80, 81, 82, 83, 84, 85]. However, no single measure that generalizes all the known interpretations of the degree of polarization had been well-established as a basis-invariant measure for high-dimensional states. A recent study established just such a measure for finite-dimensional states [86]. In Chapter 6, we will generalize this measure to quantify the intrinsic coherence of infinite-dimensional states.

The quantification of entanglement is an active topic of research in quantum information theory [20]. The well-known measures referred to as entanglement of formation and distillable entanglement have been formulated in terms of how much operational resource a state provides for certain tasks under the constraints of local operations and classical communication (LOCC) [17]. Another measure known as the relative entropy of entanglement has the geometric interpretation as the distance from the closest separable state in the Hilbert space [16]. These measures have the disadvantage that their computation in general requires extremely cumbersome optimization procedures. Yet another measure known as negativity quantifies entanglement of a state as the sum of the negative eigenvalues resulting from a partial transpose operation on the state [87, 88]. While this measure is easy to compute, it does not satisfy the property of additivity under tensor products that is desired in a valid entanglement measure. Moreover, it also has the undesirable feature that it can be zero even for an entangled state. Another related measure known as logarithmic negativity satisfies additivity but has the counterintuitive feature that it can sometimes increase under LOCC operations [88]. In summary, for general multipartite (many-party) quantum systems, no well-accepted measure exists at present. However, for the special case of two-qubit states, there is a measure called concurrence which is well-accepted as a valid measure of entanglement [18]. While this measure does not have a clear physical or operational interpretation, it has the advantage that a closed-form analytic expression in terms of the density matrix has been derived [89]. We will use concurrence to quantify the entanglement of two-qubit states of the signal-idler photons in the polarization and energy-time degrees of freedom in Chapter 4 and Chapter 5.

1.9 A basic introduction to nonlinear optics

Nonlinear optics studies the interaction of a medium with electromagnetic fields in which the optical properties of the medium are modified by the presence of the field [21]. When a medium interacts with an electric field, the electrons in the atoms of the

medium experience a Coulomb force which displaces them from their equilibrium positions. As a result, the atoms acquire a dipole moment that depends on the electric field. The dipole moment per unit volume is termed as the polarization of the medium. For simplicity, we assume the polarization $P(\mathbf{r}, t)$ and the external electric field $E(\mathbf{r}, t)$ to be scalar quantities. In situations where the electric fields are weak, the displacements of the electrons from their equilibrium positions are small. This corresponds to the regime of linear optics, in which the polarization $P(\mathbf{r}, t)$ can be written in terms of the electric field $E(\mathbf{r}, t)$ as

$$P(\mathbf{r}, t) = \epsilon_0 \chi^{(1)} E(\mathbf{r}, t), \tag{1.20}$$

where ϵ_0 is the permittivity of free space and $\chi^{(1)}$ is linear susceptibility of the medium. However, when electric field strengths are sufficiently high – which corresponds to the regime of nonlinear optics – the polarization $P(\mathbf{r}, t)$ must be expressed as a power series expansion of the form

$$P(\mathbf{r}, t) = \epsilon_0 \chi^{(1)} E(\mathbf{r}, t) + \epsilon_0 \chi^{(2)} E^2(\mathbf{r}, t) + \epsilon_0 \chi^{(3)} E^3(\mathbf{r}, t) + ... \tag{1.21}$$

Here, the quantities $\chi^{(2)}, \chi^{(3)}, ...$ are the second-order and third-order nonlinear susceptibilites of the medium, and so on. For centrosymmetric crystals, i.e, for crystals that possess inversion symmetry, the even-ordered nonlinear susceptibilities vanish [21]. On the other hand, for non-centrosymmetric crystals, all the nonlinear susceptibilities are in general finite. We will now derive the expression for the interaction Hamiltonian for a second-order process in a non-centrosymmetric crystal.

Consider a non-centrosymmetric crystal interacting with an electric field $E(\mathbf{r}, t)$. The electric field displacement $D(\mathbf{r}, t)$ inside the medium can be written as

$$D(\mathbf{r}, t) = \epsilon_0 E(\mathbf{r}, t) + P(\mathbf{r}, t). \tag{1.22}$$

Using the above expression, we can compute the energy density W of the field inside

the crystal medium as

$$\begin{aligned} W &= \frac{1}{2} D(\mathbf{r},t) \cdot E(\mathbf{r},t) \\ &= \frac{1}{2} \left[\epsilon_0 E(\mathbf{r},t) + P(\mathbf{r},t)\right] E(\mathbf{r},t) \\ &= \frac{1}{2} \left[\epsilon_0 E(\mathbf{r},t) + \epsilon_0 \chi^{(1)} E(\mathbf{r},t) + \epsilon_0 \chi^{(2)} E^2(\mathbf{r},t) + ...\right] E(\mathbf{r},t) \\ &\approx \frac{\epsilon_0}{2} \left[\left(1 + \chi^{(1)}\right) E^2(\mathbf{r},t) + \chi^{(2)} E^3(\mathbf{r},t)\right] \\ &= W_L + W_{NL} \end{aligned}$$

where W_L and W_{NL} are the linear and nonlinear interaction contributions, respectively, to the energy density. As we are interested in second-order nonlinear optical effects, we have retained terms only upto the second order from the perturbative expansion of Equation (1.21). The form of the nonlinear interaction Hamiltonian $H(t)$ can be computed as

$$H(t) = \int_V W_{NL}\, \mathrm{d}^3\mathbf{r} = \frac{\epsilon_0}{2} \int_V \mathrm{d}^3\mathbf{r}\, \chi^{(2)} E^3(\mathbf{r},t), \tag{1.23}$$

where the integration is carried out over the volume V of the crystal. We will now describe the second-order nonlinear optical process that is the topic of focus for this thesis, namely, parametric down-conversion (PDC).

1.10 Parametric down-conversion

Parametric down-conversion (PDC) is a second-order nonlinear optical process in which – as depicted in Figure 1.3 – a single photon, termed as pump, interacts with a non-centrosymmetric crystal and gets annihilated to create a pair of photons, termed as signal and idler [21]. The word parametric refers to the fact that there is no net energy transfer to the crystal medium, and the word down-conversion refers to the fact that the frequencies of the signal and idler photons are lower than the frequency of the pump photon. The constraints of energy, momentum, and

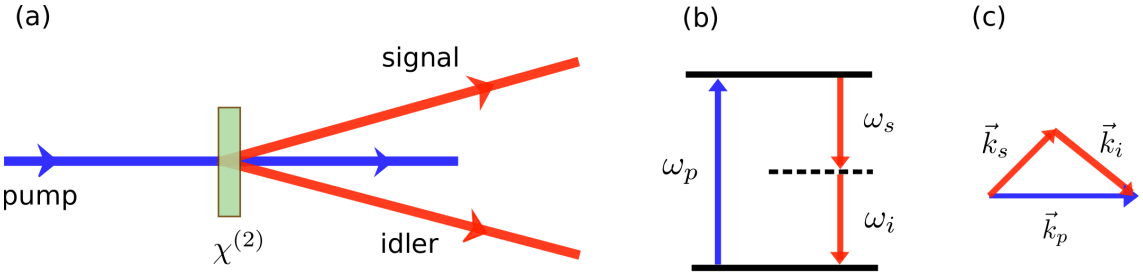

Figure 1.3: (a) Schematic depiction of parametric down-conversion (PDC) – a nonlinear optical process in which a pump photon interacts with a second-order nonlinear crystal and produces a pair of entangled photons, termed as signal and idler. (b) By virtue of energy conservation, the frequency of the pump photon is equal to the sum of the frequencies of the signal and idler photons. (c) By virtue of momentum conservation, the wave vector of the pump photon is equal to the sum of the wave vectors of the signal and idler photons.

orbital angular momentum conservation, referred to as phase-matching conditions, render the signal and idler photons entangled in the temporal, spatial, and angular degrees of freedom. In addition, using the type-I double crystal [34] and type-II [33] configurations, it is also possible to render the signal-idler photons entangled in the polarization degree of freedom.

In general, the two-photon quantum state describing the signal and idler photons depends on the physical parameters of the crystal configuration and the pump photon. These parameters can be varied experimentally to control the generated two-photon state. For instance, for a specific relative orientation of the crystal with respect to the pump photon propagation direction, the signal and idler photons are emitted in the same direction as the original pump photon. This condition is known as collinear emission. Upon changing the crystal orientation, the phase-matching conditions result in the signal and idler photons being emitted in different directions. This is known as non-collinear emission. In Chapter 3, we will explore the variation of the angular correlations of the signal-idler photons in the collinear and non-collinear emission regimes. In Chapters 4 and 5, we will further explore the dependence of the correlations of the signal and idler photons on the coherence properties of the pump photon in the polarization and temporal degrees of freedom. We will now briefly outline the derivation of the quantum interaction Hamiltonian operator for PDC from the classical interaction Hamiltonian for the process.

The classical interaction Hamiltonian of Equation (1.23) for the process of PDC takes the form [22, 24]

$$H(t) = \frac{\epsilon_0}{2} \int_V \mathrm{d}^3\mathbf{r}\chi^{(2)} E_p(\mathbf{r},t) E_s(\mathbf{r},t) E_i(\mathbf{r},t), \tag{1.24}$$

where $E_j(\mathbf{r},t)$ for $j = p, s$, and i represent the electric fields of the pump, signal and idler fields, respectively. Now as we discussed in Section 1.2, in the quantum theory the electric field amplitudes are replaced by field operators which can be expanded as in Equation (1.8) as a sum of positive and negative analytic field operators. Using the expansion, the expression for the Hamiltonian operator $\hat{H}(t)$ corresponding to the classical Hamiltonian $H(t)$ of Equation (1.24) can be computed. Each of the operators $E_j(\mathbf{r},t)$ for $j = p, s$, and i is written as a sum of their positive and negative analytic field operators, and their product is evaluated. The product has a total of eight terms corresponding to all the combinations of the analytic field operators. Among these eight terms, the contributions from six terms can be ignored as they average out to zero when the Hamiltonian is integrated with respect to time. This procedure corresponds to making the rotating wave approximation (see Section 2.3 of Ref. [90]). The terms whose contributions survive are the energy-conserving terms $\hat{E}_p^{(+)}(\mathbf{r},t)\hat{E}_s^{(-)}(\mathbf{r},t)\hat{E}_i^{(-)}(\mathbf{r},t)$ and its Hermitian conjugate $\hat{E}_p^{(-)}(\mathbf{r},t)\hat{E}_s^{(+)}(\mathbf{r},t)\hat{E}_i^{(+)}(\mathbf{r},t)$. Thus, the effective interaction Hamiltonian for PDC takes the form

$$\hat{H}(t) = \frac{\epsilon_0}{2} \int_V \mathrm{d}^3\mathbf{r}\chi^{(2)} \hat{E}_p^{(+)}(\mathbf{r},t)\hat{E}_s^{(-)}(\mathbf{r},t)\hat{E}_i^{(-)}(\mathbf{r},t) + \mathrm{H.c.} \tag{1.25}$$

We will use the above expression to compute the form of the two-photon state in the transverse spatial and temporal degrees of freedom in Chapter 3 and Chapter 5, respectively.

1.11 Correlations in parametric down-conversion

In the past, several studies have investigated the correlations between the signal and idler photons in the polarization [33, 34], temporal [22, 35, 28], spatial [23, 26, 30, 91], and angular [36, 31, 37] degrees of freedom. As the entangled states from PDC remain the most widely used entangled states, a precise characterization of their correlations is important for harnessing them in various quantum applications [77, 92, 37, 93]. In Chapter 3, we will present our experimental and theoretical characterizations of the angular correlations of these states.

In addition, it is also of fundamental interest to understand how the intrinsic correlations of the pump photon are transferred through the process of parametric down-conversion to manifest as entanglement between the signal and idler photons [22, 23, 26, 30, 29, 91]. In the past, several studies have attempted to understand how the correlations of the signal-idler photons are affected by the various pump and crystal parameters in PDC [35, 33, 34, 27]. However, studies on the transfer of correlations from the pump photon to the signal-idler photons have been carried out mainly in the spatial degree of freedom [23, 26, 30, 91]. In Chapter 4. and Chapter 5, we will study the transfer of correlations from the pump photon to the signal-idler photons in the polarization and temporal degrees of freedom.

1.12 Summary

In this chapter, we introduced the concepts of optical coherence, quantum entanglement, and parametric down-conversion. In the forthcoming chapters of this thesis, we will present our experimental and theoretical studies on the correlations of the signal and idler photons produced from PDC in various degrees of freedom. In Chapter 2, we will present a novel single-shot interferometric technique for measuring the angular correlations of a field. In Chapter 3, we will present experimental and theoretical characterizations of the angular correlations between the signal and idler photons produced from PDC of a Gaussian pump. In Chapters 4 and 5, we will

explore the transfer of correlations from the pump photon to the entangled signal-idler photons in the polarization and temporal degrees of freedom, respectively. We will show that the coherence of the pump photon predetermines the maximum achievable entanglement between the signal and idler photons. In Chapter 6, we will present the theoretical formulation of a basis-invariant measure of coherence for infinite-dimensional quantum states. This measure will now enable a basis-invariant quantification of the intrinsic correlations of the pump and signal-idler fields in the OAM, photon number, position and momentum degrees of freedom.

Chapter 2

Single-shot measurement of angular correlations

2.1 Introduction

In recent decades, the orbital angular momentum (OAM) degree of freedom of photons has gained a lot of attention for its potential applicability in the field of quantum information processing [16, 94, 36, 95, 93, 96]. This is because unlike the polarization basis which is intrinsically two-dimensional, the OAM basis is discrete and infinite-dimensional [44, 45, 28, 97]; and thus provides a natural basis for preparing high-dimensional states. In comparison to two-dimensional qubit states [56, 57, 98], high-dimensional qudit states have many distinct advantages in quantum protocols. In quantum communication, the use of high-dimensional states leads to enhanced security [99, 100, 101] and transmission bandwidth [102, 103]. For quantum computation, high-dimensional states have been shown to have more efficient gate implementations [104, 105]. Moreover, high-dimensional states also have inherent advantages for supersensitive measurements [106] and fundamental tests of quantum mechanics [107, 108, 109, 110]. Even in the classical domain, the use of high-dimensional superpositions of OAM-states can increase the system capacities and spectral efficiencies [111, 112, 113].

In this chapter, we consider an important problem that arises in high-dimensional OAM-based classical and quantum protocols, namely, the problem of measuring the OAM spectrum or distribution of an incoherent mixture of different OAM-carrying modes. The existing methods for measuring the orbital-angular-momentum (OAM) spectrum suffer from issues such as poor efficiency [36], strict interferometric stability requirements [47] or too much loss [32, 114]. Furthermore, most techniques inevitably discard part of the field and measure only a post-selected portion of the true spectrum [36, 32, 114]. Here, we propose and demonstrate an interferometric technique for measuring the true OAM spectrum of optical fields in a single-shot manner [115]. The technique directly encodes the angular coherence function in the output interferogram. In the absence of noise, a single-shot acquisition of the output interferogram is sufficient to obtain the OAM spectrum by an inverse Fourier transform. In the presence of noise, two appropriately chosen acquisitions can be used to infer the OAM spectrum in a noise-insensitive manner.

The chapter has been adapted almost verbatim from Ref. [115] and is organized here as follows: In Section 2.2, we present a brief overview of the OAM of light. In Section 2.3, we introduce the concepts of OAM spectrum and angular coherence function, and describe their Fourier relationship. In Section 2.4, we review the existing techniques for measuring the OAM spectrum and their limitations. In Section 2.5 and Section 2.6, we describe the single-shot technique and the two-shot noise elimination procedure. In Section 2.7, we present experimental results of a proof-of-concept demonstration of the technique using laboratory-synthesized fields with known spectra. In Section 2.8, we conclude with a summary of our technique.

2.2 Orbital Angular Momentum (OAM) of light

The earliest experiments aimed at measuring the angular momentum of light were performed by Raman and Bhagavantam in 1931 [116, 117]. The authors studied Rayleigh scattering of monochromatic light from different molecular gases and were led to the conclusion that a photon possesses an intrinsic spin angular momentum

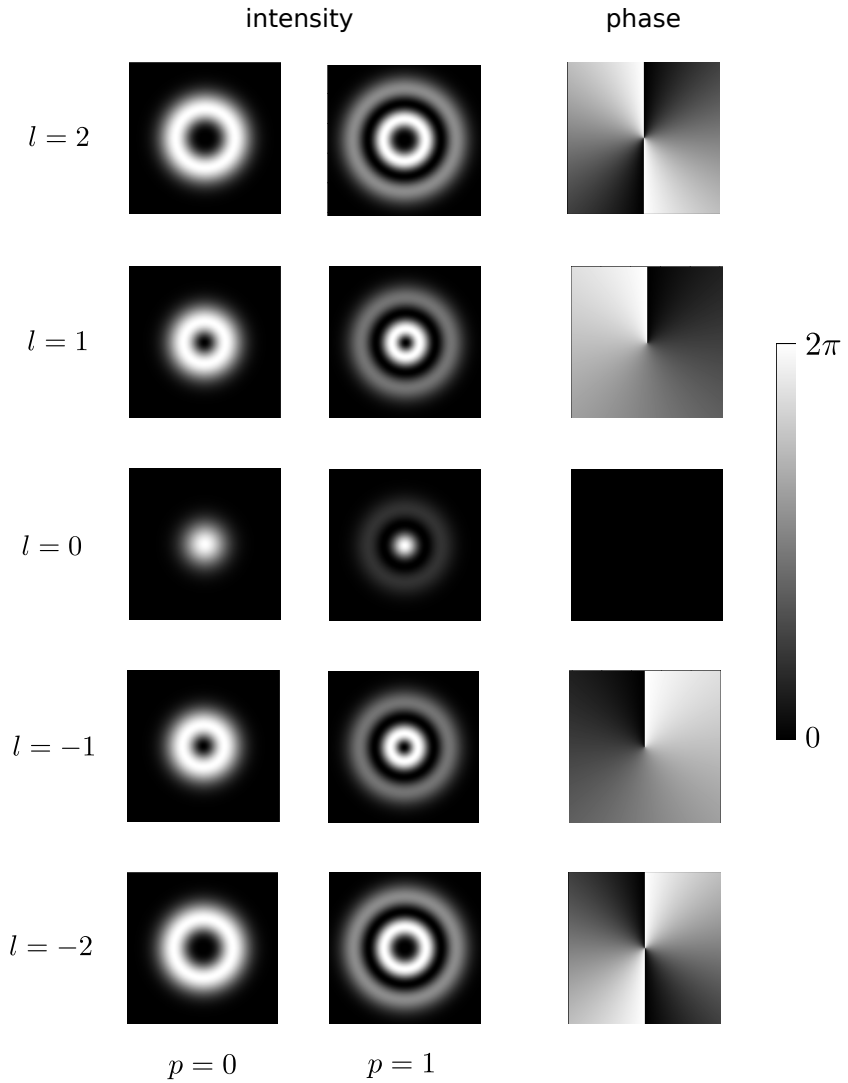

Figure 2.1: Intensity and phase profiles of Laguerre-Gauss (LG) modes with azimuthal index l and radial index p. The modes have the characteristic $e^{il\phi}$ phase profile which gives them an OAM of $l\hbar$ per photon. The sign (positive or negative) of l denotes the sense (clockwise or anti-clockwise) and the magnitude of l denotes the number of times the phase changes from 0 to 2π in the transverse plane. The radial index p only determines the radial intensity profile.

of magnitude $\hbar$. Later in 1936, Beth found that when right circularly-polarized light is passed through a birefringence plate which converts it to left-circularly polarized light, an angular momentum of $2\hbar$ per photon is transferred to the plate [118]. This was understood by assigning the right and left circularly-polarized light fields with a spin angular momentum of $\hbar$ and $-\hbar$ per photon, respectively.

In addition to spin angular momentum, light can also possess orbital angular momentum. In this context, an important discovery was made in 1992 by Allen *et al.*, who observed that certain paraxial fields known as Laguerre-Gauss (LG) modes

possess integer values of orbital angular momentum per photon in units of $\hbar$ [94]. The Laguerre-Gauss modes are exact solutions of the paraxial Helmholtz equation, and their transverse spatial electric field profiles are denoted in polar co-ordinates by the Laguerre-Gauss functions $LG_p^l(\rho, \phi)$. The azimuthal index l can take integer values from ∞ to $+\infty$, whereas the radial index p takes positive integer values from 0 to ∞. We depict the intensity and phase profiles of the first few LG modes in Figure 2.1. The functions $LG_p^l(\rho, \phi)$ take the form [119]

$$LG_p^l(\rho, \phi) = A \left(\frac{\rho\sqrt{2}}{w}\right)^{|l|} L_p^{|l|}\left(\frac{2\rho^2}{w^2}\right) \exp\left(-\frac{\rho^2}{w^2}\right) e^{il\phi}, \tag{2.1}$$

where w is the beam waist, A is a scaling constant, and $L_p^l(x)$ is the Laguerre polynominal given by

$$L_p^l(x) = \sum_{m=0}^{p} (-1)^m \frac{(l+p)!}{(p-m)!(l+m)!m!}\, x^m. \tag{2.2}$$

The azimuthal phase dependence of $e^{il\phi}$ is responsible for imparting the mode with an OAM of $l\hbar$ per photon, whereas the radial index p only determines the radial intensity profile, and not the OAM of the photons.

2.3 OAM spectrum and angular coherence function of a field

The LG modes form an orthonormal and complete basis in the transverse spatial degree of freedom. As a result, the transverse electric field profile $E_{\text{in}}(\rho, \phi)$ of any paraxial beam can be expressed in this basis as

$$E_{\text{in}}(\rho, \phi) = \sum_{l,p} A_{lp} LG_p^l(\rho, \phi) = \sum_{l,p} A_{lp} LG_p^l(\rho) e^{il\phi}, \tag{2.3}$$

where A_{lp} are stochastic complex variables. The corresponding correlation function $W(\rho_1, \phi_1; \rho_2, \phi_2)$ is

$$\begin{aligned} W(\rho_1, \phi_1; \rho_2, \phi_2) &\equiv \langle E^*_{\text{in}}(\rho_1, \phi_1) E_{\text{in}}(\rho_2, \phi_2) \rangle_e \\ &= \sum_{l,p,p'} \alpha_{lpp'} LG^{*l}_p(\rho_1, \phi_1) LG^l_{p'}(\rho_2, \phi_2), \end{aligned} \tag{2.4}$$

where $\langle \cdots \rangle_e$ represents an ensemble average over many realizations. The correlation function when integrated over the radial coordinate yields the angular coherence function

$$W(\phi_1, \phi_2) \equiv \int_0^\infty \rho d\rho W(\rho, \phi_1; \rho, \phi_2). \tag{2.5}$$

We shall consider the special class of partially coherent fields that satisfy $\langle A^*_{lp} A_{l'p'} \rangle_e = \alpha_{lpp'} \delta_{l,l'}$, where $\delta_{l,l'}$ is the Kronecker-delta function. Such fields are incoherent mixtures of different OAM-carrying modes. For such fields, the angular coherence function takes the form

$$W(\phi_1, \phi_2) \to W(\phi_1 - \phi_2) = \frac{1}{2\pi} \sum_{l=-\infty}^{\infty} S_l e^{-il(\phi_1 - \phi_2)}, \tag{2.6}$$

where $S_l = \sum_p \alpha_{lpp}$, and where we have used the identity $\int_0^\infty \rho LG^{*l}_p(\rho) LG^l_{p'}(\rho) \mathrm{d}\rho = \delta_{pp'}/2\pi$. The quantity S_l is referred to as the OAM spectrum of the field. It is normalized such that $\sum_l S_l = 1$ and $\int_0^{2\pi} W(\phi, \phi) d\phi = 1$. The Fourier transform relation of Equation (2.6) is the angular analog of the temporal Wiener-Khintchine theorem [1] for temporally-stationary fields discussed in Section 1.3 of this thesis (also see Section 2.4 of [120]). As a consequence of this relation, the OAM spectrum and the angular coherence function of a field are informationally equivalent.

[1] Interestingly, yet another relation analogous to the Wiener-Khintchine theorem is the van Cittert-Zernike theorem which relates the intensity profile of a spatially incoherent source to the far-field spatial coherence function by a Fourier transform [120]

2.4 Existing techniques for OAM spectrum measurement

Presently, there are primarily two approaches taken by existing techniques for measuring the OAM spectrum of a field. In the first approach [36], one displays a specific hologram onto a spatial light modulator (SLM) for a given input OAM-mode and then measures the intensity at the first diffraction order using a single mode fiber. This way, by placing different holograms specific to different input l in a sequential manner, one is able to measure the spectrum. However, this method is highly inefficient because the required number of measurements scales with the size of the input spectrum and also because of the non-uniform fiber-coupling efficiencies for different input l-modes [121]. Moreover, the fiber-coupling efficiencies also have a dependence on the radial indices of the input modes. As a result, the measured spectrum corresponds to a post-selected part of the true spectrum.

The second approach relies on measuring the angular coherence function of the field and then inferring the OAM-spectrum through an inverse Fourier transform. One way to measure the angular coherence function is by measuring the interference visibility in a Mach-Zehnder interferometer as a function of the Dove-prism rotation angle [47]. Although this method does not have any coupling-efficiency issue, it still requires a series of measurements for obtaining the angular coherence function. This necessarily requires that the interferometer be kept aligned for the entire range of the rotation angles. A way to bypass the interferometric stability requirement is by measuring the angular coherence function using angular double-slits [32, 114, 31]. However, this method is not suitable for fields that have very low intensities as only a very small portion of the incident field is used for detection.

Thus the existing methods for measuring the OAM spectrum information suffer from either poor efficiency [36] or strict interferometric stability requirements [47] or too much loss [32, 114]. In addition, most techniques [36, 32, 114] inevitably discard part of the field and yield only a post-selected portion of the true spectrum. We

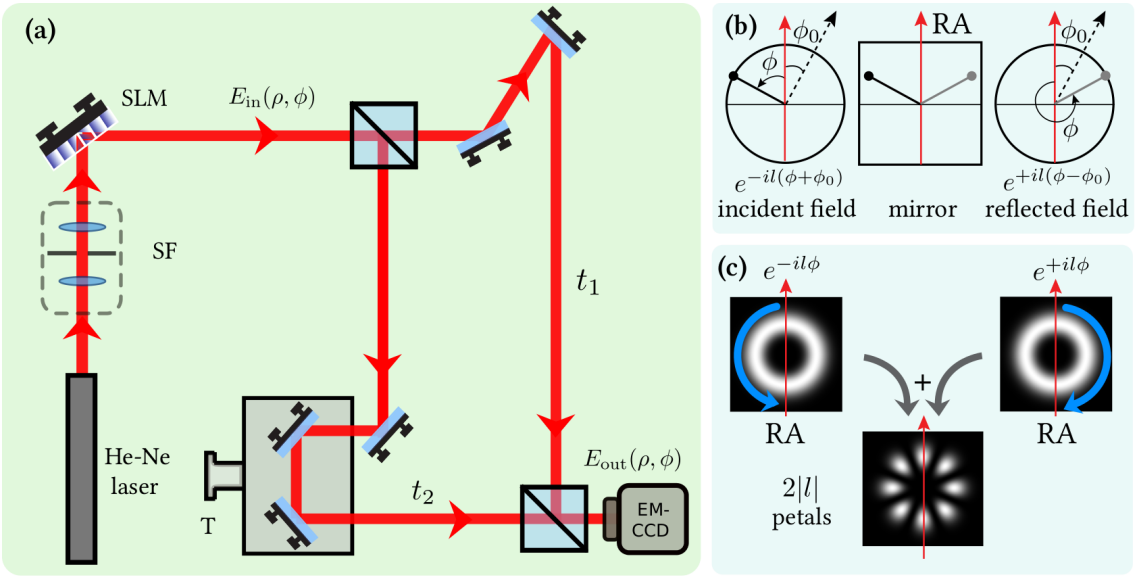

Figure 2.2: (a) Schematic of the experimental setup for single-shot measurement of OAM spectrum of lab-synthesized fields. (b) Describing how a mirror reflection changes the azimuthal phase of an LG mode. An incident beam with the azimuthal phase profile $e^{il(\phi+\phi_0)}$ transforms into a beam having the azimuthal phase profile $e^{-il(\phi-\phi_0)}$, where ϕ_0 is the angle between the reflection axis (RA) and the zero-phase axis (dashed axis) of the incident mode. (c) Illustrating the interference effect produced by the interferometer when the incident field is an $LG^{l}_{p=0}(\rho,\phi)$ mode with $l = 4$. At the output, we effectively have the interference of an $e^{il\phi}$ mode with an $e^{-il\phi}$ mode, and we obtain the output interference intensity in the form of a petal pattern with the number of petals being $2|l| = 8$. SLM: spatial light modulator; SF: spatial filter; T: translation stage.

shall now demonstrate a novel interferometric technique for measuring the true OAM spectrum in a single-shot manner. Moreover, as the technique requires only a single-shot measurement, the interferometric stability requirements are less stringent.

2.5 Description of a single-shot technique

Consider the situation shown in Figure 2.2(a). A partially coherent field of the type represented by Equations (2.3) and (2.4) enters the Mach-Zehnder interferometer having an odd and an even number of mirrors in the two arms [shown in Figure 2.2(c)]. As illustrated in Figure 2.2(d), each reflection transforms the polar coordinate as $\rho \to \rho$ and the azimuthal coordinate as $\phi + \phi_0 \to -\phi + \phi_0$ across the reflection axis (RA). Here ϕ is the angle measured from RA, and ϕ_0 is the angular-separation

between RA and the zero-phase axis of the incident mode (dashed-axis). The phase ϕ_0 does not survive in intensity expressions. So, without the loss of any generality, we take $\phi_0 = 0$ for all incident modes. Therefore, for the input incident field $E_{\text{in}}(\rho, \phi)$ of Equation (2.3), the field $E_{\text{out}}(\rho, \phi)$ at the output port becomes

$$E_{\text{out}}(\rho, \phi) = \sqrt{k_1} E_{\text{in}}(\rho, -\phi) e^{i(\omega_0 t_1 + \beta_1)} + \sqrt{k_2} E_{\text{in}}(\rho, \phi) e^{i(\omega_0 t_2 + \beta_2 + \tilde{\gamma})}. \tag{2.7}$$

Here, t_1 and t_2 denote the travel-times in the two arms of the interferometer; ω_0 is the central frequency of the field; β_1 and β_2 are the phases other than the dynamical phase acquired in the two arms; $\tilde{\gamma}$ is a stochastic phase which incorporates the temporal coherence between the two arms; k_1 and k_2 are the scaling constants in the two arms, which depend on the splitting ratios of the beam splitters, etc. The azimuthal intensity $I_{\text{out}}(\phi)$ at the output port is defined as $I_{\text{out}}(\phi) \equiv \int \rho \langle E^*_{\text{out}}(\rho, \phi) E^*_{\text{out}}(\rho, \phi) \rangle_e d\rho$, and using Equations (2.3)-(2.9), we can evaluate it to be

$$I_{\text{out}}(\phi) = \frac{1}{2\pi}(k_1 + k_2) + \gamma \sqrt{k_1 k_2} W(2\phi) e^{i\delta} + \text{c.c.} \tag{2.8}$$

Here, we have defined $\delta \equiv \omega_0(t_2 - t_1) + (\beta_2 - \beta_1)$, and $\gamma = \langle e^{i\tilde{\gamma}} \rangle$ quantifies the degree of temporal coherence. So, if the precise values of k_1, k_2, γ and δ are known then $W(2\phi)$ can be obtained by measuring $I_{\text{out}}(\phi)$ through a single-shot image of the output interferogram and subsequently the spectrum can be computed by using

$$S_l = \int_0^{2\pi} W(\phi_1 - \phi_2) e^{il(\phi_1 - \phi_2)} d\phi. \tag{2.9}$$

The single-shot nature of our scheme can be extremely useful since it makes the alignment requirements much more relaxed. Moreover, our scheme uses the entire incoming light field and therefore does not suffer from the photon-loss issue faced by schemes such as those based on using angular double-slits [32, 114].

We note that the intensity expression in Equation (2.8) is very different from the output intensity expression one obtains in a conventional Mach-Zehnder interferometer having a Dove prism [37]. In Equation (2.8), the output intensity and the

angular correlation function both depend on the detection-plane azimuthal angle ϕ. As a result, the angular correlation function $W(2\phi)$ comes out encoded in the azimuthal intensity profile $I_{\text{out}}(\phi)$. However, in the conventional Mach-Zehnder interferometer, the output intensity has no azimuthal variation; one measures only the total output intensity, and the angular correlation function is measured by measuring the interference-visibility of the total-intensity for a range of Dove prism rotation angles.

2.6 Two-shot noise elimination

Although it is in principle possible to measure the OAM spectrum in a single-shot manner as discussed above, it is practically highly difficult to do so because of the requirement of a very precise knowledge of k_1, k_2, γ, and δ. Moreover, obtaining a spectrum in this manner is susceptible to any noise in the measured $I_{\text{out}}(\phi)$, which results in errors in the measured spectrum. In particular, there could be intensity noise arising from ambient light exposures, beam intensity distortions due to imperfections in optical elements, etc, i.e, noise that neither depends on δ nor has a shot-to-shot variation. We now show that it is possible to eliminate such noise completely while also relinquishing the need for a precise knowledge of k_1, k_2, γ, and δ, just by acquiring one additional output interferogram. We present our analysis for a symmetric spectrum, that is, $S_l = S_{-l}$. (See Appendix A. for the non-symmetric case). Let us assume that the experimentally measured output azimuthal intensity $\bar{I}_{\text{out}}(\phi)$ contains some noise $I_{\text{n}}(\phi)$ in addition to the signal $I_{\text{out}}(\phi)$, that is,

$$\bar{I}_{\text{out}}(\phi) = I_{\text{n}}(\phi) + \frac{1}{2\pi}(k_1 + k_2) + 2\gamma\sqrt{k_1 k_2}W(2\phi)\cos\delta.$$

Now, suppose that we have two interferograms, $\bar{I}^{\delta_c}_{\text{out}}(\phi)$ and $\bar{I}^{\delta_d}_{\text{out}}(\phi)$, measured at $\delta = \delta_c$ and $\delta = \delta_d$, respectively. The difference in the intensities $\Delta\bar{I}_{\text{out}}(\phi) = \bar{I}^{\delta_c}_{\text{out}}(\phi) -$

$\bar{I}_{\text{out}}^{\delta_d}(\phi)$ of the two interferograms is then given by

$$\Delta\bar{I}_{\text{out}}(\phi) = \Delta I_{\text{n}}(\phi) + 2\gamma\sqrt{k_1 k_2}(\cos\delta_c - \cos\delta_d)W(2\phi),$$

where $\Delta I_{\text{n}}(\phi) = I_{\text{n}}^{\delta_c}(\phi) - I_{\text{n}}^{\delta_d}(\phi)$ is the difference in the noise intensities. In situations in which the noise neither has any explicit functional dependence on δ nor does it vary from shot to shot, $\Delta I_{\text{n}}(\phi) = 0$, and the difference intensity $\Delta\bar{I}_{\text{out}}(\phi)$ then becomes directly proportional to the angular coherence function $W(2\phi)$. Multiplying each side of the above equation by $e^{i2l\phi}$, integrating over ϕ, using the definition of Equation (2.9), and defining the measured OAM spectrum $\bar{S}_l$ as $\bar{S}_l \equiv \int_0^{2\pi} \Delta\bar{I}_{\text{out}}(\phi)e^{i2l\phi}d\phi$, we obtain

$$\bar{S}_l = 2\gamma\sqrt{k_1 k_2}(\cos\delta_c - \cos\delta_d)S_l. \tag{2.10}$$

The measured OAM-spectrum $\bar{S}_l$ is same as the true input OAM-spectrum S_l up to a scaling constant. We thus see that the OAM-spectrum can be computed in a two-shot manner without having to know the exact values of k_1, k_2, γ, δ_c or δ_d. However, in order to get a better experimental signal-to-noise ratio, it would be desirable to have $\gamma \approx 1$ by minimizing the path length difference, $k_1 \approx k_2 \approx 0.5$ by choosing precise $50:50$ beam splitters. Moreover, it is also desirable to have $\delta_c \approx 0$, and $\delta_d \approx \pi$. We will now describe a proof-of-concept experimental demonstration of this technique using laboratory synthesized fields with known spectra.

2.7 Proof-of-concept experimental demonstration

In our experiment, we spatially filtered the beam from a standard He-Ne laser of wavelength 632 nm to obtain a high purity Gaussian beam. The Gaussian beam was then incident on a Holoeye Pluto BB spatial light modulator (SLM) on which a hologram corresponding to various $LG_{p=0}^{l}$ modes were displayed. The holograms were generated using the Type 3 method of Ref.[122]. The generated $LG_{p=0}^{l}$ modes were

sequentially made incident into the interferometer and the corresponding output interferograms were imaged using an Andor iXon Ultra electron-multiplying charge-coupled device (EMCCD) camera having 512×512 pixels. To reduce pixelation-related noise, the interferograms were scaled up in size by a factor of four using a bicubic interpolation method. For each individual $LG^{l}_{p=0}$ mode the camera was exposed for about 0.4 s. The sequential acquisition was automated to ensure that δ is the same for all the modes. The azimuthal intensity $\bar{I}^{\delta}_{\text{out}}(\phi)$ plots were obtained by first precisely positioning a very narrow angular region-of-interest (ROI) at angle ϕ in the interferogram image and then integrating the intensity within the ROI up to a radius that is sufficiently large. In order to ensure minimal shot-to-shot noise variation, the interferometer was covered after the required alignment with a box and the measurements were performed only after it had stabilized in terms of ambient fluctuations. As shown in Figure 2.2(a), He-Ne laser is spatially filtered and made incident onto a Holoeye Pluto SLM. The measured interferograms and the corresponding azimuthal intensities for a few $LG^{l}_{p=0}(\rho, \phi)$ modes for $\delta_c \approx 2m\pi$, and $\delta_d \approx (2m+1)\pi$, where m is an integer, are presented in Figure 2.3(a) and Figure 2.3(b), respectively. A very good match between the theory and experiment indicates that the $LG^{l}_{p=0}(\rho, \phi)$ modes produced in our experiments are of very high quality. By controlling the strengths of the synthesized $LG^{l}_{p=0}(\rho, \phi)$ modes for l ranging from $l = -20$ to $l = 20$, we synthesize two separate fields: One with a rectangular spectrum, and the other one with a Gaussian spectrum. The representative interferogram corresponding to a particular field as input is obtained by adding individual interferograms for l ranging from $l = -20$ to $l = +20$. The serial acquisition is automated to ensure that δ is the same for all the modes. Two such representative interferograms, one with $\delta = \delta_c$ and other one with $\delta = \delta_d$ are recorded for each field. Figs. 2.3(c) and 2.3(d) show the measured output interferograms, the corresponding azimuthal intensities, and the measured spectrum $\bar{S}_l$ computed using Equation (2.10) for the synthesized Gaussian and Rectangular OAM spectrum, respectively. We find a very good match between the synthesized

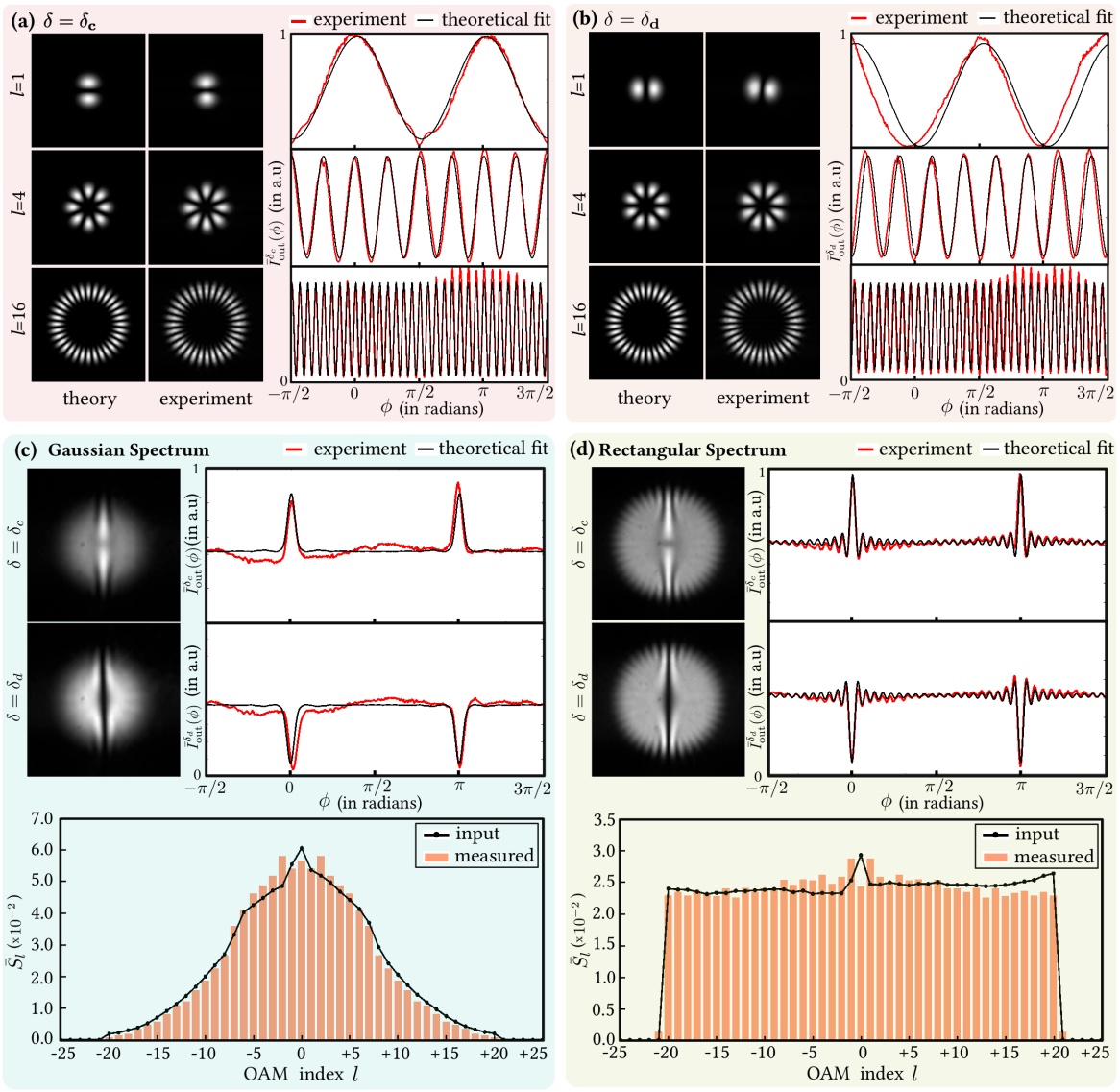

Figure 2.3: (a) and (b) Measured output interferograms and the corresponding azimuthal intensities for input $LG^l_{p=0}(\rho, \phi)$ modes with $l = 1, 4$, and 16 for $\delta = \delta_c \approx 2m\pi$ and $\delta = \delta_d \approx (2m + 1)\pi$, respectively, where m is an integer. (c) Measured output interferograms, the azimuthal intensities, and the measured spectrum for the synthesized input field with a Gaussian OAM-spectrum. (d) Measured output interferograms, the azimuthal intensities, and the measured spectrum for the synthesized input field with a Rectangular OAM-spectrum.

spectra and the measured spectra. There is some noise in the measured spectra for low values of l, which we believe could be due to SLM imperfections and various wave-front aberrations in the laser beam.

2.8 Summary

In summary, we have proposed and demonstrated an interferometric technique that measures the OAM spectrum of light fields with only two acquisitions of the output interferograms. This technique is insensitive to noise and does not require a precise characterization of the setup parameters, such as beam splitting ratios, degree of temporal coherence, etc. As the measurement comprises of only two acquisitions irrespective of the number of OAM modes in the field, this technique is highly efficient in comparison to other existing techniques. Moreover, this technique does not inherently involve any post-selection of the measured field and therefore measures the true OAM spectrum.

We finally mention some of the potential applications of this technique. First, the concept of image-inversion utilized in our technique, can be employed in more general settings to probe correlation properties and spectral characteristics of light fields in degrees of freedom other than the OAM [123]. Second, the unparalleled efficiency of our technique can be used to characterize high-dimensional OAM entangled states for information processing applications. This second application will be demonstrated in the next chapter for the high-dimensional OAM-entangled states produced from PDC of a Gaussian pump.

Chapter 3

Angular correlations in parametric down-conversion

3.1 Introduction

It is known that by virtue of orbital-angular-momentum (OAM) conservation, the two-photon signal-idler states produced from parametric down-conversion (PDC) are entangled in the OAM degree of freedom. Moreover, these states are high-dimensional entangled states, and have become a natural choice for several high-dimensional quantum information applications. To this end, there have been intense research efforts, both theoretically [92, 77, 124, 125, 32, 126, 127] and experimentally [36, 128, 31, 129, 37, 130, 115], for the precise characterization of high-dimensional OAM-entangled states produced by PDC. Although a general OAM-entangled state requires state tomography for its complete characterization, the experimentally relevant case of OAM-entangled states produced using a Gaussian pump beam can be characterized by measuring just the angular Schmidt spectrum [92, 77, 37], which is defined as the probability S_l of signal and idler photons getting detected with OAM values $l\hbar$ and $-l\hbar$, respectively.

The characterization of the angular Schmidt spectrum has been challenging, both, experimentally and theoretically. On the experimental front, several tech-

niques have been developed for measuring the angular Schmidt spectrum. The first set of techniques is based on using fiber-based projective measurements [36, 31, 128, 129, 130]. However, these techniques are very inefficient because the required number of measurements scales with the size of the input spectrum. Furthermore, these techniques measure only the projected spectrum instead of the true spectrum [121]. The second set of techniques is based on inferring the spectrum by measuring the angular coherence function [37, 32]. Although these techniques do measure the true spectrum, they either require a series of coincidence measurements and have strict interferometric stability requirements [37] or suffer from too much loss [32]. More recently, an interferometric technique has been demonstrated that can measure the true angular Schmidt spectrum in a very efficient single-shot manner [115].

On the theoretical front, Torres *et al.* have derived a formula for calculating the spectrum for collinear phase matching [77]. However, this formula involves a four-dimensional integration followed by two infinite summations over the radial indices. Although the summations have been shown to converge for certain set of experimental parameters, the convergence is not explicitly proved for an arbitrary set of parameters. Moreover, it is extremely inefficient to first calculate the contributions due to sufficiently large number of radial modes and then sum them over. Subsequent studies have analytically performed the four-dimensional integration for certain collinear phase-matching conditions [124, 125], but they still suffer from the same set of issues due to infinite summations. In a recent study by Zhang and Roux [127], the angular Schmidt spectrum in non-collinear phase matching condition was studied. However, their calculation includes contributions only from the first radial modes of the signal and idler photons, and therefore is not applicable to a generic experimental situation.

In this chapter, we derive an exact formula for calculating the true angular Schmidt spectrum of a two-photon state that does not suffer from the above mentioned issues since the infinite summations over radial modes are performed analytically. Our formula is valid for both collinear and non-collinear phase matching

conditions. Next, we use the single-shot technique developed in the previous chapter to experimentally characterize the angular Schmidt spectrum of entangled photons produced by PDC of a Gaussian pump from collinear to highly non-collinear emission regimes.

The contents of this chapter, which appear almost verbatim from Ref. [131], are organized as follows: In Section 3.2, we derive the form of the two-photon state produced from PDC in the transverse spatial representation. In Section 3.3, we present the definition of angular Schmidt spectrum of the two-photon state produced from PDC. In Section 3.4, we present the derivation of the analytic formula for computing the angular Schmidt spectrum. In Section 3.5, we present our experimental characterization of the angular Schmidt spectrum of down-converted photons from collinear to non-collinear emission regimes. In Section 3.6, we conclude with a summary of this chapter.

3.2 Two-photon state produced from parametric down-conversion

We will now derive the spatial representation of the two-photon state produced from PDC. We closely follow the calculations presented in Ref. [29, 22, 132]. As derived in Section 1.10, the interaction Hamiltonian $\hat{H}(t')$ for the process of PDC is given by Equation (1.25) written as

$$\hat{H}(t') = \frac{\epsilon_0}{2} \int_{\mathbb{V}} \mathrm{d}^3\boldsymbol{r} \chi^{(2)} \hat{E}_p^{(+)}(\boldsymbol{r}, t') \hat{E}_s^{(-)}(\boldsymbol{r}, t') \hat{E}_i^{(-)}(\boldsymbol{r}, t') + H.c, \tag{3.1}$$

where $\mathbb{V}$ is the interaction volume inside the nonlinear crystal, $\chi^{(2)}$ is the second-order non-linear susceptibility of the crystal medium, $\hat{E}_j^{(+)}(r, t')$ and $\hat{E}_j^{(-)}(r, t')$ are the positive and negative complex analytic field operators of the field with $j = p, s$ or i corresponding to the pump, signal or idler, respectively. The field operators can

be expanded in the plane-wave representation as

$$\hat{E}_p^{(+)}(\boldsymbol{r},t') = \int_{-\infty}^{+\infty} A_p \mathrm{d}^3\boldsymbol{k}_p\, V(\boldsymbol{k}_p)\, e^{i(\boldsymbol{k}_p\cdot\boldsymbol{r}-\omega_p t')} \tag{3.2a}$$

$$\hat{E}_s^{(-)}(\boldsymbol{r},t') = \int_{-\infty}^{+\infty} A_s^* \mathrm{d}^3\boldsymbol{k}_s\, \hat{a}_s^\dagger(\boldsymbol{k}_s)\, e^{-i(\boldsymbol{k}_s\cdot\boldsymbol{r}-\omega_s t')} \tag{3.2b}$$

$$\hat{E}_i^{(-)}(\boldsymbol{r},t') = \int_{-\infty}^{+\infty} A_i^* \mathrm{d}^3\boldsymbol{k}_i\, \hat{a}_i^\dagger(\boldsymbol{k}_i)\, e^{-i(\boldsymbol{k}_i\cdot\boldsymbol{r}-\omega_i t')} \tag{3.2c}$$

We have used the notation, $\boldsymbol{r} = (\rho, z)$ and $\boldsymbol{k}_j = (\boldsymbol{q}_j, k_{jz})$. The scaling factors A_j are assumed to be constant in the typical frequency range of the signal-idler photons. The above electric field operators satisfy $[\hat{E}_j^{(+)}(\boldsymbol{r}_1,t_1'), \hat{E}_k^{(+)}(\boldsymbol{r}_2,t_2')] = [\hat{E}_j^{(-)}(\boldsymbol{r}_1,t_1'), \hat{E}_k^{(-)}(\boldsymbol{r}_2,t_2')] = 0$ where $j,k = p,s,i$. Also, $[\hat{E}_j^{(+)}(\boldsymbol{r}_1,t_1'), \hat{E}_k^{(-)}(\boldsymbol{r}_2,t_2')]$ is in general not zero, but one can evaluate it from Eq. (3.2) using the commutation relations $[\hat{a}_j(\boldsymbol{k}_i), \hat{a}_k^\dagger(\boldsymbol{k}_j)] = \delta_{jk}$ and $[\hat{a}_j(\boldsymbol{k}_j), \hat{a}_k(\boldsymbol{k}_k)] = [\hat{a}_j^\dagger(\boldsymbol{k}_j), \hat{a}_k^\dagger(\boldsymbol{k}_k)] = 0$ where $j,k = p,s$, and i. The pump field, whose Fourier-domain complex amplitude of the pump is denoted as $V(\boldsymbol{k}_p)$, is assumed to be strong enough to be treated classically. Using equations (3.2), we can express Equation (3.1) as

$$\hat{H}(t') = \frac{A_p A_s^* A_i^* \epsilon_0 \chi^{(2)}}{2} \int_{\mathbb{V}} \mathrm{d}^3\boldsymbol{r} \iiint \mathrm{d}^3\boldsymbol{k}_p \mathrm{d}^3\boldsymbol{k}_s \mathrm{d}^3\boldsymbol{k}_i V(\boldsymbol{k}_p) \hat{a}_s^\dagger(\boldsymbol{k}_s) \hat{a}_i^\dagger(\boldsymbol{k}_i) \times e^{i(\boldsymbol{k}_p-\boldsymbol{k}_s-\boldsymbol{k}_i)\cdot\boldsymbol{r}}\, e^{-i(\omega_p-\omega_s-\omega_i)t'}$$

The state of the signal-idler field at $t' = 0$ is given by

$$|\psi(t'=0)\rangle = \exp\left[-\frac{i}{\hbar}\int_{-t_{int}}^{0} \mathrm{d}t' \hat{H}(t')\right] |\psi(-t_{int})\rangle. \tag{3.3}$$

The state $|\psi(-t_{int})\rangle$ of the signal-idler field before the PDC process is just the vacuum state, i.e, $|\psi(-t_{int})\rangle = |\mathrm{vac}\rangle_s |\mathrm{vac}\rangle_i$. We note that as the Hamiltonian $\hat{H}(t')$ is explicitly time-dependent, it need not commute with itself at different times. As a result, we must strictly expand the output state in terms of the time-ordered Dyson series. However, assuming the parametric interaction to be weak, we will retain only the first two terms of the Dyson series, which are in fact identical to those of

the usual Taylor series expansion for a time-independent Hamiltonian [133]. The first term is the vacuum state, and can be ignored as it does not contribute photon detection events. The second term is written as

$$|\psi_2\rangle = \frac{A_p A_s^* A_i^* \epsilon_0 \chi^{(2)}}{2i\hbar} \int_{-t_{int}}^{0} \mathrm{d}t' \iint_S \mathrm{d}^2\boldsymbol{\rho} \int_0^L \mathrm{d}z \iiint \mathrm{d}^2\boldsymbol{q}_p \mathrm{d}^2\boldsymbol{q}_s \mathrm{d}^2\boldsymbol{q}_i \iiint \mathrm{d}k_{pz}\mathrm{d}k_{sz}\mathrm{d}k_{iz}$$
$$\times V(\boldsymbol{k}_p)\hat{a}_s^\dagger(\boldsymbol{k}_s)\hat{a}_i^\dagger(\boldsymbol{k}_i) e^{i[(\boldsymbol{q}_p-\boldsymbol{q}_s-\boldsymbol{q}_i)\cdot\boldsymbol{\rho}+(k_{pz}-k_{sz}-k_{iz})z]}\, e^{-i(\omega_p-\omega_s-\omega_i)t'} |0\rangle_s |0\rangle_i.$$

Note that $\hat{a}_s^\dagger(\boldsymbol{k}_s)\hat{a}_i^\dagger(\boldsymbol{k}_i)|0\rangle_s|0\rangle_i = |\boldsymbol{k}_s\rangle|\boldsymbol{k}_i\rangle$, where $|\boldsymbol{k}_s\rangle|\boldsymbol{k}_i\rangle$ denotes a two-photon state in which the signal photon has wavevector $\boldsymbol{k}_s$, and idler photon has wavevector $\boldsymbol{k}_i$. We now assume that the interaction time t_{int} is much longer than the time scale of the down-conversion process, but is much smaller than the time interval between successive down-conversion events [24, 134]. Under this assumption, the time integration can be carried out from $-\infty$ to $+\infty$, which yields $\delta(\omega_p - \omega_s - \omega_i)$. Also, the area of interaction S is typically much smaller than the transverse area of the crystal. Under this condition, the integral over the transverse spatial position with respect to $\mathrm{d}^2\boldsymbol{\rho}$ can be performed from $-\infty$ to $+\infty$ to yield $\delta(\boldsymbol{q}_p - \boldsymbol{q}_s - \boldsymbol{q}_i)$. Moreover, the integral with respect to $\mathrm{d}z$ over the longitudinal size L of the crystal can be carried out analytically. Performing the above steps, we obtain

$$|\psi_2\rangle = A \iiint \mathrm{d}^2\boldsymbol{q}_p \mathrm{d}^2\boldsymbol{q}_s \mathrm{d}^2\boldsymbol{q}_i \iiint \mathrm{d}k_{pz}\mathrm{d}k_{sz}\mathrm{d}k_{iz} V(\boldsymbol{k}_p)\delta(\boldsymbol{q}_p - \boldsymbol{q}_s - \boldsymbol{q}_i)$$
$$\times \delta(\omega_p - \omega_s - \omega_i)\,\mathrm{sinc}\left(\frac{\Delta k_z L}{2}\right) \exp\left(i\frac{\Delta k_z L}{2}\right) |\boldsymbol{k}_s\rangle|\boldsymbol{k}_i\rangle,$$

where $\mathrm{sinc}(x) \equiv \sin(x)/x$ and $\Delta k_z \equiv (k_{pz} - k_{sz} - k_{iz})$. We now assume that the signal-idler photons with a narrow bandwidth around the central frequency $\omega_p/2$, corresponding to degenerate parametric down-conversion. This is typically achieved by introducing wavelength filters before detection. We also assume that the pump is extraordinarily polarized (as in type-I PDC from a negative uniaxial crystal) [132] and that the pump and signal-idler fields satisfy the paraxial approximation. The

state $|\psi_2\rangle$ can then be expressed in the transverse momentum representation as [77]

$$|\psi_2\rangle = A \iint \mathrm{d}^2\boldsymbol{q}_s \mathrm{d}^2\boldsymbol{q}_i \, V(\boldsymbol{q}_s + \boldsymbol{q}_i, z = 0) \, \mathrm{sinc}\left(\frac{\Delta k_z L}{2}\right) \exp\left(i\frac{\Delta k_z L}{2}\right) |\boldsymbol{q}_s\rangle |\boldsymbol{q}_i\rangle \quad (3.4)$$

where $V(\boldsymbol{q}_p, z = 0)$ is the transverse momentum representation of the pump field at the crystal location $z = 0$. We will now present our theoretical work on the calculation of the angular Schmidt spectrum of two-photon states produced from parametric down-conversion.

3.3 Angular Schmidt spectrum

Consider the parametric down-conversion of a pump field with OAM index $l_p = 0$, for eg, a Gaussian pump. By virtue of conservation of OAM in PDC [36, 77, 92], the OAM indices l_s and l_i of the generated signal and idler photons, respectively, must satisfy $l_s + l_i = 0$. When the detection system is sensitive only to the OAM-mode index, the two-photon state $|\psi_2\rangle$ has the following Schmidt-decomposed form [32]:

$$|\psi_2\rangle = \sum_{l=-\infty}^{\infty} \sqrt{S_l} |l\rangle_s | - l\rangle_i. \quad (3.5)$$

Here $|l\rangle_s$ and $|l\rangle_i$ represent modes with OAM-mode indices l and $-l$ for the signal and idler photons, respectively. The corresponding probabilities S_l are collectively referred to as the angular Schmidt spectrum of the two-photon state. The angular Schmidt spectrum quantifies the dimensionality and the entanglement of the state [92, 77, 37].

3.4 Derivation of the analytic formula

Consider a general two-photon state $|\psi_2\rangle$ of signal-idler photons written in the transverse-momentum basis as [22]:

$$|\psi_2\rangle = \iint_{-\infty}^{\infty} \Phi(\boldsymbol{q_s}, \boldsymbol{q}_i)|\boldsymbol{q}_s\rangle_s|\boldsymbol{q}_i\rangle_i d\boldsymbol{q}_s d\boldsymbol{q}_i, \tag{3.6}$$

where $\Phi(\boldsymbol{q_s}, \boldsymbol{q}_i)$ is the wavefunction of the down-converted photons in the transverse-momentum basis. The state $|\psi_2\rangle$ can also be represented in the Laguerre-Gaussian (LG) basis [77, 124, 125, 32] as:

$$|\psi_2\rangle = \sum_{l_s}\sum_{l_i}\sum_{p_s}\sum_{p_i} C_{l_i,p_i}^{l_s,p_s}|l_s, p_s\rangle_s|l_i, p_i\rangle_i. \tag{3.7}$$

Here $|l_s, p_s\rangle_s$ represents the state of the signal photon in the Laguerre-Gaussian (LG) basis defined by the OAM-mode index l_s and the radial index p_s, etc. Using Equations (3.6) and (3.7), the complex coefficients $C_{l_i,p_i}^{l_s,p_s}$ can be written as,

$$C_{l_i,p_i}^{l_s,p_s} = \iint \Phi(\boldsymbol{q}_s, \boldsymbol{q}_i) LG_{p_s}^{*l_s}(\boldsymbol{q}_s) LG_{p_i}^{*l_i}(\boldsymbol{q}_i) d\boldsymbol{q}_s d\boldsymbol{q}_i. \tag{3.8}$$

Here $LG_{p_s}^{l_s}(\boldsymbol{q}_s) = \langle \boldsymbol{q}_s | l_s, p_s\rangle$ is the momentum-basis representation of state $|l_s, p_s\rangle_s$ [77, 124]. Transforming to the cylindrical coordinates, we write $C_{l_i,p_i}^{l_s,p_s}$ as,

$$C_{l_i,p_i}^{l_s,p_s} = \int_0^{\infty}\int_{-\pi}^{\pi} \Phi(\rho_s, \rho_i, \phi_s, \phi_i) LG_{p_s}^{*l_s}(\rho_s, \phi_s) LG_{p_i}^{*l_i}(\rho_i, \phi_i) \rho_s \rho_i d\rho_s d\rho_i d\phi_s d\phi_i, \tag{3.9}$$

where $\boldsymbol{q}_s \equiv (q_{sx}, q_{sy}) = (\rho_s \cos\phi_s, \rho_s \sin\phi_s)$, $\boldsymbol{q}_i \equiv (q_{ix}, q_{iy}) = (\rho_i \cos\phi_i, \rho_i \sin\phi_i)$, $d\boldsymbol{q}_s = \rho_s d\rho_s d\phi_s$, and $d\boldsymbol{q}_i = \rho_i d\rho_i d\phi_i$. The probability $P_{l_i}^{l_s}$, that the signal and idler photons are detected with OAMs $l_s\hbar$ and $l_i\hbar$, respectively, is calculated by summing over radial indices:

$$P_{l_i}^{l_s} = \sum_{p_s=0}^{\infty}\sum_{p_i=0}^{\infty} |C_{l_i,p_i}^{l_s,p_s}|^2. \tag{3.10}$$

Equations (3.9) and (3.10) were used in Refs. [77, 124, 125] for calculating the spectra of OAM-entangled states. We note that in order to calculate the angular Schmidt spectrum using the above formula one needs to first choose a beam waist for the signal and idler LG bases in Equations (3.9) and then perform the summations in Equation (3.10) over a sufficiently large number of modes. As a result, even for certain collinear phase-matching conditions, in which the four-dimensional integral can be analytically performed [124, 125], the above formula suffers from convergence issues.

We now derive a formula for the angular Schmidt spectrum that neither requires a beam waist to be chosen nor involves infinite summations and is applicable to both collinear and non-collinear phase matching conditions. To this end, we first rewrite Equation (3.10) using the relation $LG^{l_s}_{p_s}(\rho_s,\phi_s) = LG^{l_s}_{p_s}(\rho_s)e^{il_s\phi_s}$, etc., as

$$P^{l_s}_{l_i} = \iiiint_0^\infty \iiiint_{-\pi}^{\pi} \Phi(\rho_s,\rho_i,\phi_s,\phi_i)\Phi^*(\rho'_s,\rho'_i,\phi'_s,\phi'_i) \sum_{p_s=0}^{\infty} LG^{*l_s}_{p_s}(\rho_s)LG^{l_s}_{p_s}(\rho'_s) \times \sum_{p_i=0}^{\infty} LG^{*l_i}_{p_i}(\rho_i)LG^{l_i}_{p_i}(\rho'_i)e^{+i(l_s\phi_s+l_i\phi_i)}e^{-i(l_s\phi'_s+l_i\phi'_i)}\rho_s\rho_i\rho'_s\rho'_i\mathrm{d}\rho_s\mathrm{d}\rho_i\mathrm{d}\rho'_s\mathrm{d}\rho'_i\,\mathrm{d}\phi_s\mathrm{d}\phi_i\mathrm{d}\phi'_s\mathrm{d}\phi'_i. \tag{3.11}$$

We then use the identity $\sum_{p=0}^{\infty} LG^{p}_{l}(\rho)LG^{*p}_{l}(\rho') = (1/\pi)\delta(\rho^2-\rho'^2)$ over indices p_s and p_i and obtain

$$P^{l_s}_{l_i} = \iiiint_0^\infty \iiiint_{-\pi}^{\pi} \Phi(\rho_s,\rho_i,\phi_s,\phi_i)\Phi^*(\rho'_s,\rho'_i,\phi'_s,\phi'_i)\frac{1}{\pi^2}\delta(\rho_s^2-\rho_s'^2)\delta(\rho_i^2-\rho_i'^2) \times e^{+i(l_s\phi_s+l_i\phi_i)}e^{-i(l_s\phi'_s+l_i\phi'_i)}\rho_s\rho_i\rho'_s\rho'_i\mathrm{d}\rho_s\mathrm{d}\rho_i\mathrm{d}\rho'_s\mathrm{d}\rho'_i\,\mathrm{d}\phi_s\mathrm{d}\phi_i\mathrm{d}\phi'_s\mathrm{d}\phi'_i. \tag{3.12}$$

After evaluating the delta function integrals and rearranging the remaining terms, we obtain

$$P^{l_s}_{l_i} = \frac{1}{4\pi^2}\iint_0^\infty \left| \iint_{-\pi}^{\pi} \Phi(\rho_s,\rho_i,\phi_s,\phi_i)e^{i(l_s\phi_s+l_i\phi_i)}d\phi_s d\phi_i \right|^2 \rho_s\rho_i d\rho_s d\rho_i. \tag{3.13}$$

We can now compute the angular Schmidt spectrum $S_l = P^l_{-l}$ of two-photon states produced from a Gaussian pump. Upon substituting $l_s = -l_i = l$, which follows from OAM conservation in PDC of a Gaussian pump, we obtain

$$S_l = \frac{1}{4\pi^2} \iint_0^\infty \left| \iint_{-\pi}^{\pi} \Phi(\rho_s, \rho_i, \phi_s, \phi_i) e^{il(\phi_s - \phi_i)} d\phi_s d\phi_i \right|^2 \rho_s \rho_i d\rho_s d\rho_i. \tag{3.14}$$

Equations (3.13) and (3.14) are the main theoretical results. Equation (3.13) provides a formula for calculating the probability $P^{l_s}_{l_i}$ that the signal and idler photons are detected with OAMs $l_s\hbar$ and $l_i\hbar$, respectively for a general two-photon state. Equation (3.14) calculates the angular Schmidt spectrum of two-photon states produced from a Gaussian pump. In contrast to the previously obtained formulas [77, 124, 125, 127], Equations (3.13) and (3.14) neither require a beam waist to be chosen nor involve infinite summations. As a result, these formulas can provide improvement of several orders of magnitude in the spectrum computation time. Moreover, unlike the non-collinear phase-matching results in Ref. [127], which is applicable only for a given pair of radial modes of the signal and idler photons, these formulas are applicable to a generic set of non-collinear phase matching conditions and geometries.

3.5 Experimental and theoretical characterizations

The experimental characterizations of angular Schmidt spectrum so far have suffered from poor efficiency and stringent stability requirements [36, 37]. Note that from Equation (3.5), we can compute the density matrices $\rho_s = \mathrm{Tr}_i\left(|\psi_2\rangle\langle\psi_2|\right)$ and $\rho_i = \mathrm{Tr}_s\left(|\psi_2\rangle\langle\psi_2|\right)$ for the individual signal and idler photons by performing partial trace operations on the two-photon state. We obtain

$$\rho_s = \sum_l S_l |l\rangle\langle l| \qquad \text{and} \qquad \rho_i = \sum_l S_{-l} |l\rangle\langle l|. \tag{3.15}$$

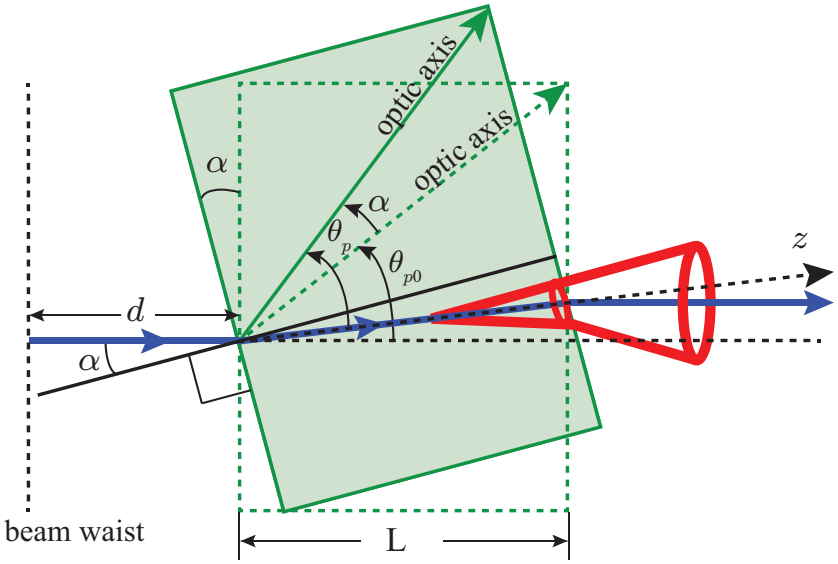

Figure 3.1: Schematic of phase matching in PDC.

For a Gaussian pump, it is known that $S_l = S_{-l}$, i.e, the angular Schmidt spectrum is symmetric [77, 92]. Thus, the OAM spectrum of the one-photon signal-idler field is identical to the angular Schmidt spectrum of the entangled two-photon state. We shall now use the single-shot technique developed in Chapter 2 to measure the angular Schmidt spectrum of entangled photons produced from type-I PDC of a Gaussian pump.

3.5.1 Modeling the experiment

Let us consider the situation shown in Figure 3.1. A Gaussian pump beam undergoes Type-I PDC inside a nonlinear crystal of thickness L. We take the pump photon to be extra-ordinary polarized and the signal and idler photons to be ordinary polarized. The beam waist of the pump field is located at a distance d behind the front surface of the crystal. The crystal is rotated by an angle α with respect to the incident direction of the pump beam, and the z-axis is defined to be the direction of the refracted pump beam inside the crystal. The angles that the optic axes of the unrotated and rotated crystals make with the pump beam inside the crystal are

denoted by θ_{p0} and θ_p, respectively. Using Figure 3.1, one can show that

$$\theta_p = \theta_{p0} + \sin^{-1}\left(\sin\alpha/\eta_p\right), \tag{3.16}$$

where η_p is the refractive index of the extraordinary pump photons. By changing θ_p, one can go from collinear to non-collinear down-conversion. Note from Equation (3.4) and Equation (3.6) that

$$\Phi(\boldsymbol{q}_s, \boldsymbol{q}_i) = A\, V(\boldsymbol{q}_s + \boldsymbol{q}_i, z = 0)\,\mathrm{sinc}\left(\frac{\Delta k_z L}{2}\right)\exp\left(i\frac{\Delta k_z L}{2}\right) \tag{3.17}$$

The spectral amplitude $V(\boldsymbol{q}_p, z = -d)$ of the pump field at the beam waist location $z = -d$ is given by

$$V(\boldsymbol{q}_p, z = -d) = C\exp\left(-\frac{|\boldsymbol{q}_p|^2 w_p^2}{4}\right), \tag{3.18}$$

where w_p is the width of the beam at the wait location. The spectral amplitude $V(\underline{\mathrm{q}}_p, z = 0)$ at the crystal location $z = 0$ is (see Appendix B. for the detailed calculation)

$$V(\boldsymbol{q}_s + \boldsymbol{q}_i, z = 0) = C\exp\left(-\frac{|\boldsymbol{q}_s + \boldsymbol{q}_i|^2 w_p^2}{4}\right)\, e^{ik_{pz}d}, \tag{3.19}$$

where C is a constant, k_p is the magnitude of the pump wavevector. We have used $\boldsymbol{q}_p = \boldsymbol{q}_s + \boldsymbol{q}_i$, which implies transverse momentum conservation in PDC.

Next, we obtain the expressions for k_{sz}, k_{iz} and k_{pz} from Ref. [132] (a sign typo in the expression for k_{pz} in Ref. [132] has been corrected here. See Ref. [135] for the detailed calculation):

$$\begin{aligned}
k_{s_z} &= \sqrt{\left(2\pi n_{so}/\lambda_s\right)^2 - |\boldsymbol{q}_s|^2}, \\
k_{i_z} &= \sqrt{\left(2\pi n_{io}/\lambda_i\right)^2 - |\boldsymbol{q}_i|^2}, \quad \text{and} \\
k_{p_z} &= -\alpha_p q_{px} + \sqrt{\left(2\pi\eta_p/\lambda_p\right)^2 - \beta_p^2 q_{px}^2 - \gamma_p^2 q_{py}^2},
\end{aligned} \tag{3.20}$$

where

$$\begin{aligned}
\eta_p &= n_{pe}\gamma_p, \\
\gamma_p &= n_{po}/\sqrt{n_{po}^2 \sin^2\theta_p + n_{pe}^2 \cos^2\theta_p}, \\
\alpha_p &= \frac{(n_{po}^2 - n_{pe}^2)\sin\theta_p \cos\theta_p}{(n_{po}^2 \sin^2\theta_p + n_{pe}^2 \cos^2\theta_p)}, \\
\text{and} \quad \beta_p &= \frac{n_{po}n_{pe}}{(n_{po}^2 \sin^2\theta_p + n_{pe}^2 \cos^2\theta_p)}.
\end{aligned} \tag{3.21}$$

Here n_{so} denotes the ordinary refractive index of the signal photon at wavelength λ_s, etc. We use the above relations to compute Δk_z. Then, we substitute Δk_z, and $V(\boldsymbol{q}_s + \boldsymbol{q}_i, z = 0)$ from Equation (3.19) into Equation (3.14) to calculate the angular Schmidt spectrum. We note that the formula in Equation (3.14) represents angular Schmidt spectrum just inside the nonlinear crystal. Nevertheless, in situations in which α is of the order of only a few degrees, the angle of refraction is small so that the angular Schmidt spectrum inside and outside the crystal can be regarded to be the same.

3.5.2 Methods

We define the measured OAM spectrum as

$$\bar{S}_l \equiv \int_{-\pi}^{\pi} \Delta\bar{I}_{\text{out}}(\phi) e^{i2l\phi} d\phi, \tag{3.22}$$

where $\Delta\bar{I}_{\text{out}}(\phi) = \bar{I}_{\text{out}}^{\delta_c}(\phi) - \bar{I}_{\text{out}}^{\delta_d}(\phi)$ is the difference in the azimuthal intensities $\bar{I}_{\text{out}}^{\delta_c}(\phi)$ and $\bar{I}_{\text{out}}^{\delta_d}(\phi)$ of the two output interferograms recorded at $\delta = \delta_c$ and $\delta = \delta_d$, respectively, and where δ denotes the overall phase difference between the two arms of the interferometer [115]. In the experimentally recorded interferograms, there could be intensity noise due to stray light exposures, imperfections in optical elements, etc. When the noise intensities in the two interferograms are the same, it has been shown that the normalized measured OAM-spectrum $\bar{S}_l$ is equal to the true normalized OAM-spectrum S_l [32, 115].

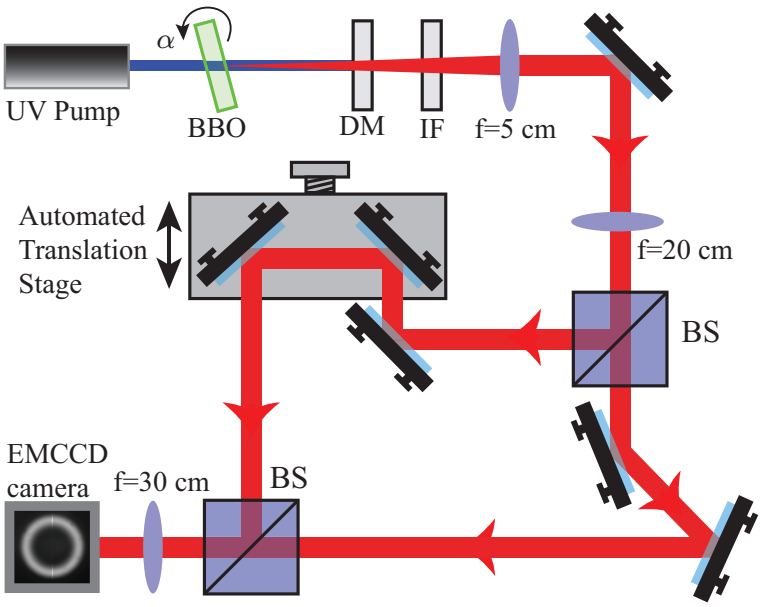

Figure 3.2: Experimental setup for measuring the angular Schmidt spectrum. BBO: β-Barium Borate crystal; DM: Dichroic mirror; IF: 10-nm wavelength-bandwidth interference filter; BS: beam splitter.

In the setup of Figure 3.2, an ultraviolet continuous-beam pump laser (100 mW) of wavelength $\lambda_p = 405$ nm and beam-waist width $w_p = 388$ μm was used to produce Type-I PDC inside a β-barium borate (BBO) crystal. The beam waist of the pump field was located at $d = 100$ cm behind the front surface of the crystal. The crystal was mounted on a goniometer which was rotated in steps of 0.04 degrees in order to change α and thereby θ_p. For a given setting of crystal and pump parameters, output interferograms and thereby the azimuthal intensities $\bar{I}^{\delta_c}_{\text{out}}(\phi)$ and $\bar{I}^{\delta_d}_{\text{out}}(\phi)$ were recorded for two values of δ, namely δ_c and δ_d, which differed by about half a wavelength [115]. The recording of the interferograms was done using an Andor Ixon Ultra EMCCD camera (512×512 pixels) with an acquisition time of 16 seconds. From a given pair of $\bar{I}^{\delta_c}_{\text{out}}(\phi)$ and $\bar{I}^{\delta_d}_{\text{out}}(\phi)$, $\Delta\bar{I}_{\text{out}}(\phi)$ was obtained and the angular Schmidt spectrum was then estimated using Equation (3.22). In our experiments, $\lambda_s = \lambda_i = 810$ nm, $\lambda_p = 405$ nm, and $L = 2$ mm. We have used the following refractive index values taken from Ref. [136]: $n_{po} = 1.6923, n_{pe} = 1.5680$ and $n_{so} = n_{io} = 1.6611$.

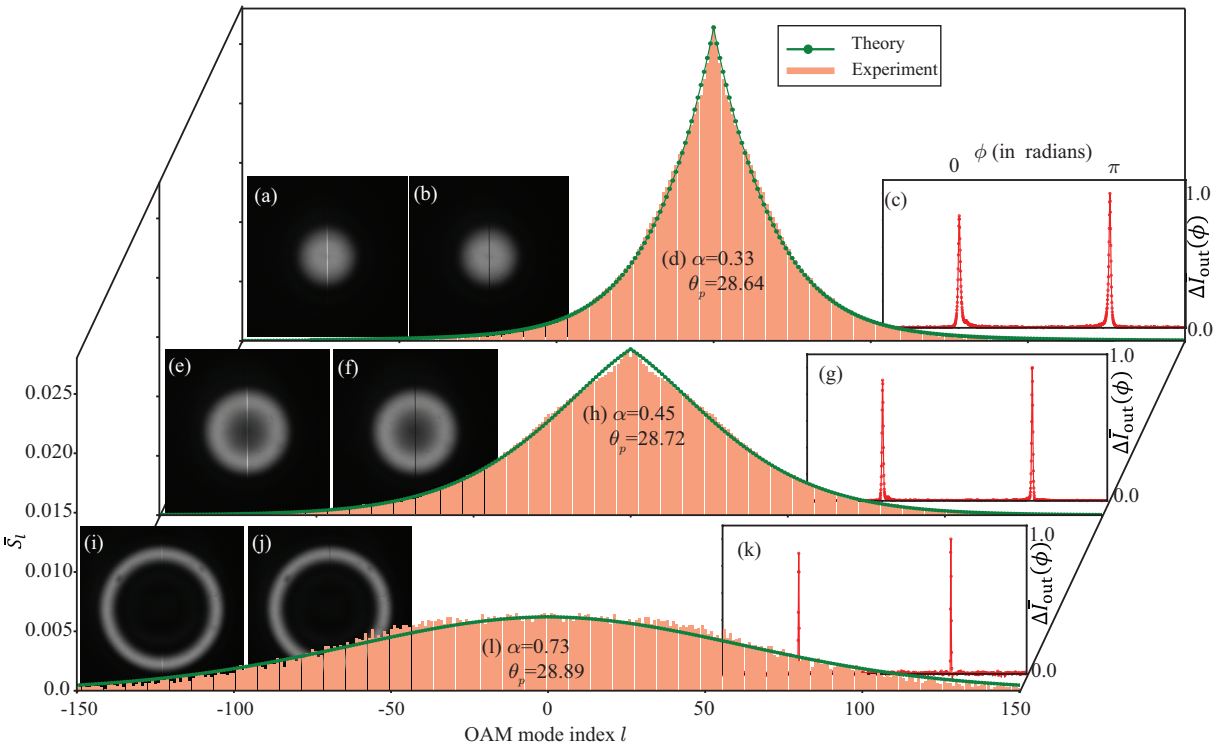

Figure 3.3: (a), (b) The measured output interferograms at $\delta = \delta_c$ and $\delta = \delta_d$, respectively, (c) the difference $\Delta\bar{I}(\phi)$ in the azimuthal intensities of the two inteferograms, (d) The normalized measured spectrum as computed using Equation (3.22) and the normalized theoretical spectrum as calculated using Equation (3.13), for $\alpha = 0.33$ and θ_p =28.64. (e), (f), (g), (h) are the corresponding plots for $\alpha = 0.45$ and θ_p =28.72. (i), (j), (k), (l) are the corresponding plots for $\alpha = 0.73$ and θ_p =28.89.

3.5.3 Experimental observations

Figure 3.3 shows the details of our measurements for three different values of θ_p. For each θ_p, we have plotted the measured output interferograms at $\delta = \delta_c$ and $\delta = \delta_d$, the difference azimuthal intensity $\Delta\bar{I}_{\text{out}}(\phi)$ along with the normalized spectrum as computed using Equation (3.22) and the normalized theoretical spectrum as calculated using Equation (3.14). The angular Schmidt number was calculated using the formula $K_a = 1/\left(\sum_l \bar{S}_l^2\right)$. The experimentally measured angular Schmidt numbers along with the theoretical predictions at various θ_p values have been plotted in Figure 3.4. We note that for our theoretical plots, θ_{p0} was the only fitting parameter, and once it was chosen, the subsequent θ_p values were calculated simply by substituting the rotation angle α in Equation (3.16). We find that the angular

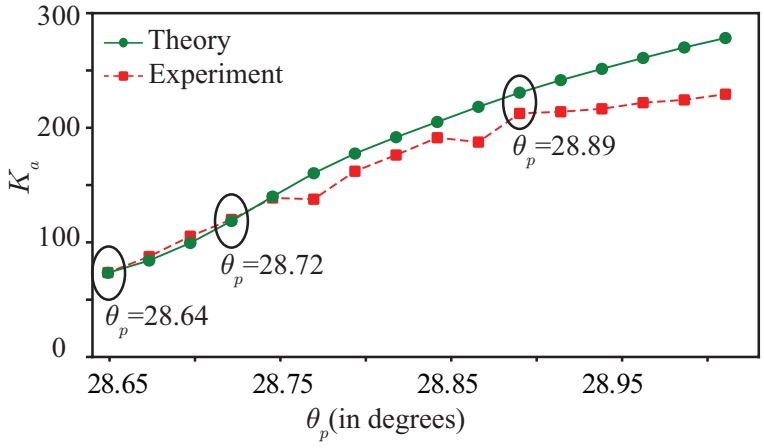

Figure 3.4: (color online) Experimentally measured and theoretically estimated angular Schmidt number K_a versus θ_p.

Schmidt spectrum becomes broader with increasing non-collinearity. We measured very broad angular Schmidt spectra with the corresponding Schmidt numbers up to 229, which to the best of our knowledge is the highest ever reported angular Schmidt number. We find excellent agreement between the theory and experiment, except for extremely non-collinear conditions, in which case the experimentally measured Schmidt numbers are slightly lower than the theoretical predictions. The main reason for this discrepancy is the limited resolution of our EMCCD camera. In order to generate the azimuthal intensity plots, we use a narrow angular region of interest (ROI) [115], the minimum possible size of which is fixed by the pixel size of the EMCCD camera. In the case of non-collinear down-conversion, the intensities in the interferograms are concentrated at regions away from the center. Therefore, the corresponding $\Delta\bar{I}_{\text{out}}(\phi)$ plots have lesser angular resolution and thus they get estimated to be wider than their true widths. This results in a progressively lower estimate of the Schmidt numbers with increasing non-collinearity.

3.5.4 Some numerical predictions

We use Equation (3.14) for studying how w_p and L affect the angular Schmidt number K_a. Figure 3.5(a) shows the theoretical dependence of K_a on w_p for fixed L, θ_p and d. Figure 3.5(b) shows the theoretical dependence of K_a on L for fixed

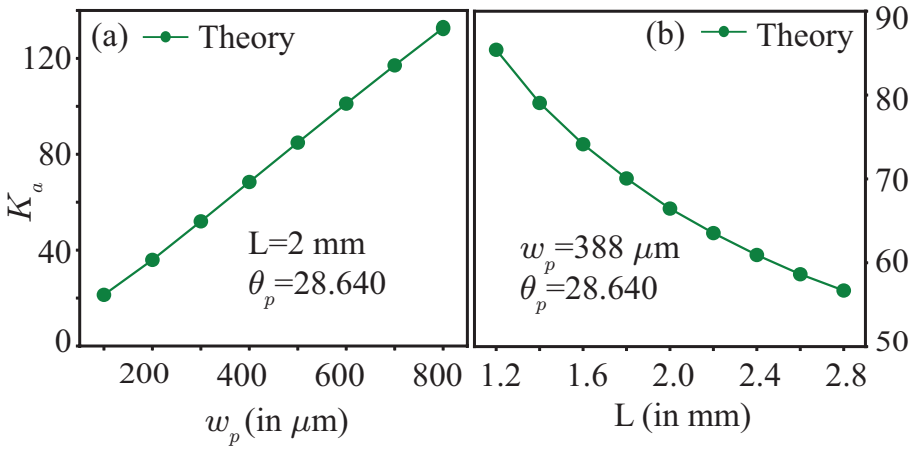

Figure 3.5: (color online) (a) and (b) Theoretical dependence of the angular Schmidt number on the width of the pump beam waist w_p and crystal thickness L, respectively.

w_p, θ_p, and d. We find that K_a increases as a function of w_p, while it decreases as a function of L. Thus, in addition to θ_p, it is also possible to vary w_p and L in order to tune the angular Schmidt spectrum of the two-photon state from PDC.

3.6 Summary

In summary, we have derived in this chapter an exact formula for the angular Schmidt spectrum of OAM-entangled photons produced by PDC. We have shown that our formula yields the true theoretical spectrum without any convergence issue as has been the case with the previously derived formulas. Furthermore, we have used our theoretical formulation to experimentally characterize the angular Schmidt spectrum for non-collinear phase matching in PDC. The results reported in this chapter can be very relevant for the ongoing intensive research efforts towards harnessing high-dimensional OAM entanglement for quantum information applications [137, 96].

Chapter 4

Polarization correlations in parametric down-conversion

4.1 Introduction

The wave-particle duality, that is, the simultaneous manifestation of both particle and wave behavior, is among the most characteristic features of a quantum system. There are many processes in which a quantum system gets annihilated to produce a new quantum system consisting of either equal or a higher number of particles. An example is the nonlinear optical process of parametric down-conversion (PDC), in which an input pump photon gets annihilated to produce two entangled photons called the signal and idler photons [138]. Another example is the four-wave mixing process, in which two input pump photons get annihilated to produce two new photons [21]. In such processes, it is known that physical quantities such as energy, momentum, and angular momentum are conserved [138, 36]. However, it is not very well understood how in such processes the intrinsic correlations that constitute the coherence of the annihilated quantum system get transferred to the generated new quantum system.

One of the main difficulties in addressing questions related to the transfer of correlations is the lack of a well-established basis-invariant measure for quantifying

the intrinsic correlations in multi-dimensional systems in terms of a single scalar quantity [1]. For a one-particle quantum system with a two-dimensional Hilbert space, the coherence of the system can be completely specified. For example, the coherence of the two-dimensional polarization state of a one-photon system can be quantified in terms of the degree of polarization [139, 3]. Two-photon systems have a four-dimensional Hilbert space in the polarization degree of freedom and are described by two-qubit states [33]. In the last several years much effort has gone into quantifying the entanglement of the two-qubit states [17, 140, 141, 142, 89, 143, 18, 144], and among the available entanglement quantifiers, Wootters's concurrence [143, 18] is the most widely used one.

In the context of signal-idler photons produced by PDC, the two-qubit polarization-entangled states have been extensively studied [33, 34, 145] and are now seen to hold a lot of promise for practical quantum-information protocols [146, 147]. However, to the best of our knowledge, the correlations in the down-converted polarization-entangled states have not been studied from the perspective of how these correlations are dictated by the polarization correlations in the pump field. In degrees of freedom other than polarization, some aspects of how one-photon pump correlations transfer to two-photon signal-idler correlations have previously been investigated [28, 30, 31, 26, 148]. In particular, Ref. [30] studied correlation transfer in PDC in the spatial degree of freedom. Although the spatial degree of freedom provides an infinite dimensional basis, correlations in Ref. [30] were quantified in restricted two-dimensional subspaces only. More specifically, the spatial correlations in the pump field were quantified in terms of a spatial two-point correlation function; and for quantifying spatial correlations of the signal and idler fields, spatial two-qubit states with only two non-zero diagonal elements were considered. It was then shown that the maximum achievable concurrence of spatial two-qubit states is bounded by the degree of spatial correlations of the pump field. In this chapter, we study

[1] This problem was addressed subsequent to the work of this chapter by Ref.[86], which establishes a basis-invariant measure of coherence for finite-dimensional systems. In Chapter 6. of this thesis, we generalize the measure of Ref.[86] to quantify the intrinsic coherence of infinite-dimensional systems

correlation transfer from one-photon to two-photon systems, not in any restricted subspace, but in the complete space of the polarization degree of freedom. We quantify intrinsic one-photon correlations in terms of the degree of polarization and the two-photon correlations in terms of concurrence.

The contents of the chapter, which appear almost verbatim from Ref. [149], are organized as follows. In Section 4.2, we present a brief description of the degree of polarization, which will be used to quantify the intrinsic polarization correlations or coherence of the pump photon in a basis-invariant manner. In Section 4.3, we briefly describe the prescription to compute Wootters' concurrence, a well-accepted measure of entanglement for arbitrary two-qubit states. In Section 4.4, we present the most general bound on the concurrence of two-qubit polarization entangled states produced from PDC in terms of the degree of polarization of the pump. Subsequently, in Section 4.5 we discuss the corresponding bound for two-qubit states signal-idler that have only two non-zero diagonal elements in the computational basis. In Sec. 4.6, we discuss an example experimental setup in which a wide variety of two-qubit states can be produced. By numerically varying different tunable parameter of the setup, we simulate a large number of two-qubit states, calculate the corresponding concurrences and illustrate how the bounds derived in Section 4.4 and Section 4.5 are obeyed. In Section 4.7 we present the conclusions of the chapter.

4.2 Degree of polarization of the pump photon

We begin by noting that the state of a normalized quasi-monochromatic pump field may be described by a 2×2 density matrix [3] given by

$$J = \begin{bmatrix} \langle E_H E_H^* \rangle & \langle E_H E_V^* \rangle \\ \langle E_H^* E_V \rangle & \langle E_V E_V^* \rangle \end{bmatrix}, \tag{4.1}$$

which is referred to as the 'polarization matrix.' The complex random variables E_H and E_V denote the horizontal and vertical components of the electric field, respec-

tively, and $\langle \cdots \rangle$ denotes an ensemble average. By virtue of a general property of 2×2 density matrices, J has a decomposition of the form,

$$J = P\,|\psi_{\rm pol}\rangle\langle\psi_{\rm pol}| + (1-P)\,\bar{\mathbb{1}}, \tag{4.2}$$

where $|\psi_{\rm pol}\rangle$ is a pure state representing a completely polarized field, and $\bar{\mathbb{1}}$ denotes the normalized 2×2 identity matrix representing a completely unpolarized field [3]. This means that any arbitrary field can be treated as a unique weighted mixture of a completely polarized part and a completely unpolarized part. The fraction P corresponding to the completely polarized part is called the degree of polarization and is a basis-invariant measure of polarization correlations in the field. If we denote the eigenvalues of J as ϵ_1 and ϵ_2, then it follows that $P = |\epsilon_1 - \epsilon_2|$ [3]. Furthermore, the eigenvalues are connected to P as $\epsilon_1 = (1+P)/2$ and $\epsilon_2 = (1-P)/2$.

4.3 Concurrence of the signal-idler photons

Concurrence is a measure of entanglement formulated by Wootters for quantifying the entanglement of general two-qubit states [18]. While the concurrence does not have any definite operational or physical interpretation, it is a well-accepted measure of entanglement for two-qubit states. For a general two-qubit state ρ, the concurrence is computed as

$$C(\rho) = \max\{0, \sqrt{\kappa_1} - \sqrt{\kappa_2} - \sqrt{\kappa_3} - \sqrt{\kappa_4}\}, \tag{4.3}$$

where κ_i's are the eigenvalues of the state ζ defined as

$$\zeta = \rho(\sigma_y \otimes \sigma_y)\rho^*(\sigma_y \otimes \sigma_y). \tag{4.4}$$

Here σ_y is the usual Pauli operator, and ρ^* is the complex conjugate of ρ. For a general ρ, we have $0 \leq C(\rho) \leq 1$. If ρ is a maximally entangled state, then $C(\rho) = 1$, whereas if ρ is a separable state then $C(\rho) = 0$. Our aim is to quantify the upper

limit on the concurrence of the two-qubit signal-idler states in terms of the degree of polarization P of the pump photon.

4.4 General upper bound

We now investigate the PDC-based generation of polarization entangled two-qubit signal-idler states ρ from a quasi-monochromatic pump field J (see Figure 4.1). The nonlinear optical process of PDC is a very low-efficiency process [21]. Most of the pump photons do not get down-converted and just pass through the nonlinear medium. Only a very few pump photons do get down-converted, and in our description, only these photons constitute the ensemble containing the pump photons. We further assume that the probabilities of the higher-order down-conversion processes are negligibly small so that we do not have in our description the down-converted state containing more than two photons. With these assumptions, we represent the state of the down-converted signal and idler photons by a 4×4, two-qubit density matrix in the polarization basis $\{|H\rangle_s|H\rangle_i, |H\rangle_s|V\rangle_i, |V\rangle_s|H\rangle_i, |V\rangle_s|V\rangle_i\}$. In what follows, we will be applying some results from the theory of majorization [150] in order to study the propagation of correlations from the 2×2 pump density matrix J to the 4×4 two-qubit density matrix ρ. This requires us to equalize the dimensionalities of the pump and the two-qubit states. We therefore represent the pump field by a 4×4 matrix σ, where

$$\sigma \equiv \begin{pmatrix} 1 & 0 \\ & \\ 0 & 0 \end{pmatrix} \otimes J. \tag{4.5}$$

We denote the eigenvalues of σ in non-ascending order as $\{\epsilon_1, \epsilon_2, \epsilon_3, \epsilon_4) \equiv ((1+P)/2$ $, (1-P)/2, 0, 0\}$ and the eigenvalues of ρ in non-ascending order as $\{\lambda_1, \lambda_2, \lambda_3, \lambda_4\}$.

Let us represent the two-qubit generation process $\sigma \to \rho$ by a completely positive map $\mathcal{E}$ (see Figure 4.1) such that $\rho = \mathcal{E}(\sigma) = \sum_i M_i \sigma M_i^\dagger$, where M_i's are the Sudarshan-Kraus operators for the process [16, 151, 152, 153]. We restrict our

analysis only to maps that satisfy the following two conditions for all σ: (i) No part of the system can be discarded, that is, there must be no postselection. This means that the map must be trace-preserving, which leads to the condition that $\sum_i M_i^\dagger M_i = \mathbb{1}$; (ii) Coherence may be lost to, but not gained from degrees of freedom external to the system. In other words, the von Neumann entropy cannot decrease. This condition holds if and only if the map is unital, that is, $\sum_i M_i M_i^\dagger = \mathbb{1}$. The above two conditions together imply that the process $\sigma \to \rho$ is doubly-stochastic [154]. The characteristic implication of double-stochasticity is that the two-qubit state is majorized by the pump state, that is $\rho \prec \sigma$. This means that the eigenvalues of ρ and σ satisfy the following relations:

$$\lambda_1 \leq \epsilon_1, \tag{4.6a}$$

$$\lambda_1 + \lambda_2 \leq \epsilon_1 + \epsilon_2, \tag{4.6b}$$

$$\lambda_1 + \lambda_2 + \lambda_3 \leq \epsilon_1 + \epsilon_2 + \epsilon_3, \tag{4.6c}$$

$$\lambda_1 + \lambda_2 + \lambda_3 + \lambda_4 = \epsilon_1 + \epsilon_2 + \epsilon_3 + \epsilon_4. \tag{4.6d}$$

We must note that condition (i) may seem not satisfied in some of the experimental schemes for producing polarization entangled two-qubit states. For example, in the scheme for producing a polarization Bell state using Type-II phase-matching [33], only one of the polarization components of the pump photon is allowed to engage in the down-conversion process; the other polarization component, even if present, simply gets discarded away. Nevertheless, our formalism is valid even for such two-qubit generation schemes. In such schemes, the state σ represents that part of the pump field which undergoes the down-conversion process so that condition (i) is satisfied.

Now, for a general realization of the process $\sigma \to \rho$, the generated density matrix ρ can be thought of as arising from a process $\mathcal{N}$, that can have a non-unitary part, followed by a unitary-only process $\mathcal{U}$, as depicted in Figure 4.1. This means that we have $\sigma \to \chi \equiv \mathcal{N}(\sigma) \to \rho \equiv \mathcal{U}(\chi)$. The process $\mathcal{N}$ generates the two-

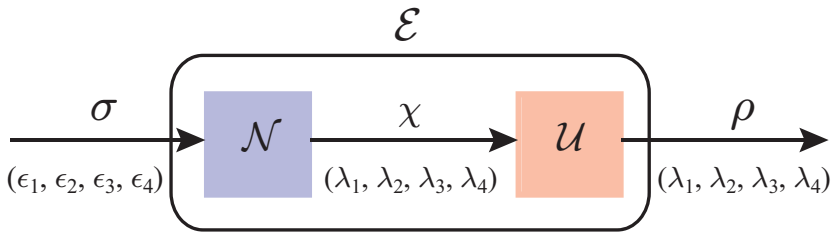

Figure 4.1: Modelling the generation of two-qubit states ρ from σ through a doubly stochastic process.

qubit state χ with eigenvalues $\{\lambda_1, \lambda_2, \lambda_3, \lambda_4\}$ which are different from the eigenvalues $\{\epsilon_1, \epsilon_2, \epsilon_3, \epsilon_4\}$ of σ, except when $\mathcal{N}$ consists of unitary-only transformations, in which case the eigenvalues of χ remain the same as those of σ. The unitary part $\mathcal{U}$ transforms the two-qubit state χ to the final two-qubit state ρ. This action does not change the eigenvalues but can change the concurrence of the two-qubit state. The majorization relations of Equation (4.6) dictate how the two sets of eigenvalues are related and thus quantify the effects due to $\mathcal{N}$. We quantify the effects due to $\mathcal{U}$ by using the result from Refs. [155, 156, 89] for the maximum concurrence achievable by a two-qubit state under unitary transformations. According to this result, for a two-qubit state ρ with eigenvalues in non-ascending order denoted as $\lambda_1, \lambda_2, \lambda_3, \lambda_4$, the concurrence $C(\rho)$ obeys the inequality:

$$C(\rho) \leq \max\{0, \lambda_1 - \lambda_3 - 2\sqrt{\lambda_2 \lambda_4}\}; \tag{4.7}$$

the bound is saturable in the sense that there always exists a unitary transformation $\mathcal{U}(\chi) = \rho$ for which the equality holds true [156]. Now, from Equation (4.7), we clearly have $C(\rho) \leq \lambda_1$. And, from the majorization relation of Equation (4.6a), we find that $\lambda_1 \leq \epsilon_1 = (1 + P)/2$. Therefore, for a general doubly-stochastic process $\mathcal{E}$, we arrive at the inequality:

$$C(\rho) \leq \frac{1 + P}{2}. \tag{4.8}$$

We stress that this bound is tight, in the sense that there always exists a pair of $\mathcal{N}$ and $\mathcal{U}$ for which the equality in the above equation holds true. In fact, the saturation of Equation (4.8) is achieved when $\mathcal{N}$ consists of unitary-only process and when $\mathcal{U}$

is such that it yields the maximum concurrence for ρ as allowed by Equation (4.7). This can be verified, first, by noting that when $\mathcal{N}$ is unitary the process $\chi = \mathcal{N}(\sigma)$ preserves the eigenvalues to yield $(\lambda_1, \lambda_2, \lambda_3, \lambda_4) = ((1+P)/2, (1-P)/2, 0, 0)$, and second, by substituting these eigenvalues in Equation (4.7) which then yields $(1+P)/2$ as the maximum achievable concurrence. Equation (4.8) is the central result of this chapter which clearly states that the intrinsic polarization correlations of the pump field in PDC predetermine the maximum entanglement that can be achieved by the generated two-qubit signal-idler states. We note that while Equation (4.8) has been derived keeping in mind the physical context of parametric down-conversion, the derivation does not make any specific reference to the PDC process or to any explicit details of the two-qubit generation scheme. As a result, Equation (4.8) is also applicable to processes other than PDC that would produce a two-qubit state from a single source qubit state via a doubly stochastic process.

4.5 Restricted bound for 2D states

We now recall that our present work is directly motivated by previous studies in the spatial degree of freedom for two-qubit states with only two nonzero diagonal entries in the computational basis [30]. Therefore, we next consider this special class of two-qubit states in the polarization degree of freedom. We refer to such states as '2D states' in this chapter and represent the corresponding density matrix as $\rho^{(2D)}$. Since such states can only have two nonzero eigenvalues, the majorization relations of Equation (4.6) reduce to: $\lambda_1 \leq \epsilon_1$ and $\lambda_1 + \lambda_2 = \epsilon_1 + \epsilon_2 = 1$. Owing to its 2×2 structure, the state $\rho^{(2D)}$ has a decomposition of the form [3],

$$\rho^{(2D)} = \tilde{P}|\psi^{(2D)}\rangle\langle\psi^{(2D)}| + (1-\tilde{P})\bar{\mathbb{1}}^{(2D)}, \tag{4.9}$$

where $|\psi^{(2D)}\rangle$ is a pure state and $\bar{\mathbb{1}}^{(2D)}$ is a normalized 2×2 identity matrix. As in Equation (4.2), the pure state weightage $\tilde{P}$ can be shown to be related to the eigenvalues as $\tilde{P} = \lambda_1 - \lambda_2$. It is known that the concurrence is a convex function

on the space of density matrices [18], that is, $C(\sum_i p_i\rho_i) \leq \sum_i p_i C(\rho_i)$, where $0 \leq p_i \leq 1$ and $\sum_i p_i = 1$. Applying this property to Equation (4.9) along with the fact that $C(\bar{\mathbb{1}}^{(2D)}) = 0$, we obtain that the concurrence $C(\rho^{(2D)})$ of a 2D state satisfies $C(\rho^{(2D)}) \leq \tilde{P}$. Now since $\tilde{P} = \lambda_1 - \lambda_2 = 2\lambda_1 - 1$, and $\lambda_1 \leq \epsilon_1$, we get $\tilde{P} \leq 2\epsilon_1 - 1 = \epsilon_1 - \epsilon_2 = P$, or $\tilde{P} \leq P$. We therefore arrive at the inequality,

$$C(\rho^{(2D)}) \leq P. \tag{4.10}$$

Thus, for 2D states the upper bound on concurrence is the degree of polarization itself. This particular result is in exact analogy with the result shown previously for 2D states in the spatial degree of freedom that the maximum achievable concurrence is bounded by the degree of spatial correlations of the pump field itself [30].

Our entire analysis leading upto Equation (4.8) and Equation (4.10) describes the transfer of one-particle correlations, as quantified by P, to two-particle correlations and their eventual manifestation as entanglement, as quantified by concurrence. For 2D states, which have a restricted Hilbert space available to them, the maximum concurrence that can get manifested is P. Thus, restricting the Hilbert space appears to restrict the degree to which pump correlations can manifest as the entanglement of the generated two-qubit state. However, when there are no restrictions on the available Hilbert space, the maximum concurrence that can get manifested is $(1+P)/2$. This leads to the somewhat non-intuitive consequence that even an unpolarized pump field ($P = 0$) can produce two-qubit states with non-zero concurrence (upto $C(\rho) = 0.5$). This is attributed to the fact that the one-particle correlations of the pump field are allowed to manifest in the full unrestricted Hilbert space of the two-particle state of the signal-idler photons. We note that our general result as derived in Equation (4.8) remains applicable even in situations where the entanglement in a generated two-qubit state is transferred to another two-qubit state [157, 158, 159, 160] or where a two-qubit state is made to go through a turbulent atmosphere [161]. As long as the trace-preserving and entropy non-decreasing conditions are satisfied the upper bound on entanglement in such transfers still remain

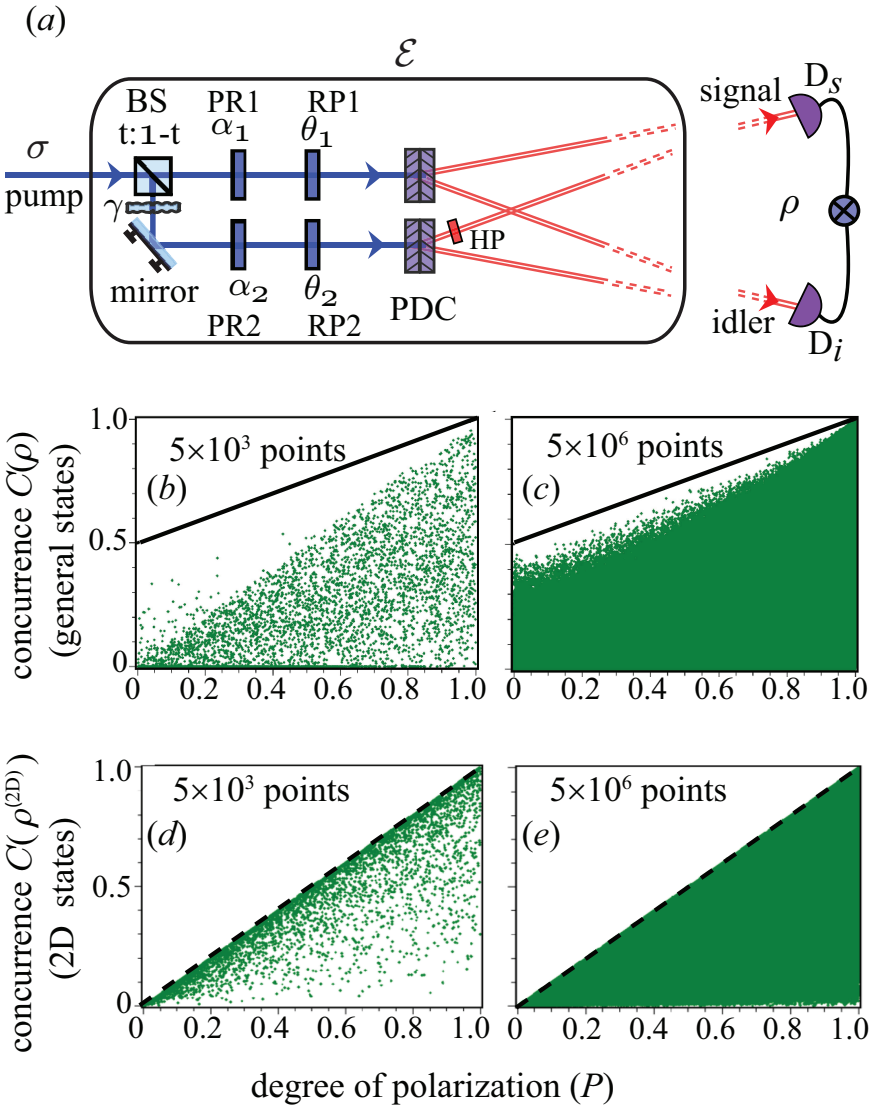

Figure 4.2: (a) An example experimental scheme for producing a wide range of two-qubit states. BS: beam-splitter, PR: phase retarder, RP: rotation plate, HP: half-wave plate; D_s and D_i are photon detectors in a coincidence-counting setup. (b) and (c) are the scatter plots of concurrences of states numerically generated by randomly varying all the tunable parameters. (d) and (e) are the scatter plots of concurrence of 2D states, numerically generated by keeping $t = 1$ and varying all the remaining tunable parameters.

dictated by Equation (4.8).

4.6 An illustrative experimental scheme

We now illustrate the bounds derived in this chapter in an example experimental scheme. The scheme shown in Figure 4.2(a) can produce a wide range of two-qubit states in a doubly-stochastic manner. A pump field with the degree of polarization

P is split into two arms by a non-polarizing beam-splitter (BS) with splitting ratio $t : 1-t$. We represent the horizontal and vertical polarization components of the field hitting the PDC crystals in arm (1) as E_{H1} and E_{V1}, respectively. The phase retarder (PR1) introduces a phase difference α_1 between E_{H1} and E_{V1}. The rotation plate (RP1) rotates the polarization vector by angle θ_1. The corresponding quantities in arm (2) have similar representations. The stochastic variable γ introduces a decoherence between the pump fields in the two arms. Its action is described as $\langle e^{i\gamma}\rangle = \mu\, e^{i\gamma_0}$, where $\langle\cdots\rangle$ represents the ensemble average, μ is the degree of coherence and γ_0 is the mean value of γ [3]. The entangled photons in each arm are produced using type-I PDC in a two-crystal geometry [34]. The purpose of the half-wave plate (HP) is to convert the two-photon state vectors $|H\rangle_s|H\rangle_i$ and $|V\rangle_s|V\rangle_i$, into $|V\rangle_s|H\rangle_i$ and $|H\rangle_s|V\rangle_i$, respectively. Therefore, a typical realization $|\psi_\gamma\rangle$ of the two-qubit state in the ensemble detected at D_s and D_i can be represented as $|\psi_\gamma\rangle = E_{V1}|H\rangle_s|H\rangle_i + E_{H1}|V\rangle_s|V\rangle_i + e^{i\gamma}\,(E_{V2}|H\rangle_s|V\rangle_i + E_{H2}|V\rangle_s|H\rangle_i)$. The two-qubit density matrix is then $\rho = \langle|\psi_\gamma\rangle\langle\psi_\gamma|\rangle =$

$$\begin{bmatrix} \langle E_{V1}E_{V1}^*\rangle & \langle E_{V1}E_{V2}^*e^{-i\gamma}\rangle & \langle E_{V1}E_{H2}^*e^{-i\gamma}\rangle & \langle E_{V1}E_{H1}^*\rangle \\ \langle E_{V2}E_{V1}^*e^{i\gamma}\rangle & \langle E_{V2}E_{V2}^*\rangle & \langle E_{V2}E_{H2}^*\rangle & \langle E_{V2}E_{H1}^*e^{i\gamma}\rangle \\ \langle E_{H2}E_{V1}^*e^{i\gamma}\rangle & \langle E_{H2}E_{V2}^*\rangle & \langle E_{H2}E_{H2}^*\rangle & \langle E_{H2}E_{H1}^*e^{i\gamma}\rangle \\ \langle E_{H1}E_{V1}^*\rangle & \langle E_{H1}E_{V2}^*e^{-i\gamma}\rangle & \langle E_{H1}E_{H2}^*e^{-i\gamma}\rangle & \langle E_{H1}E_{H1}^*\rangle \end{bmatrix}.$$

For calculating the matrix elements of ρ, we represent the polarization vector of the pump field before the BS as $(E_H, E_V)^T$ and thus write E_{H1} and E_{V1} as

$$\begin{bmatrix} E_{H1} \\ E_{V1} \end{bmatrix} = \eta_1 \begin{bmatrix} \cos\theta_1 & \sin\theta_1 \\ -\sin\theta_1 & \cos\theta_1 \end{bmatrix} \begin{bmatrix} 1 & 0 \\ 0 & e^{i\alpha_1} \end{bmatrix} \begin{bmatrix} E_H \\ E_V \end{bmatrix}, \tag{4.11}$$

where $\eta_1 = \sqrt{t}$, and the two matrices represent the transformations by PR1 and RP1. E_{H2} and E_{V2} are calculated in a similar manner, with the corresponding quantity $\eta_2 = \sqrt{1-t}\; e^{i\gamma}$. Without the loss of generality, we assume $\langle E_H^* E_H\rangle =$

$\langle E_V^* E_V\rangle = 1/2$ and $\langle E_H^* E_V\rangle = P/2$, and calculate the matrix elements to be

$$
\begin{aligned}
\langle E_{V1(2)} E^*_{V1(2)}\rangle &= |\eta_{1(2)}|^2\big(1 - P\cos\alpha_{1(2)}\sin 2\theta_{1(2)}\big)/2,\\
E_{H1(2)} E^*_{H1(2)}\rangle &= |\eta_{1(2)}|^2\big(1 + P\cos\alpha_{1(2)}\sin 2\theta_{1(2)}\big)/2,\\
\langle E_{V1(2)} E^*_{H1(2)}\rangle &= |\eta_{1(2)}|^2\, P\big(\cos\alpha_{1(2)}\cos 2\theta_{1(2)} + i\sin\alpha_{1(2)}\big)/2,\\
\langle E_{V1} E^*_{V2} e^{-i\gamma}\rangle &= \mu|\eta_1\eta_2|\big(\sin\theta_1\sin\theta_2 + \cos\theta_1\cos\theta_2 e^{i(\alpha_1-\alpha_2)}\\
&\quad - P\cos\theta_1\sin\theta_2 e^{i\alpha_1} - P\sin\theta_1\cos\theta_2 e^{-i\alpha_2}\big)e^{-i\gamma_0}/2,\\
\langle E_{V1} E^*_{H2} e^{-i\gamma}\rangle &= \mu|\eta_1\eta_2|\big(-\sin\theta_1\cos\theta_2 + \cos\theta_1\sin\theta_2 e^{i(\alpha_1-\alpha_2)}\\
&\quad + P\cos\theta_1\cos\theta_2 e^{i\alpha_1} - P\sin\theta_1\sin\theta_2 e^{-i\alpha_2}\big)e^{-i\gamma_0}/2,\\
\langle E_{V2} E^*_{H1} e^{i\gamma}\rangle &= \mu|\eta_1\eta_2|\big(-\cos\theta_1\sin\theta_2 + \sin\theta_1\cos\theta_2 e^{-i(\alpha_1-\alpha_2)}\\
&\quad - P\sin\theta_1\sin\theta_2 e^{-i\alpha_1} + P\cos\theta_1\cos\theta_2 e^{i\alpha_2}\big)e^{i\gamma_0}/2,\\
\langle E_{H2} E^*_{H1} e^{i\gamma}\rangle &= \mu|\eta_1\eta_2|\big(\cos\theta_1\cos\theta_2 + \sin\theta_1\sin\theta_2 e^{-i(\alpha_1-\alpha_2)}\\
&\quad + P\sin\theta_1\cos\theta_2 e^{-i\alpha_1} + P\cos\theta_1\sin\theta_2 e^{i\alpha_2}\big)e^{i\gamma_0}/2.
\end{aligned}
$$

Here, $t, \alpha_1, \alpha_2, \theta_1, \theta_2,\ \mu$, and γ_0 are the tunable parameters. We numerically vary these parameters with a uniform random sampling and simulate a large number of two-qubit states. Figure 4.2(b) and Figure 4.2(c) are the scatter plots of concurrences of 5×10^3 and 5×10^6 two-qubit states, respectively, numerically generated by varying all the tunable parameters. Figure 4.2(d) and Figure 4.2(e) are the scatter plots of concurrence of 5×10^3 and 5×10^6 2D states, respectively, numerically generated by keeping $t = 1$ and varying all the remaining tunable parameters. The solid black lines are the general upper bound $C(\rho) = (1 + P)/2$ and the dashed black lines are the upper bound $C(\rho) = P$ for 2D states. The unfilled gaps in the scatter plots can be filled in either by sampling more data points or by adopting a different sampling strategy. To this end, we note that one possible setting for which the general upper bound $C(\rho) = (1 + P)/2$ can be achieved for any value of P is: $t = 0.5, \theta_1 = -\pi/4, \theta_2 = 0, \alpha_1 = \pi/2, \alpha_2 = \pi, \mu = 1$ and $\gamma_0 = 0$. Thus, even an unpolarized pump field ($P = 0$) can be made to produce two-qubit signal-idler

states with non-zero entanglement (upto $C(\rho) = 0.5$) by a suitable choice of the tunable parameters. This is due to the fact that the setup is capable of producing a wide variety of two-qubit states, which in general, reside in the full unrestricted four-dimensional Hilbert space.

4.7 Summary

In summary, we have investigated how one-particle correlations transfer to manifest as two-particle correlations in the physical context of PDC. We have shown that if the generation process is trace-preserving and entropy-nondecreasing, the concurrence $C(\rho)$ of the generated two-qubit state ρ follows an intrinsic upper bound with $C(\rho) \leq (1+P)/2$, where P is the degree of polarization of the pump photon. For the special class of two-qubit states $\rho^{(2D)}$ that is restricted to have only two nonzero diagonal elements, the upper bound on concurrence is the degree of polarization itself, that is, $C(\rho^{(2D)}) \leq P$. The surplus of $(1+P)/2-P = (1-P)/2$ in the maximum achievable concurrence for arbitrary two-qubit states can be attributed to the availability of the entire 4×4 computational space, as opposed to 2D states which only have a 2×2 computational block available to them.

We note that the polarization correlations of a pump field do not impose serious limitations on the degree of entanglement of the signal and idler photons, insofar as its practical achievability in realistic experiments is concerned. The main motivation behind this study is from the fundamental perspective of understanding how one-particle correlations transfer to manifest as two-particle correlations. The results derived in this chapter can have two important implications. The first one is towards exploring whether correlations too follow a quantifiable conservation principle just as physical observables such as energy and momentum do. The second one could be towards deducing the upper bound on the correlations in a generated high-dimensional quantum system, purely from the knowledge of the correlations in the source. In light of the recent experiment on generation of three-photon entangled states from a single source photon [162], this formalism may prove useful in deter-

mining upper bounds on the entanglement of such multipartite systems, for which no well-accepted measure exists. We believe that this approach based on intrinsic source correlations could complement the existing information-theoretic approaches [17, 140, 141, 142, 89, 143, 18, 144] towards quantifying entanglement.

Chapter 5

Temporal correlations in parametric down-conversion

5.1 Introduction

Coherence and entanglement are intimately related concepts. The recent attempts at developing a resource-based theory of coherence also reveal such relations [163, 164, 165, 166]. One of the physical processes in which the relations between coherence and entanglement can be systematically explored is parametric down-conversion (PDC)—a nonlinear optical process in which a pump photon interacts with a nonlinear crystal to produce a pair of entangled photons, termed as signal and idler [138]. Using the PDC photons, coherence and entanglement effects have been observed in several degrees of freedom including polarization [167], time-energy [41, 168, 169, 170, 28, 42, 171, 172, 35, 173], position and momentum [27, 174, 30], and orbital angular momentum (OAM) [175, 31, 37, 32].

There have been several studies on how coherence and entanglement properties of the down-converted field are affected by different PDC setting and pump field parameters [22, 23, 26, 176, 177, 27, 178]. However, regarding how the intrinsic correlations of the pump field get transferred to manifest as two-photon coherence and entanglement, there have been efforts mostly in the polarization and spatial

degrees of freedom [26, 179, 30, 149]. In the spatial degree of freedom, a general spatially partially coherent field was considered and it was shown that the spatial coherence properties of the pump field get entirely transferred to that of the down-converted two-photon field [30]. However, in the temporal degree of freedom, the effects due to the temporal correlations of the pump field have only been studied in two limiting situations: one, in which the constituent frequency components are completely correlated (fully-coherent pulsed field) [24, 25, 35, 180, 181] and the other, in which the constituent frequency components are completely uncorrelated (continuous-wave field) [41, 168, 169, 170, 28, 42, 171, 172, 134, 182, 183, 184, 185]. In this chapter, we study the coherence transfer in PDC for a general temporally partially coherent pump field and explicitly quantify this correlation transfer for the special case of a partially coherent Gaussian Schell-model field [186], in which the correlations between the constituent frequency components have a Gaussian distribution.

The contents of this chapter, which appear almost verbatim from Ref. [187], are organized as follows. In Section 5.2, we describe a general model of two-photon interference in terms of two time parameters. In Section 5.4, we show that the temporal coherence properties of a general pump get entirely transferred to the down-converted two-photon field. Specifically, we derive the two-photon temporal coherence functions for both infinitely-fast and time-averaged detection schemes and show that in each scheme the coherence function factorizes into two separate coherence functions with one of them carrying the entire statistical information of the pump field. In Section 5.5, we derive the explicit form of the two-photon coherence function for a Gaussian-Schell pump field. In Section 5.6, we show that the entanglement of time-energy entangled two-qubit states is bounded by the degree of temporal coherence of the partially coherent pump field. Finally, in Section 5.7 we present the conclusions of our study.

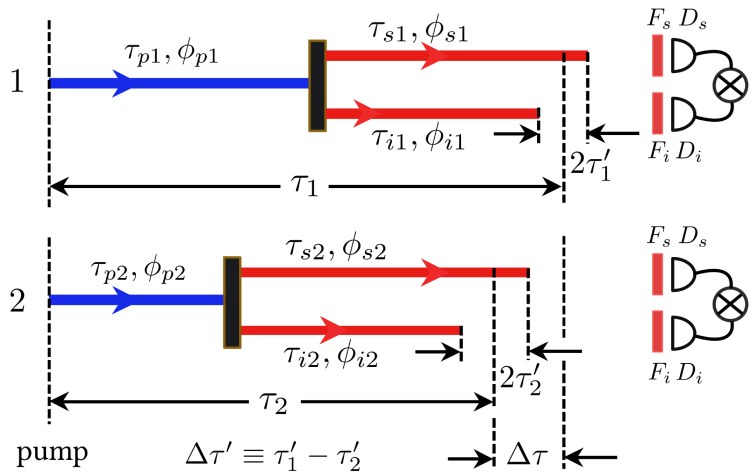

Figure 5.1: Schematic representation of two-photon interference using the two-photon path diagrams. A pump photon has two alternatives 1 and 2 through which it can be annihilated to produce photon pairs which pass through filters F_s and F_i and are detected in coincidence at detectors D_s and D_i.

5.2 Understanding two-photon interference using path diagrams

Alternatives 1 and 2 are the two pathways by which a pump photon is down-converted and the down-converted signal and idler photons are detected in coincidence at single-photon detectors D_s and D_i, respectively. There are six independent time parameters in this setting. The subscripts p, s and i denote the pump, signal and idler respectively. We adopt the convention that a signal photon is the one that arrives at detector D_s while an idler photon is the one that arrives at detector D_i. The symbol τ denotes the traversal time of a photon while ϕ denotes the phase, other than the dynamical phase, accumulated by a photon. Thus, τ_{s1} denotes the traversal time of the signal photon in alternative 1, etc. The various signal, idler and pump quantities are used to define the following parameters:

$$\begin{aligned}
\Delta\tau &\equiv \tau_1 - \tau_2 \equiv \left(\tau_{p1} + \frac{\tau_{s1} + \tau_{i1}}{2}\right) - \left(\tau_{p2} + \frac{\tau_{s2} + \tau_{i2}}{2}\right), \\
\Delta\tau' &\equiv \tau_1' - \tau_2' \equiv \left(\frac{\tau_{s1} - \tau_{i1}}{2}\right) - \left(\frac{\tau_{s2} - \tau_{i2}}{2}\right), \\
\Delta\phi &\equiv \phi_1 - \phi_2 \equiv (\phi_{p1} + \phi_{s1} + \phi_{i1}) - (\phi_{p2} + \phi_{s2} + \phi_{i2}). \qquad (5.1)
\end{aligned}$$

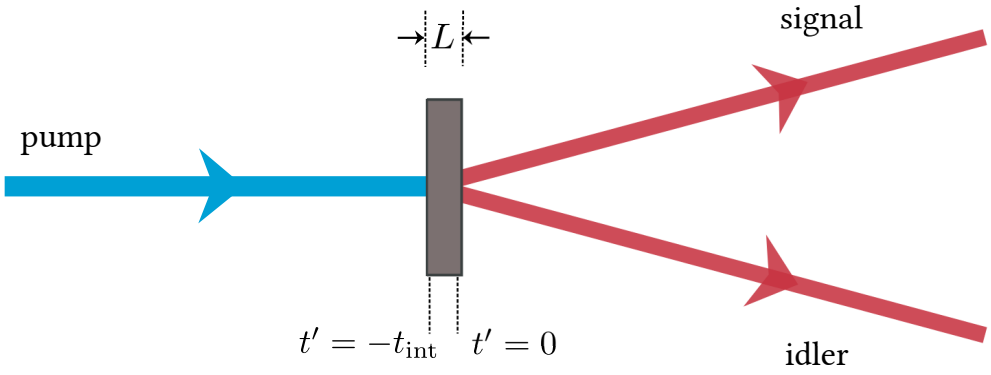

Figure 5.2: The pump photon starts interacting with a crystal of thickness L at time $t' = -t_{\text{int}}$. The interaction continues till $t' = 0$ at which the the signal and idler photons are emitted from the crystal.

The parameters defined above are identical to those defined in Ref. [28], except for τ_1', τ_2' and $\Delta\tau'$, which have been scaled down by a factor of 2. It is found that this rescaling imparts the equations in this chapter a neat and symmetric form.

5.3 Two-photon state produced from PDC

We present the derivation of the form of the two-photon state in the temporal degree of freedom as presented previously in Refs. [29, 134, 188, 24]. In Chapter 1, we described the basic physics of PDC and derived the expression 1.25 for the effective Hamiltonian operator for PDC which is given by

$$\hat{H}(t') = \frac{\epsilon_0}{2} \int_V \mathrm{d}^3\mathbf{r} \chi^{(2)} \hat{E}_p^{(+)}(\mathbf{r}, t') \hat{E}_s^{(-)}(\mathbf{r}, t') \hat{E}_i^{(-)}(\mathbf{r}, t') + \text{H.c.} \tag{5.2}$$

Recall that V is the volume of the interaction region in the crystal and $\chi^{(2)}$ is the second-order nonlinear susceptibility of the crystal medium. As depicted in Figure 5.2, let us assume that the pump photon starts interacting with the crystal at $t' = -t_{\text{int}}$ and gets annihilated by $t' = 0$ to generate the signal and idler photons. We further assume that the crystal is embedded in a passive linear medium with suitable refractive index so that we can neglect refraction effects at the air-crystal interface [22, 26].

We will now derive a simplified form of the Hamiltonian that focuses on the

temporal characteristics of the pump and signal-idler photons. We assume that the transverse area of the crystal is very large. Moreover, in a typical two-photon interference experiment, pinholes are placed to ensure that the transverse wave-vectors $\mathbf{q}_s$ and $\mathbf{q}_i$ are perfectly phase-matched such that $\mathbf{q}_s + \mathbf{q}_i = \mathbf{q}_p$, where $\mathbf{k}_p \equiv (\mathbf{q}_p, k_{pz}), \mathbf{k}_s \equiv (\mathbf{q}_s, k_{sz})$ and $\mathbf{k}_i \equiv (\mathbf{q}_i, k_{iz})$ are the wave-vectors for the pump, signal and idler photons, respectively. Incorporating these assumptions, it can be shown that the effective Hamiltonian for PDC is given by

$$\hat{H}(t') = \frac{\epsilon_0}{2} \int_{-L}^{0} \mathrm{d}z \chi^{(2)} \hat{E}_p^{(+)}(z,t') \hat{E}_s^{(-)}(z,t') \hat{E}_i^{(-)}(z,t') + \mathrm{H.c}, \tag{5.3}$$

where L is the thickness of the crystal. In most experiments, the pump field is sufficiently intense and may therefore be treated classically. The electric fields can be expanded as

$$\hat{E}_p^{(+)}(z,t') = \int_0^{\infty} \mathrm{d}\omega_p A_p V(\omega_p) e^{i(k_{pz}(\omega_p)z - \omega_p t')} e^{i(\omega_p \tau_p + \phi_p)}, \tag{5.4a}$$

$$\hat{E}_s^{(-)}(z,t') = \int_0^{\infty} \mathrm{d}\omega_s A_s^* \hat{a}_s^{\dagger}(\omega_s) e^{-i(k_{sz}(\omega_s)z - \omega_s t')}, \tag{5.4b}$$

$$\hat{E}_i^{(-)}(z,t') = \int_0^{\infty} \mathrm{d}\omega_i A_i^* \hat{a}_i^{\dagger}(\omega_i) e^{-i(k_{iz}(\omega_i)z - \omega_i t')}. \tag{5.4c}$$

Here A_p, A_s and A_i are scaling factors which vary slowly in the frequency range of experimental interest and can be taken to be constants. The function $V(\omega_p)$ is the complex spectral amplitude of the pump field at frequency ω, and the phase factor $e^{i(\omega_p \tau_p + \phi_p)}$ has been included to incorporate phase changes in the pump photon in its propagation before interacting with the crystal. Here τ_p represents the traversal time of the pump photon, and ϕ_p is the net non-dynamical phase (such as geometric phase) that it acquires during propagation. Substituting Equations (5.4) in Equation (5.3), we obtain

$$\hat{H}(t') = \frac{\epsilon_0 \chi^{(2)} A_p A_s^* A_i^*}{2} \int_{-L}^{0} \mathrm{d}z \iiint_0^{\infty} \mathrm{d}\omega_p \mathrm{d}\omega_s \mathrm{d}\omega_i V(\omega_p) \hat{a}_s^{\dagger}(\omega_s) \hat{a}_i^{\dagger}(\omega_i) e^{i(\omega_s + \omega_i - \omega_p)t'} \times e^{i[k_{pz}(\omega_p) - k_{sz}(\omega_s) - k_{iz}(\omega_i)]z} + \mathrm{H.c.} \tag{5.5}$$

At time $t' = -t_{\text{int}}$, there are no photons in the signal and idler modes. Therefore, the state of the field is given by $|\psi(-t_{\text{int}}) = |\text{vac}\rangle_s|\text{vac}\rangle_i$, which denotes the vacuum state. The state $|\psi(0)\rangle$ at time $t' = 0$ at the end of the interaction can be computed using Schrodinger's equation as

$$|\psi(0)\rangle = \exp\left[\frac{1}{i\hbar}\int_{-t_{\text{int}}}^{0} \mathrm{d}t' \hat{H}(t')\right] |\psi(t' = t_{\text{int}})\rangle. \tag{5.6}$$

In most experiments, the PDC interaction is sufficiently weak so that the above equation can be approximated by the first two terms of a perturbative expansion. The first term is the vacuum state which does not contribute to photon detections can be ignored. The second term correspond to the two-photon state $|\psi\rangle$ is given by

$$|\psi\rangle = \frac{\epsilon_0 \chi^{(2)} A_p A_s^* A_i^*}{2i\hbar} \int_{-t_{\text{int}}}^{0} \mathrm{d}t' \int_{-L}^{0} \mathrm{d}z \iiint_{0}^{\infty} \mathrm{d}\omega_p \mathrm{d}\omega_s \mathrm{d}\omega_i V(\omega_p) e^{i(\omega_s+\omega_i-\omega_p)t'} \times e^{i[k_{pz}(\omega_p)-k_{sz}(\omega_s)-k_{iz}(\omega_i)]z} \hat{a}_s^\dagger(\omega_s)\hat{a}_i^\dagger(\omega_i)|\text{vac}\rangle_s|\text{vac}\rangle_i. \tag{5.7}$$

Note that only the first term in the Hamiltonian has contributed to generating the above state. The contribution from its Hermitian conjugate vanishes identically.

We now assume that the interaction time t_{int} is significantly large compared to the time-scale over which PDC takes place in the medium. As a result, the integration over the time variable t' can be performed over the entire range from negative to positive infinity to yield $\delta(\omega_p - \omega_s - \omega_i)$. We perform the integration over the pump frequency to obtain

$$|\psi\rangle = A \iint d\omega_s d\omega_i V(\omega_p)\Phi(\omega_s, \omega_i) e^{i(\omega_p \tau_p + \phi_p)} |\omega_s\rangle_s |\omega_i\rangle_i, \tag{5.8}$$

where A is a constant and $\Phi(\omega_s, \omega_i)$ is called the phase-matching function, and is given by

$$\Phi(\omega_s, \omega_i) = \int_{-L}^{0} \mathrm{d}z e^{i[k_{pz}(\omega_p)-k_{sz}(\omega_s)-k_{iz}(\omega_i)]z}. \tag{5.9}$$

The form of the phase-matching function is determined by the crystal parameters such as refractive indices for the different fields and polarizations, length and orientation of the crystal with respect to the pump, etc. We now study the transfer of temporal correlations from the pump to the two-photon state.

5.4 Transfer of temporal coherence in PDC

5.4.1 Detection with infinitely fast detectors

We follow the formalism worked out in Ref. [28] and represent a general two-alternative two-photon interference of the PDC photons by the two-photon path diagrams shown in Figure 5.1. The pump is a general temporally partially coherent field. The two-photon state $|\psi\rangle_1$ produced in alternative 1 in the weak down-conversion limit is given by [134, 24]:

$$|\psi\rangle_1 = A_1 \iint d\omega_s d\omega_i V(\omega_p)\Phi_1(\omega_s,\omega_i)e^{i(\omega_p\tau_{p1}+\phi_{p1})}|\omega_s\rangle_{\omega_{s1}}|\omega_i\rangle_{\omega_{i1}}, \tag{5.10}$$

where $\Phi_1(\omega_s,\omega_i)$ is the phase-matching function in alternative 1. The two-photon state $|\psi\rangle_2$ in alternative 2 can be similarly defined. The complete two-photon state $|\psi\rangle$ at the detectors is the sum of the two-photon states in alternatives 1 and 2 and can be written as $|\psi\rangle = |\psi\rangle_1 + |\psi\rangle_2$. The corresponding density matrix ρ of the state at the detectors is therefore:

$$\hat{\rho} = \big\langle |\psi\rangle\langle\psi| \big\rangle. \tag{5.11}$$

Here $\langle\cdots\rangle$ represents an ensemble average over infinitely many realizations of the two-photon state.

We now denote the positive frequency parts of the electric fields at detectors D_s and D_i by $\hat{E}_s^{(+)}(t)$ and $\hat{E}_i^{(+)}(t)$, respectively, and write them as

$$\hat{E}_s^{(+)}(t) = \kappa_{s1}\hat{E}_{s1}^{(+)}(t-\tau_{s1}) + \kappa_{s2}\hat{E}_{s2}^{(+)}(t-\tau_{s2}), \tag{5.12a}$$

$$\hat{E}_i^{(+)}(t) = \kappa_{i1}\hat{E}_{i1}^{(+)}(t-\tau_{i1}) + \kappa_{i2}\hat{E}_{i2}^{(+)}(t-\tau_{i2}), \tag{5.12b}$$

where $\kappa_{s1(2)}$ and $\kappa_{i1(2)}$ are scalar amplitudes and where

$$\hat{E}_{s1}^{(+)}(t-\tau_{s1}) = e^{i\phi_{s1}} \int_0^\infty d\omega f_{s1}(\omega-\omega_{s0})\hat{a}_{s1}(\omega)e^{-i\omega(t-\tau_{s1})}, \tag{5.13}$$

is the positive frequency parts of the electric field at detector D_s in alternative 1, etc. The function $f_{s1}(\omega-\omega_{s0})$ is the amplitude transmission function of the filter F_s placed at detector D_s, etc. The filters F_s and F_i are centered at frequencies ω_{s0} and ω_{i0}, respectively, and we assume the phase-matching condition $\omega_{p0} = \omega_{s0} + \omega_{i0}$, where ω_{p0} is the central frequency of the pump field $V(\omega_p)$. The coincidence count rate $R_{si}^{(2)}(t_s, t_i)$ of the two detectors is the probability per (unit time)^2 that a signal photon is detected at time t_s and the corresponding idler photon is detected at time t_i, and it is given by $R_{si}^{(2)}(t_s,t_i) = \mathrm{Tr}\{\hat{\rho}\,\hat{E}_s^{(-)}(t_s)\,\hat{E}_i^{(-)}(t_i)\hat{E}_i^{(+)}(t_i)\,\hat{E}_s^{(+)}(t_s)\}$ [4]. Using the definitions and expressions of Equations (5.1)-(5.13), we evaluate $R_{si}^{(2)}(t_s,t_i)$ to be

$$R_{si}^{(2)}(t_s,t_i) = \kappa_1^2 R^{(2)}(t_s,t_i,\tau_{s1},\tau_{i1}) + \kappa_2^2 R^{(2)}(t_s,t_i,\tau_{s2},\tau_{i2}) \times +\kappa_1\kappa_2\Gamma^{(2)}(t_s,t_i,\tau_{s1},\tau_{i1},\tau_{s2},\tau_{i2})e^{-i\Delta\phi} + \text{c.c.}, \tag{5.14a}$$

where $\kappa_1 = \kappa_{s1}\kappa_{i1}$, $\kappa_2 = \kappa_{s2}\kappa_{i2}$,

$$\Gamma^{(2)}(t_s,t_i,\tau_{s1},\tau_{i1},\tau_{s2},\tau_{i2}) = \mathrm{Tr}\big\{\hat{\rho}\,\hat{E}_{s1}^{(-)}(t_s-\tau_{s1})\hat{E}_{i1}^{(-)}(t_i-\tau_{i1})\hat{E}_{i2}^{(+)}(t_i-\tau_{i2})\hat{E}_{s2}^{(+)}(t_s-\tau_{s2})\big\}, \tag{5.14b}$$

and

$$R^{(2)}(t_s,t_i,\tau_{s1},\tau_{i1}) = \Gamma^{(2)}(t_s,t_i,\tau_{s1},\tau_{i1},\tau_{s1},\tau_{i1}). \tag{5.14c}$$

Equation (5.14) is the interference law for the two-photon field. The first and the second terms are the coincidence count rates in alternatives 1 and 2, respectively. The interference term $\Gamma^{(2)}(t_s,t_i,\tau_{s1},\tau_{i1},\tau_{s2},\tau_{i2})$ appears when both the alternatives are present, and it will be referred to as the two-photon cross-correlation function of the down-converted field. We now make the assumption that the spectral width

$\Delta\omega_{p0}$ of the pump field is much smaller than the central frequency ω_{p0} and the spectral widths of the phase-matching functions and filter functions. As a result, the phase-matching and filter functions can be taken to be approximately constant in the frequency range $(\omega_{p0} - \Delta\omega_{p0}/2, \omega_{p0} + \Delta\omega_{p0}/2)$. This assumption remains valid for most PDC experiments employing continuous wave pump field [41, 168, 169, 170, 28, 42, 171, 172, 185] and pulsed pump field [24, 25, 35, 180, 181] and may only be invalid for experiments employing ultrashort pulsed pump fields [189, 190, 191]. We use the relations $\omega_p = \omega_s + \omega_i$, $\omega_d = \omega_s - \omega_i$, $\omega_{p0} = \omega_{s0} + \omega_{i0}$, $\omega_{d0} = \omega_{s0} - \omega_{i0}$ and define the integration variables $\bar{\omega}_p = \omega_p - \omega_{p0}$ and $\bar{\omega}_d = \omega_d - \omega_{d0}$. Using Equations (5.1)-(5.14), we obtain after a long but straightforward calculation:

$$\Gamma^{(2)}(t_s, t_i, \tau_{s1}, \tau_{i1}, \tau_{s2}, \tau_{i2}) = \Gamma_p\left(\tau_1 - \frac{t_s + t_i}{2}, \tau_2 - \frac{t_s + t_i}{2}\right) \times \Gamma_d\left(\tau_1' - \frac{t_s - t_i}{2}, \tau_2' - \frac{t_s - t_i}{2}\right), \quad (5.15)$$

where,

$$\Gamma_p\left(\tau_1 - \frac{t_s + t_i}{2}, \tau_2 - \frac{t_s + t_i}{2}\right) = e^{-i\omega_{p0}\Delta\tau} \iint d\bar{\omega}_p' d\bar{\omega}_p'' \left\langle V^*(\bar{\omega}_p' + \omega_{p0}) V(\bar{\omega}_p'' + \omega_{p0}) \right\rangle \times \exp\left[-i\bar{\omega}_p'\left(\tau_1 - \frac{t_s + t_i}{2}\right)\right] \exp\left[i\bar{\omega}_p''\left(\tau_2 - \frac{t_s + t_i}{2}\right)\right], \quad (5.16)$$

and,

$$\Gamma_d\left(\tau_1' - \frac{t_s - t_i}{2}, \tau_2' - \frac{t_s - t_i}{2}\right) = e^{-i\omega_{d0}\Delta\tau'} \iint d\bar{\omega}_d' d\bar{\omega}_d'' \left\langle g_1^*(\bar{\omega}_d')\, g_2(\bar{\omega}_d'') \right\rangle \times \exp\left[-i\bar{\omega}_d'\left(\tau_1' - \frac{t_s - t_i}{2}\right)\right] \exp\left[i\bar{\omega}_d''\left(\tau_2' - \frac{t_s - t_i}{2}\right)\right], \quad (5.17)$$

with

$$g_1(\omega) = \Phi_1\left(\omega_{s0} + \frac{\omega}{2}, \omega_{i0} - \frac{\omega}{2}\right) f_{s1}\left(\frac{\omega}{2}\right)\, f_{i1}\left(-\frac{\omega}{2}\right),$$

etc. The ensemble average $\left\langle V^*(\bar{\omega}_p' + \omega_{p0}) V(\bar{\omega}_p'' + \omega_{p0}) \right\rangle$ is the cross-spectral den-

sity function of the pump field. It is at once clear from Equation (5.16) that the coherence function $\Gamma_p\left(\tau_1 - \frac{t_s+t_i}{2}, \tau_2 - \frac{t_s+t_i}{2}\right)$ and the cross-spectral density function $\left\langle V^*(\bar{\omega}'_p + \omega_{p0})V(\bar{\omega}''_p + \omega_{p0})\right\rangle$ are connected through the generalized Wiener-Khintchine relation [3] with parameters $\tau_1 - (t_s + t_i)/2$ and $\tau_2 - (t_s + t_i)/2$. So, in terms of the two-photon time parameters $\tau_1 - (t_s + t_i)/2$ and $\tau_2 - (t_s + t_i)/2$, the coherence function $\Gamma_p\left(\tau_1 - \frac{t_s+t_i}{2}, \tau_2 - \frac{t_s+t_i}{2}\right)$ has the same functional form as that of the cross-correlation function of the pump field. The function $\langle g_1^*(\bar{\omega}'_d)\, g_2(\bar{\omega}''_d)\rangle$ is also in the form of a cross-spectral density function, and as is clear from Equation (5.17), it forms a generalized Wiener-Khintchine relation with the coherence function $\Gamma_d\left(\tau'_1 - \frac{t_s-t_i}{2}, \tau'_2 - \frac{t_s-t_i}{2}\right)$. Therefore, the function $\Gamma_d\left(\tau'_1 - \frac{t_s-t_i}{2}, \tau'_2 - \frac{t_s-t_i}{2}\right)$ not only carries all the information about the phase-matching conditions and the crystal parameters but also carries information about any statistical randomness that the down-converted photons go through [192]. It is interesting to note that any statistical randomness encountered by the photons after the down-conversion affects only $\Gamma_d\left(\tau'_1 - \frac{t_s-t_i}{2}, \tau'_2 - \frac{t_s-t_i}{2}\right)$ and has no effect on $\Gamma_p\left(\tau_1 - \frac{t_s+t_i}{2}, \tau_2 - \frac{t_s+t_i}{2}\right)$.

We thus find that the two-photon cross-correlation function factorizes into two separate coherence functions. The coherence function $\Gamma_p\left(\tau_1 - \frac{t_s+t_i}{2}, \tau_2 - \frac{t_s+t_i}{2}\right)$ carries the entire statistical information of the pump field, and in this way the temporal correlation properties of the pump photon get entirely transferred to the down-converted photons. This result is the temporal analog of the effect described in Ref. [30] in which it was shown that in PDC the spatial coherence properties of the pump field gets entirely transferred to the down-converted two-photon field. However, the present chapter extends beyond just establishing this analogy. For example, in Ref. [30], the effect due to the phase-matching function was completely ignored, but in the present chapter, we have included it through the coherence function $\Gamma_d\left(\tau'_1 - \frac{t_s-t_i}{2}, \tau'_2 - \frac{t_s-t_i}{2}\right)$. Moreover, like most spatial-interference schemes, Ref. [30] does not employ a detection scheme that involves space-averaging. However, most time-domain experiments employ time-averaged detection schemes. Therefore, in the present chapter, we also work out how time-averaged detection schemes affect

the temporal coherence transfer in PDC.

5.4.2 Time-averaged detection scheme

In most experiments, one does not measure the instantaneous coincidence rate $R^{(2)}_{si}(t_s, t_i)$ of Equation (5.14). Instead, one measures the time-averaged coincidence count rate, averaged over the photon collection time $T_{\rm pc}$ and the coincidence time-window $T_{\rm ci}$. The time-averaged two-photon cross-correlation function $\bar{\Gamma}^{(2)}$ can be found by first expressing it as

$$\begin{aligned}\bar{\Gamma}^{(2)} &= \left\langle\left\langle \Gamma^{(2)}(t_s, t_i, \tau_{s1}, \tau_{i1}, \tau_{s2}, \tau_{i2})\right\rangle\right\rangle_{t_s,t_i} \\ &= \left\langle \Gamma_p\left(\tau_1 - \frac{t_s+t_i}{2}, \tau_2 - \frac{t_s+t_i}{2}\right)\right\rangle_{\frac{t_s+t_i}{2}} \left\langle \Gamma_d\left(\tau_1' - \frac{t_s-t_i}{2}, \tau_2' - \frac{t_s-t_i}{2}\right)\right\rangle_{\frac{t_s-t_i}{2}},\end{aligned} \tag{5.18}$$

and then integrating it with respect to $(t_s + t_i)/2$ over $T_{\rm pc}$ and with respect to $(t_s - t_i)/2$ over $T_{\rm ci}$. In most experiments, the coincidence time-window $T_{\rm ci}$ spans a few nanoseconds, which is much longer than the inverse frequency-bandwidth of $g(\omega)$, typically of the order of picoseconds. The photon collection time $T_{\rm pc}$ is usually a few seconds and is much longer than the inverse frequency-bandwidth of the pump field $V(\omega_p)$, typically of the order of microseconds. Thus we perform the above time-averaging in the limit $T_{pc}, T_{ci} \to \infty$ to obtain

$$\begin{aligned}\bar{\Gamma}^{(2)} &= \bar{\Gamma}_p(\tau_1, \tau_2)\,\bar{\Gamma}_d(\tau_1', \tau_2') \\ &= \sqrt{\bar{I}_1\bar{I}_2}\sqrt{\bar{G}_1\bar{G}_2}\;\; \bar{\gamma}_p(\Delta\tau)\,\bar{\gamma}_d(\Delta\tau') \\ &= \bar{R}^{(2)}\bar{\gamma}_p(\Delta\tau)\,\bar{\gamma}_d(\Delta\tau').\end{aligned} \tag{5.19}$$

Here $\bar{I}_1 = \bar{\Gamma}_p(\tau_1, \tau_1)$, $\bar{G}_1 = \bar{\Gamma}_d(\tau_1', \tau_1')$, $\bar{R}^{(2)} \equiv \sqrt{\bar{I}_1\bar{I}_2}\sqrt{\bar{G}_1\bar{G}_2}$, $\bar{\gamma}_p(\Delta\tau) = \bar{\Gamma}_p(\tau_1, \tau_2)/\sqrt{\bar{I}_1\bar{I}_2}$, and $\bar{\gamma}_d(\Delta\tau) = \bar{\Gamma}_d(\tau_1', \tau_2')/\sqrt{\bar{G}_1\bar{G}_2}$, etc. The function $\bar{\gamma}_p(\Delta\tau)$ satisfies $0 \le |\bar{\gamma}_p(\Delta\tau)| \le 1$ and diminishes over a $\Delta\tau$-scale given by the inverse pump bandwidth $1/\Delta\omega_{p0}$. The function $\bar{\gamma}_d(\Delta\tau')$ also satisfies $0 \le |\bar{\gamma}_d(\Delta\tau')| \le 1$ and diminishes over a $\Delta\tau'$-scale

given by the inverse frequency-bandwidth $1/\Delta\omega_{d0}$. The temporal widths of $\bar{\gamma}_p(\Delta\tau)$ and $\bar{\gamma}_d(\Delta\tau')$ limit the ranges over which fringes could be observed as functions of $\Delta\tau'$ and $\Delta\tau$, respectively, in a time-averaged two-photon interference experiment.

The coincidence count rate of Equation (5.14) in the time-averaged scheme therefore becomes

$$\bar{R}_{si}^{(2)} = \kappa_1^2\bar{R}^{(2)} + \kappa_2^2\bar{R}^{(2)} + \kappa_1\kappa_2\bar{R}^{(2)}\bar{\gamma}_p\left(\Delta\tau\right)\bar{\gamma}_d\left(\Delta\tau'\right)e^{i(\omega_{p0}\Delta\tau+\omega_{d0}\Delta\tau'+\Delta\phi)} + \text{c.c.} \quad (5.20)$$

A similar expression was reported in Ref. [28], where various temporal two-photon interference effects have been described. The time averaged coherence function $\bar{\gamma}_p\left(\Delta\tau\right)$ has the same functional form as the time-averaged coherence function of the pump field. The time-averaged coherence function $\bar{\gamma}_d\left(\Delta\tau'\right)$ depends on the phase-matching function and the crystal parameters, and its functional form shows up in the Hong-Ou-Mandel (HOM) [41] and HOM-like effects [170, 193].

5.5 The special case of a Gaussian Schell-model pump field

In the last section, we considered PDC with a very general non-stationary pump field and described how the temporal coherence properties of the pump field get transferred to the down-converted two-photon field. In this section, we consider the pump field to be a widely-studied class of non-stationary fields, namely, the Gaussian Schell-model field, also known as the non-stationary Gaussian pulsed fields [186].

The cross-spectral density function of a Gaussian Schell-model field is given by [186]

$$\left\langle V^*(\omega''+\omega_0)V(\omega'+\omega_0)\right\rangle = A\exp\left[-\frac{(\omega'^2+\omega''^2)}{4\left(\Delta\omega_{p0}\right)^2}\right]\exp\left[-\frac{(\omega'-\omega'')^2}{2\left(\Delta\omega_c\right)^2}\right]., \quad (5.21)$$

where $\Delta\omega_{p0}$ is the frequency bandwidth of the field. The parameter $\Delta\omega_c$ is called the spectral correlation width and it quantifies the frequency-separation up to which dif-

ferent frequency components are phase-correlated. The limit $\Delta\omega_c \to 0$ corresponds to a continuous-wave, stationary field in which case the constituent frequency components are completely uncorrelated. The other limit $\Delta\omega_c \to \infty$ corresponds to a fully-coherent pulsed field in which case the constituent frequency components are perfectly phase-correlated. The corresponding temporal correlation function $\Gamma_{\mathrm{GS}}(t_1, t_2)$ can be calculated by using the generalized Wiener-Khintchine theorem [186]:

$$\Gamma_{\mathrm{GS}}(t_1, t_2) = \sqrt{I(t_1)I(t_2)}\gamma_{\mathrm{GS}}(\Delta t), \tag{5.22}$$

where we have denote $\Delta t = t_1 - t_2$ and $I(t_{1(2)}) = (2\pi\Delta\omega_{p0}A/T)\exp[-t_{1(2)}^2/(2T^2)]$. Also, we have denoted the degree of temporal coherence as $\gamma_{\mathrm{GS}}(\Delta t) = \exp[-(\Delta t)^2/(2\tau_{\mathrm{coh}}^2)]$. The quantity $\tau_{\mathrm{coh}} = (\Delta\omega_c/\Delta\omega_{p0})\left[1/(2\Delta\omega_{p0})^2 + 1/(\Delta\omega_c)^2\right]^{1/2}$ is the coherence time of the field and $T = \left[1/(2\Delta\omega_{p0})^2 + 1/(\Delta\omega_c)^2\right]^{1/2}$ is a measure of the temporal width of the non-stationary Gaussian pulse. The limit $\Delta\omega_c \to \infty$ yields $\tau_{\mathrm{coh}} \to \infty$ as expected for a fully-coherent field, and the other limit $\Delta\omega_c \to 0$ yields $\tau_{\mathrm{coh}} = 1/\Delta\omega_{p0}$ as expected for a continuous-wave, stationary field.

Now, we assume that $\Gamma_d\left(\tau_1' - \frac{t_s - t_i}{2}, \tau_2' - \frac{t_s - t_i}{2}\right) = 1$ and take the pump field to be the Gaussian Schell-model field given by Equation (5.21). Equation (5.15) then becomes:

$$\begin{aligned}\Gamma^{(2)}(t_s, t_i, \tau_1, \tau_2) &= \Gamma_p\left(\tau_1 - \frac{t_s + t_i}{2}, \tau_2 - \frac{t_s + t_i}{2}\right) \\ &= \sqrt{I\left(\tau_1 - \frac{t_s + t_i}{2}\right) I\left(\tau_2 - \frac{t_s + t_i}{2}\right)}\gamma_p(\Delta\tau),\end{aligned} \tag{5.23}$$

where

$$I\left(\tau_1 - \frac{t_s + t_i}{2}\right) = \frac{2\pi\Delta\omega_{p0}A}{T}\exp\left[-\frac{\left(\tau_1 - \frac{t_s+t_i}{2}\right)^2}{2T^2}\right], \text{ etc,}$$

$$\text{and} \qquad \gamma_p(\Delta\tau) = \exp\left[-\frac{\Delta\tau^2}{2\tau_{\mathrm{coh}}^2}\right].$$

As expected from Equation (5.15), we find that in terms of $\tau_1 - \frac{t_s+t_i}{2}$ and $\tau_2 - \frac{t_s+t_i}{2}$, the two-photon cross-correlation function in Equation (5.23) assumes the same functional form as does the cross-correlation function in Equation (5.22) in terms of t_1 and t_2. When integrated over t, Equation (5.23) yields

$$\bar{\Gamma}^{(2)} = \bar{\Gamma}_p(\tau_1, \tau_2) = \sqrt{\bar{I}_1 \bar{I}_2}\bar{\gamma}_p(\Delta\tau), \tag{5.24}$$

with $\bar{I}_1 = \bar{I}_2 = (2\pi)^{\frac{3}{2}}\Delta\omega_{p0}A$ and $\bar{\gamma}_p(\Delta\tau) = \exp\{-\Delta\tau^2/(2\bar{\tau}_{\text{coh}}^2)\}$ where $\bar{\tau}_{\text{coh}} = 1/\Delta\omega_{p0}$ is a measure of the coherence time. The time averaging washes out effects due to frequency correlations. Thus, only in the case of a stationary pump field $\bar{\gamma}_p(\Delta\tau) = \gamma_p(\Delta\tau)$ and $\bar{\tau}_{\text{coh}} = \tau_{\text{coh}}$.

5.6 Pump temporal coherence and two-qubit energy-time entanglement

Two-qubit states are the necessary ingredients for many quantum information protocols [58, 13, 14] and have been realized by exploiting the entanglement of PDC photons in several degrees of freedom including polarization [33], time-energy [42, 35, 180, 173, 194, 184, 185], position-momentum [195, 174, 196], and orbital angular momentum (OAM) [197, 198, 110, 31]. There have been previous studies describing how correlations of the pump field in polarization and spatial degrees of freedom affect the entanglement of the generated two-qubit states. In the polarization degree of freedom it was shown [149] that the degree of polarization P of the pump photon puts an upper bound of $(1 + P)/2$ on the concurrence of the generated two-qubit state. In the spatial degree of freedom, effects of pump spatial coherence on the entanglement of the generated spatial two-qubit state have been worked out for two-qubit state that have only two non-zero diagonal elements, and for such states it has been shown that the concurrence is bounded by the degree of spatial coherence of the pump field [30]. However, to the best of our knowledge, no such relation has

so far been derived for the time-energy entangled two-qubit states.

There are two generic methods by which one makes a PDC-based time-energy entangled two-qubit state. In the first method, one uses a continuous-wave pump field, either single-mode [42] or multi-mode [184, 185]. In the second method, one uses a pulsed pump field [35, 180, 173, 194]. In both these methods, a combination of post-selection strategies, such as selecting a faster coincidence detection-window, using arrival time of pump photon as a trigger etc., one makes sure that there are only two alternative pathways in which the signal and idler photons reach their respective detectors. The two alternative pathways form the two dimensional qubit space for the signal and idler photons. We represent by $|s1\rangle$ the state of the signal photon in alternative 1, etc. Therefore, the density matrix $\rho_{2\text{qubit}}$ of the two-qubit state can be written in the basis $\{|s1\rangle|i1\rangle, |s1\rangle|i2\rangle, |s2\rangle|i1\rangle, |s2\rangle|i2\rangle\}$ as:

$$\rho = \begin{pmatrix} a & 0 & 0 & c \\ 0 & 0 & 0 & 0 \\ 0 & 0 & 0 & 0 \\ c^* & 0 & 0 & b \end{pmatrix} \tag{5.25}$$

where the diagonal terms a and b are the probabilities that the signal and idler photons are detected in states $|s1\rangle|i1\rangle$ and $|s2\rangle|i2\rangle$, respectively, and the off-diagonal term c is a measure of coherence between states $|s1\rangle|i1\rangle$ and $|s2\rangle|i2\rangle$. In an experimental situation, the density matrix ρ can be represented by the two alternative pathways of Figure 5.1. Therefore, using Equation (5.20), we write $a = \eta\kappa_1^2\bar{R}^{(2)}$ and $b = \eta\kappa_2^2\bar{R}^{(2)}$, where $\eta = 1/[\kappa_1^2\bar{R}^{(2)} + \kappa_2^2\bar{R}^{(2)}]$ is the constant of proportionality. The off-diagonal term is given by

$$c = \eta\kappa_1\kappa_2\bar{R}^{(2)}\bar{\gamma}_p(\Delta\tau)\bar{\gamma}_d(\Delta\tau')e^{i(\omega_{p0}\Delta\tau+\omega_{d0}\Delta\tau'+\Delta\phi)}. \tag{5.26}$$

The entanglement of $\rho_{2\text{qubit}}$, as quantified by Wootters's concurrence $C(\rho_{2\text{qubit}})$ [18],

can be shown to be

$$C(\rho_{2\text{qubit}}) = 2|c| = \frac{\kappa_1\kappa_2\bar{R}^{(2)}}{\kappa_1^2\bar{R}^{(2)} + \kappa_2^2\bar{R}^{(2)}}\bar{\gamma}_p(\Delta\tau)\bar{\gamma}_d(\Delta\tau'). \tag{5.27}$$

The pre-factor $\kappa_1\kappa_2\bar{R}^{(2)}/(\kappa_1^2\bar{R}^{(2)} + \kappa_2^2\bar{R}^{(2)})$ is no greater than 1, and $\bar{\gamma}_d(\Delta\tau')$ also satisfies $0 \leq |\bar{\gamma}_d(\Delta\tau')| \leq 1$. We therefore arrive at the relation: $C(\rho_{2\text{qubit}}) \leq \bar{\gamma}_p(\Delta\tau)$. Therefore, we find that the concurrence $C(\rho_{2\text{qubit}})$ of the time-energy two-qubit state is bounded from above by the degree of coherence of the pump photon and thus that the temporal correlations of the pump field set an upper bound on the attainable concurrence for a two-qubit state of the form of Equation (5.25). This result is the temporal analog of the results obtained in the polarization [149] and spatial [30] degrees of freedom. However, unlike in the spatial degree of freedom, which does not involve any space-averaged detection scheme, the results derived in this chapter show that even for the time-averaged detection schemes, the temporal correlation properties of the pump do directly decide the upper limit on entanglement that a time-energy entangled two-qubit state can achieve.

5.7 Summary

In conclusion, we have shown that in parametric down-conversion the coherence properties of a temporally partially coherent pump field get entirely transferred to the down-converted entangled two-photon field. Under the assumption that the frequency-bandwidth of the down-converted signal-idler photons is much larger than that of the pump, we have worked out the temporal coherence functions of the down-converted field for both infinitely-fast and time-averaged detection schemes. We have shown that in each scheme the coherence function factorizes into two separate coherence functions with one of them carrying the entire statistical information of the pump field. Taking the pump to be a Gaussian Schell-model field, we have derived explicit expressions for the coherence functions. Finally, we have shown that the concurrence of time-energy entangled two-qubit states is bounded by the degree

of temporal coherence of the pump field. This result extends previously obtained results in the spatial [30] and polarization [149] degrees of freedom to the temporal degree of freedom and can thus have important implications for understanding how correlations of the pump field in general manifest as two-particle entanglement. Our results can also be important for time-energy two-qubit based quantum communication applications. This is because it has been recognized that energy-time entangled two-qubit states are better than the polarization two-qubit states for long-distance quantum information [190, 191], and our results show that the temporal coherence properties of the pump field can be used as a parameter for tailoring the two-qubit time-energy entanglement. Our work can also have implication for PDC-based heralded single photons sources since the degree of purity of heralded photons depends on the correlations in the pump field, and therefore it can be tailored by controlling the coherence properties of the pump field.

Chapter 6

Intrinsic correlations of infinite-dimensional states

6.1 Introduction

According to its definition from optical coherence theory [3], coherence refers to the ability of a light field to superpose with itself and exhibit interference. While the contrast of the interference can be used to quantify coherence in a specific basis [1, 2], it has been recognized that the intrinsic coherence of a light field must be quantified in a basis-invariant manner [4, 78, 80, 199, 83, 82, 84, 85]. A basis-invariant quantification of coherence was first carried out by Wolf [78], who formulated a measure known as the degree of polarization, denoted as P_2, for two-dimensional polarization states of light. The quantity P_2 has the following known interpretations that justify its uniqueness as an intrinsic measure of coherence for two-dimensional states [78], namely: (i) it is the norm of the Bloch vector representing the state, (ii) it is the Frobenius distance between the state and the fully incoherent identity state [199], (iii) it is the distance between the origin and the center of mass of 2 point masses of magnitudes equal to the eigenvalues of the state that are both kept at unit distance from the origin in a Euclidean space of unit dimension [200], (iv) it is the maximum contrast or visibility of an interference experiment, (v) it is the

maximum pairwise-coherence of the state over all orthonormal bases, and (vi) it is the weightage of the pure part of the state. An analogous measure, which we denote as P_N, was first obtained by Barakat [79, 80], and independently by Samson and Olson [81] by generalizing the Bloch vector interpretation of P_2 to N-dimensional states. Recently, following up on previous studies by Setälä *et al.* [83, 82] and Luis [84] on three-dimensional and four-dimensional states, respectively, Yao *et al.* [85] generalized the Frobenius distance interpretation of P_2 to yield an analogous measure P_N for N-dimensional states, where N is a positive integer. The center-of-mass interpretation of Ref. [200] also yields a measure P_N, which is the distance between the origin and the center of mass of N point masses of magnitudes equal to the eigenvalues of the state that are kept mutually equidistant and at unit distance from the origin in a Euclidean space of $(N-1)$ dimensions. In a recent study [86], we demonstrated that P_N also generalizes the other three interpretations of P_2, and therefore argued that P_N is the analogous basis-invariant measure of coherence for finite-N-dimensional systems. In this chapter, we will generalize P_N to the $N \to \infty$ limit to quantify the intrinsic coherence P_∞ of infinite-dimensional states in the orbital angular momentum (OAM), photon number, position and momentum representations.

The measure P_∞ for states in the OAM representation can be useful for optical communication protocols that harness high-dimensional superpositions of OAM states of photons [201]. For instance, P_∞ can be used for quantifying the coherence degradation of superposition states over free-space [202] and fiber-based [112] long distance transmission. In addition, P_∞ can also be useful in studies that characterize OAM-entangled pure states through measurements of angular coherence [37, 115, 131]. In the photon number representation, P_∞ can be used to quantify the coherence of Gaussian states for continuous-variable quantum protocols [203, 204, 205]. In the position and momentum representations, we expect P_∞ to be useful for studying how the spatial coherence of light fields is affected by turbulent environments [206, 207, 208]. Until now the spatial coherence of light fields has only

been quantified in a restricted basis-dependent manner in terms of cross-correlation functions and cross-spectral density functions [3, 2]. In contrast, the measure P_∞ can be used to quantify the spatial coherence of the entire field in a basis-invariant manner. Moreover, P_∞ can also be useful in theoretical studies on decoherence in open quantum systems [209, 210, 211].

The generalization procedure to obtain P_∞ from P_N involves the following subtleties: Firstly, all the known interpretations of P_N have been defined under the assumption that N is finite. Secondly, if we consider the analytic expression for P_N of a normalized N-dimensional state represented by the density operator ρ [85, 86], namely,

$$P_N = \sqrt{\frac{N\mathrm{Tr}(\rho^2) - 1}{N - 1}}, \tag{6.1}$$

and heuristically evaluate its limit as $N \to \infty$, we obtain $P_\infty = \sqrt{\mathrm{Tr}(\rho^2)}$, where ρ is now a normalized infinite-dimensional state. However, this limiting procedure is not always legitimate because an infinite-dimensional state need not be normalizable [212]. Moreover, the trace operation is not well-defined in infinite-dimensional vector spaces, and can lead to divergent results [213]. In addition, infinite-dimensional vector spaces are generally associated with issues pertaining to the convergence of infinite summations, the order in which several summations are performed, and the validity of various limiting procedures [44].

These issues were studied by Pegg and Barnett initially in the number-phase representations in their attempt to formulate a well-behaved Hermitian phase operator [214, 215], and subsequently in the OAM-angle representations in their quantum treatment of rotation angles [44]. Specifically, the authors developed rigorous formalisms in which the infinite-dimensional representations are viewed as limits of physically indistinguishable finite-dimensional representations. They demonstrated that if physical quantities are evaluated in the finite-dimensional representations with the limit of the infinite dimensionality being imposed only at the final stage of the calculation, then the issues associated with infinite-dimensional spaces are circumvented while still yielding physically consistent, non-divergent results.

In this chapter, we use the Pegg-Barnett procedure to extend the measure P_N to the $N \to \infty$ limit and quantify the intrinsic coherence P_∞ of infinite-dimensional states. We organize the chapter as follows: In Section 6.2, we consider states in the OAM-angle and photon number representations. Using the existing Pegg-Barnett formalisms for these representations, we show that P_∞ for a normalized physical state ρ is given by $P_\infty = \sqrt{\mathrm{Tr}(\rho^2)}$. In Section 6.3, we consider states in the position and momentum representations. We first explicitly develop a Pegg-Barnett-type formalism for position and momentum, and subsequently use the formalism to show that $P_\infty = \sqrt{\mathrm{Tr}(\rho^2)}$, for a normalized physical state ρ. In Section 6.4, we present the conclusions and future outlook of this chapter.

6.2 OAM-angle and photon number representations

6.2.1 OAM-Angle

We begin with a description of the infinite-dimensional improper vector space representation of the OAM degree of freedom [44]. The OAM eigenstates, denoted by $|l\rangle$, where $l = -\infty, ..., -1, 0, 1, ..., \infty$, constitute a discrete basis, whereas the angle eigenstates denoted by $|\theta\rangle$, where $\theta \in [0, 2\pi)$, form a continuous basis. By orthonormality and completeness, these basis vectors satisfy

$$\langle l|l'\rangle = \delta_{ll'}, \qquad \langle\theta|\theta'\rangle = \delta(\theta - \theta'), \tag{6.2a}$$

$$\sum_{l=-\infty}^{+\infty} |l\rangle\langle l| = 1, \qquad \int_0^{2\pi} |\theta\rangle\langle\theta| \, \mathrm{d}\theta = 1 \tag{6.2b}$$

$$|l\rangle = \frac{1}{\sqrt{2\pi}} \int_0^{2\pi} e^{+il\theta} |\theta\rangle \, \mathrm{d}\theta, \tag{6.2c}$$

$$|\theta\rangle = \frac{1}{\sqrt{2\pi}} \sum_{l=-\infty}^{+\infty} e^{-il\theta} |l\rangle. \tag{6.2d}$$

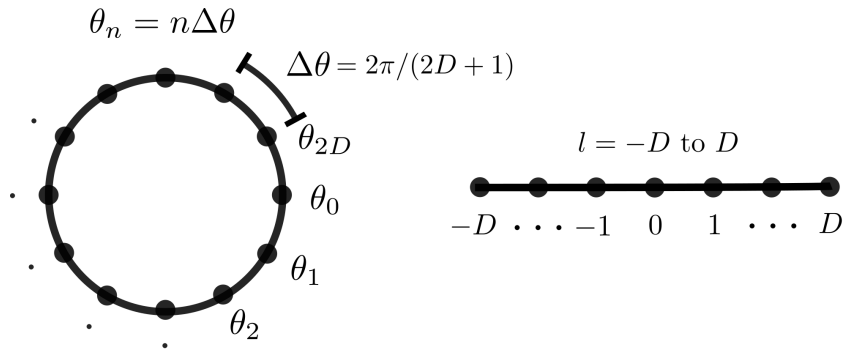

Figure 6.1: In the proper representation constructed by Pegg and Barnett, OAM eigenvectors $|l\rangle$ for $l = -D, ..., +D$, and angle eigenvectors $|\theta_n\rangle$ where $\theta_n = n\Delta\theta$ for $n = 0, 1, ..., 2D$, with $\Delta\theta = 2\pi/(2D+1)$ span a $(2D+1)$-dimensional space. In order to derive P_∞ of an infinite-dimensional state ρ, we first calculate P_{2D+1} in this finite representation and then take the limit of $D \to \infty$ or $\Delta\theta \to 0$ at the end of the calculation.

Such a vector space is referred to as improper because some states in this space may not be normalizable. For instance, notice from Equation (6.2d) that the state $|\theta\rangle$ is not normalizable. Other formal issues associated with this space have been described in detail in Ref. [44]. In the Pegg-Barnett formalism, the above infinite-dimensional vector space is substituted by a finite-dimensional vector space spanned by the eigenvectors $|l\rangle$, where $l = -D, ..., -1, 0, 1, ..., D$, with D being an arbitrarily-large but finite positive integer. We will now review the Pegg-Barnett derivation of the corresponding angle eigenvectors in this finite-dimensional space [44].

We denote the finite-dimensional OAM operator as $\hat{L}$. As $\hat{L}$ must be a generator of translations in angle space, an angle state $|\theta\rangle$ must satisfy [212]

$$\exp\big(-i\hat{L}\eta/\hbar\big)|\theta\rangle = |\theta + \eta\rangle. \tag{6.3}$$

If $|\alpha_0\rangle$ is defined as the state corresponding to the angular origin, then

$$|\theta\rangle = \exp\big(-i\hat{L}\theta/\hbar\big)|\alpha_0\rangle. \tag{6.4}$$

Now, similarly an angle operator $\hat{\theta}_\alpha$ must be a generator of translations in the OAM space. This implies that

$$\exp\big(im\hat{\theta}_\alpha\big)|l\rangle = |l + m\rangle \tag{6.5}$$

Now let us suppose that,

$$|\alpha_0\rangle = \sum_{l=-D}^{+D} a_l |l\rangle. \tag{6.6}$$

Operating $\exp(im\hat{\theta}_\alpha/\hbar)$ on $|\alpha_0\rangle$ and using Equation (6.5) on Equation (6.6) yields

$$|\alpha_0\rangle = \sum_{l=-D}^{+D} a_l |l+m\rangle. \tag{6.7}$$

Now since the above equation is true for all m, it follows that the coefficients a_l must be independent of l. Upon normalizing the state, we obtain $a_l = (1/\sqrt{2D+1})$. Using Equation (6.35) we find

$$|\theta\rangle = \sum_{l=-D}^{+D} \frac{e^{-il\theta}}{\sqrt{2D+1}} |l\rangle. \tag{6.8}$$

We now note that

$$\begin{aligned} \langle\theta|\theta'\rangle &= \sum_{l=-D}^{+D} \frac{e^{+il(\theta-\theta')}}{(2D+1)} \\ &= \frac{1}{(2D+1)} \frac{\sin\left[(2D+1)(\theta-\theta')/2\right]}{\sin\left[(\theta-\theta')/2\right]}. \end{aligned} \tag{6.9}$$

This implies that $\langle\theta|\theta'\rangle = 0$ only when $(\theta - \theta') = 2\pi n/(2D+1)$, where n is a non-zero integer. Thus, a corresponding angle basis is given by the eigenstates $|\theta_n\rangle$ with eigenvalues

$$\theta_n = \alpha_0 + n\Delta\theta \quad (n = 0, 1, ..., 2l)\,. \tag{6.10}$$

Here α_0 is an arbitrary reference angle which fixes a particular basis, and can be assumed to be zero. The angular separation $\Delta\theta = 2\pi/(2D+1)$ between the consecutive angle eigenvalues can be made arbitrarily close to zero by making D arbitrarily

large. By orthonormality and completeness, the basis vectors $|l\rangle$ and $|\theta_n\rangle$ satisfy

$$\langle l|l'\rangle = \delta_{ll'}, \qquad \langle \theta_n|\theta_k\rangle = \delta_{nk}, \tag{6.11a}$$

$$\sum_{m=-D}^{+D} |l\rangle\langle l| = 1, \qquad \sum_{n=0}^{2D} |\theta_n\rangle\langle\theta_n| = 1, \tag{6.11b}$$

and are related to each other as

$$|l\rangle = \frac{1}{\sqrt{2D+1}} \sum_{n=0}^{2D} e^{+il\theta_n} |\theta_n\rangle, \tag{6.12a}$$

$$|\theta_n\rangle = \frac{1}{\sqrt{2D+1}} \sum_{l=-D}^{+D} e^{-il\theta_n} |l\rangle. \tag{6.12b}$$

In this way, Pegg and Barnett constructed a finite-dimensional representation for OAM and angle. We depict this representation in Figure 1. Such a representation is referred to as proper because all states in this space are normalizable. The authors also proved that it is a physically consistent representation by demonstrating that the finite-dimensional commutator $[\hat{\theta}_\alpha, \hat{L}]$ is physically indistinguishable from its infinite-dimensional counterpart $[\hat{\theta}_\alpha, \hat{L}] = i\hbar$ in the $D \to \infty$ limit.

We now consider a general state ρ, whose form in the improper representation is given by

$$\rho = \sum_{l=-\infty}^{+\infty} \sum_{l'=-\infty}^{+\infty} c_{ll'} |l\rangle\langle l'|. \tag{6.13}$$

Using equations (6.2), it can be shown that ρ has the angle-basis representation

$$\rho = \int_0^{2\pi} \int_0^{2\pi} W(\theta, \theta') \, |\theta\rangle\langle\theta'| \, \mathrm{d}\theta \, \mathrm{d}\theta', \tag{6.14}$$

where

$$W(\theta, \theta') = \frac{1}{2\pi} \sum_{l=-\infty}^{+\infty} \sum_{l'=-\infty}^{+\infty} c_{ll'} \, e^{+i(l\theta - l'\theta')}. \tag{6.15}$$

The above relation expresses the Fourier relationship between the OAM cross-correlation elements $c_{ll'}$ and the angular correlation function $W(\theta, \theta')$. Our aim is to characterize the intrinsic coherence of the state ρ in terms of $c_{mm'}$ and $W(\theta, \theta')$.

According to the Pegg-Barnett procedure, the state ρ can be represented in the arbitrarily-large $(2D+1)$-dimensional space as

$$\rho = \lim_{D\to\infty} \sum_{l=-D}^{+D} \sum_{l'=-D}^{+D} c_{ll'} \, |l\rangle\langle l'|, \tag{6.16}$$

where $\mathrm{Tr}(\rho) = \sum_{l=-D}^{+D} c_{ll} = 1$. However, as emphasized by Pegg and Barnett [44], the limit of $D \to \infty$ must be imposed only at the final stage of calculating physical quantities. This implies that we can compute the intrinsic coherence P_∞ of ρ by first computing P_{2D+1} for ρ using Equation (6.1), and then taking the limit of D going to infinity at the end of the calculation. Following this procedure, we obtain

$$P_\infty = \lim_{D\to\infty} \sqrt{\frac{2D+1}{2D}\Big[\sum_{l=-D}^{D} \sum_{l'=-D}^{D} |c_{ll'}|^2 - \frac{1}{2D+1}\Big]}. \tag{6.17}$$

Using the above limiting formula, P_∞ can be calculated for any arbitrary state. However, in this study we will mainly be concerned with physical states. If ρ is a physical state, then it can only contain contributions from OAM eigenstates upto some finite absolute OAM value, say M. This implies that $c_{ll'} = 0$ for all $|l|, |l'| > M$, where M can be arbitrarily large but still less than D. In addition, a physical state must also be normalizable, i.e, $\mathrm{Tr}(\rho) = \sum_{l=-\infty}^{+\infty} c_{ll} = 1$. Incorporating these facts in Equation(6.17), we obtain

$$P_\infty = \sqrt{\sum_{l=-\infty}^{+\infty} \sum_{l'=-\infty}^{+\infty} |c_{ll'}|^2} = \sqrt{\mathrm{Tr}(\rho^2)}. \tag{6.18}$$

The above equation can be used to compute the intrinsic coherence P_∞ of any physical state in the OAM representation.

We will now obtain the expression for P_∞ in terms of the angle representation $W(\theta, \theta')$. Using equations (6.11), (6.12), and (6.16), it follows that

$$\rho = \lim_{D\to\infty} \sum_{n=0}^{2D} \sum_{k=0}^{2D} \bar{W}_{\theta_n\theta_k} \, |\theta_n\rangle\langle\theta_k|, \tag{6.19}$$

where

$$\bar{W}_{\theta_n,\theta_k} = \frac{1}{2D+1} \sum_{l=-D}^{+D} \sum_{l'=-D}^{+D} c_{ll'}\, e^{+i(l\theta_n - l'\theta_k)} \tag{6.20}$$

are the discrete matrix elements of ρ in the angle basis. As ρ is normalized, we have $\sum_{n=0}^{2D} \bar{W}_{\theta_n\theta_n} = 1$. Using Equation (6.1), we compute $P_\infty = \lim_{l\to\infty} P_{2D+1}$ in terms of $\bar{W}_{\theta_n\theta_k}$ to obtain

$$P_\infty = \lim_{D\to\infty} \sqrt{\frac{2D+1}{2D}\Big[\sum_{n=0}^{2D}\sum_{k=0}^{2D} |\bar{W}_{\theta_n\theta_k}|^2 - \frac{1}{2D+1}\Big]}. \tag{6.21}$$

We will now obtain the relation between $W(\theta,\theta')$ and $\bar{W}_{\theta_n\theta_k}$ for a physical state. We note that for a physical state, $W(\theta,\theta')$ must be a continuous function normalizable to unity. Therefore, as $D\to\infty$ or $\Delta\theta = 2\pi/(2D+1) \to 0$ the relation between $W(\theta,\theta')$ and $\bar{W}_{\theta_n\theta_k}$ must be such that the condition $\sum_{n=0}^{2l} \bar{W}_{\theta_n\theta_n} = 1$ must imply $\int_0^{2\pi} W(\theta,\theta)\,\mathrm{d}\theta = 1$. We notice that substituting $W(\theta_n,\theta_n) = \lim_{\Delta\theta\to 0} \bar{W}_{\theta_n\theta_n}/\Delta\theta$ in $\sum_{n=0}^{2l} \bar{W}_{\theta_n\theta_n} = 1$ leads to $\lim_{\Delta\theta\to 0} \sum_{n=0}^{2\pi/\Delta\theta-1} W(n\Delta\theta, n\Delta\theta)\Delta\theta = 1$, which according to Riemann's definition of an integral, is equivalent to $\int_0^{2\pi} W(\theta,\theta)\mathrm{d}\theta = 1$. Now as the relation between $W(\theta,\theta')$ and $\bar{W}_{\theta_n\theta_k}$ must be independent of the arguments, it follows that

$$W(\theta_n,\theta_k) = \lim_{\Delta\theta\to 0} \bar{W}_{\theta_n\theta_k}/\Delta\theta. \tag{6.22}$$

We use the above Equation (6.22) to substitute for $\bar{W}_{\theta_n\theta_k}$ in Equation (6.21), which upon simplification yields

$$\begin{aligned} P_\infty &= \lim_{D\to\infty} \sqrt{\sum_{n=0}^{2D}\sum_{k=0}^{2D} |W(\theta_n,\theta_k)|^2\,(\Delta\theta)^2} \\ &= \lim_{\Delta\theta\to 0} \sqrt{\sum_{n=0}^{(2\pi/\Delta\theta-1)}\ \sum_{k=0}^{(2\pi/\Delta\theta-1)} |W(n\Delta\theta, k\Delta\theta)|^2 \Delta\theta\Delta\theta}. \end{aligned}$$

The above equation can be expressed in integral form using Riemann's definition as

$$P_\infty = \sqrt{\int_0^{2\pi}\int_0^{2\pi} |W(\theta,\theta')|^2\,\mathrm{d}\theta\,\mathrm{d}\theta'} = \sqrt{\mathrm{Tr}(\rho^2)}. \tag{6.23}$$

It may be verified using Equation (6.15) that the above equation is equivalent to Equation (6.18), as expected from basis invariance. Thus, we have characterized the intrinsic coherence of infinite-dimensional states in the OAM and angle representations.

Example: States of photons in parametric down-conversion

As an illustrative application, we compute P_∞ of photons produced from parametric down-conversion (PDC) of a Gaussian pump field. By virtue of OAM conservation, the two-photon signal-idler state measured by a detection system sensitive only to the OAM index is known to take the form $|\psi_2\rangle = \sum_l \sqrt{S_l}|l\rangle_s|-l\rangle_i$, where $S_l = S_{-l}$ and $\sum_l S_l = 1$ [32]. The individual signal and idler photons are described by the reduced density operator $\rho = \mathrm{Tr}_i(|\psi\rangle\langle\psi|) = \mathrm{Tr}_s(|\psi\rangle\langle\psi|)$, where $\mathrm{Tr}_{i(s)}$ denotes a partial trace over the idler (signal) photon. The state ρ has the diagonal form

$$\rho = \sum_{l=-\infty}^{+\infty} S_l|l\rangle\langle l|. \tag{6.24}$$

The distribution of the probabilities S_l is referred to as the angular Schmidt spectrum of the two-photon entangled state [77, 92]. The angular Schmidt number $K_a = 1/\sum_l S_l^2$ is a useful measure for quantifying the effective dimensionality of the entangled state. Using Equation (6.18), we compute P_∞ of ρ and obtain

$$P_\infty = \sqrt{\mathrm{Tr}(\rho^2)} = \sqrt{\sum_{l=-\infty}^{+\infty} S_l^2} = \frac{1}{\sqrt{K_a}}. \tag{6.25}$$

Thus, P_∞ of the individual photons is inversely proportional to the square root of the angular Schmidt number of the two-photon state. We expect P_∞ to be useful for studies characterizing OAM-entangled states produced from PDC [37, 115, 131].

6.2.2 Photon number

We now consider the infinite-dimensional photon number representation of light fields. It is known that like OAM and angle, the photon number and optical phase are conjugate physical observables. The difference is that while the OAM operator eigenvalues can take all integer values from $-\infty$ to $+\infty$, the photon number operator eigenvalues can take only integer values from 0 to ∞. In their construction of a Hermitian phase operator, Pegg and Barnett have developed a proper formalism for photon number and optical phase representations [215, 214]. Therefore, the formulation of P_∞ for states in the photon number representation can be obtained in an entirely analogous manner as for the OAM-angle case.

Consider a general state expressed in the photon number representation as

$$\rho = \sum_{n=0}^{\infty} \sum_{n'=0}^{\infty} a_{nn'} |n\rangle\langle n'|, \tag{6.26}$$

where $|n\rangle$ for $n = 0, 1, ..., \infty$ are the eigenstates of the photon number operator. Following the Pegg-Barnett procedure, we now consider the finite-dimensional vector space spanned by the vectors $|n\rangle$, where $n = 0, 1, ..., D$ with D being an arbitrarily large integer. Using Equation (6.1) to compute the intrinsic coherence P_{D+1} of ρ and taking the limit of s tending to infinity, we obtain

$$P_\infty = \lim_{D\to\infty} \sqrt{\frac{D+1}{D}\Big[\sum_{n=0}^{D}\sum_{n'=0}^{D} |a_{nn'}|^2 - \frac{1}{D+1}\Big]}. \tag{6.27}$$

We will now restrict our attention to physical states. As defined in Ref. [214], a physical state is one which can be generated from the vacuum through a finite interaction with a finite energy source for a finite time. For such a state, $a_{nn'} = 0$ for $n, n' > K$, where K is arbitrarily large but still smaller than D. Moreover, such a state must be normalizable such that $\mathrm{Tr}(\rho) = \sum_{n=0}^{\infty} a_{nn} = 1$. Using Equation (6.27)

for a physical state, we obtain

$$P_\infty = \sqrt{\sum_{n=0}^{\infty}\sum_{n'=0}^{\infty}|a_{nn'}|^2} = \sqrt{\mathrm{Tr}(\rho^2)}. \tag{6.28}$$

Using the above equation, we can compute the intrinsic coherence P_∞ for physical states in the photon number representation.

Example: Single-mode thermal state

For purposes of illustration, we now compute the intrinsic coherence of a single-mode thermal field. Such a field is represented in the photon number basis as (see section 1.5 of [216])

$$\rho = \sum_{n=0}^{\infty}(1 - e^{-\beta\hbar\omega})e^{-n\beta\hbar\omega}|n\rangle\langle n|, \tag{6.29}$$

where $\mathrm{Tr}(\rho) = 1$. We have denoted $\beta = 1/k_B T$, where k_B is Boltzmann's constant and T is the effective temperature for the field. Using Equation (6.28), we compute P_∞ for ρ to obtain

$$P_\infty = \sqrt{\mathrm{Tr}(\rho^2)} = \sqrt{\frac{1 - e^{-\beta\hbar\omega}}{1 + e^{-\beta\hbar\omega}}} = \sqrt{\tanh\left(\frac{\beta\hbar\omega}{2}\right)}. \tag{6.30}$$

We notice that in the limit of $T \to 0$ or $\beta \to \infty$ where ρ is the pure vacuum state, we have $P_\infty = 1$. On the other hand, in the limit of $T \to \infty$ or $\beta \to 0$ where ρ represents an incoherent mixture of all possible number states with equal probabilities, we have $P_\infty = 0$.

6.3 Position and momentum representations

6.3.1 Improper Representation

We shall now consider the infinite-dimensional continuous-variable position and momentum representations. For conceptual clarity, we present our analysis for a one-dimensional configuration space labeled by the co-ordinate x, whose corresponding

canonical momentum space is labeled by the co-ordinate p. A general state ρ in the position representation is written as

$$\rho = \int_{-\infty}^{+\infty} \int_{-\infty}^{+\infty} G(x, x') \, |x\rangle\langle x'| \, \mathrm{d}x \, \mathrm{d}x'. \tag{6.31}$$

Similarly, in the momentum representation ρ takes the general form

$$\rho = \int_{-\infty}^{+\infty} \int_{-\infty}^{+\infty} \Gamma(p, p') \, |p\rangle\langle p'| \, \mathrm{d}p \, \mathrm{d}p', \tag{6.32}$$

where the Fourier relation between position and momentum representations implies

$$\Gamma(p, p') = \frac{1}{2\pi\hbar} \iint_{-\infty}^{+\infty} G(x, x') \, e^{-i(px - p'x')/\hbar} \, \mathrm{d}x \, \mathrm{d}x'. \tag{6.33}$$

The continuous matrix elements $G(x, x')$ and $\Gamma(p, p')$ represent the cross-correlation functions in the position and momentum representations, respectively. We seek a formulation of P_∞ of ρ in terms of $G(x, x')$ and $\Gamma(p, p')$. To the best of our knowledge, a Pegg-Barnett-type formalism for position and momentum has not been constructed so far. In what follows, we develop such a formalism using a strategy similar to the one adopted by Pegg and Barnett for OAM-angle and number-phase pair of variables. An important distinction is that in contrast with the OAM-angle and number-phase pairs, the position-momentum pair has both the physical observables being continuous and unbounded.

6.3.2 Construction of a Proper Representation

Consider an arbitrarily-large but finite region $[-p_{\max}, p_{\max}]$ in momentum space. We sample $(2D + 1)$ equally-spaced momentum values p_j in this region, where $j = -D, ..., 0, ..., D$, with D also being arbitrarily large but finite. The spacing between consecutive values is $\Delta p = p_{\max}/D$, which is made arbitrarily close to zero. Using the $(2D+1)$ eigenstates $|p_j\rangle$ corresponding to the eigenvalues $p_j = j\Delta p$ of the momentum operator, we will develop a consistent $(2D + 1)$-dimensional proper representation

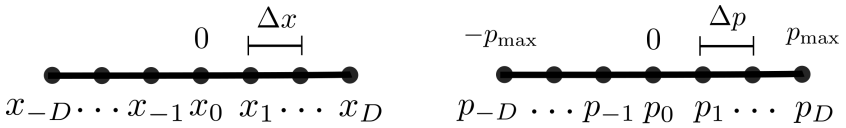

Figure 6.2: In the proper representation that we construct in this chapter, the position eigenvectors $|x_m\rangle$ for $m = -D, ..., 0, ...D$, and momentum eigenvectors $|p_j\rangle$ for $j = -D, ..., 0, ..., D$ span a $(2D + 1)$-dimensional space. In order to derive P_∞ for an infinite-dimensional state ρ in the position and momentum representations, we first calculate P_{2D+1} and take the limit of $D \to \infty$ and $p_{\max} \to \infty$ such that $1/\Delta p = D/p_{\max} \to \infty$ at the end of the calculation.

for position and momentum. We will then use this representation to compute P_{2D+1} of a general state, and then take the limit of $D \to \infty$ and $p_{\max} \to \infty$, subject to the condition that $1/\Delta p = D/p_{\max} \to \infty$ to obtain the expression for P_∞.

We note that a momentum operator $\hat{p}$ must be a generator of translations in position space. Therefore, a position state $|x\rangle$ must satisfy [212]

$$\exp\left(-i\hat{p}\eta/\hbar\right)|x\rangle = |x + \eta\rangle. \tag{6.34}$$

If we define $|x_0\rangle$ as the state corresponding to the position zero, then

$$|x\rangle = \exp\left(-i\hat{p}x/\hbar\right)|x_0\rangle. \tag{6.35}$$

Now, similarly a position operator $\hat{x}$ must be a generator of translations in momentum space. This implies that

$$\exp\left(+ip_k\hat{x}/\hbar\right)|p_j\rangle = |p_{j+k}\rangle, \tag{6.36}$$

where the translations are cyclic such that $\exp\left(ip_1\hat{x}/\hbar\right)|p_D\rangle = |p_{-D}\rangle$. In direct analogy with the derivation of Equation (6.8), we can use equations (6.35) and (6.36) to show that the position state is given by

$$|x\rangle = \sum_{j=-D}^{+D} \frac{e^{-ip_j x/\hbar}}{\sqrt{2D+1}}|p_j\rangle. \tag{6.37}$$

We now note that

$$\begin{aligned}\langle x|x'\rangle &= \sum_{j=-D}^{+D} \frac{e^{+ij(x-x')\Delta p/\hbar}}{(2D+1)} \\ &= \frac{1}{(2D+1)} \frac{\sin\left[(2D+1)(x-x')\Delta p/2\hbar\right]}{\sin\left[(x-x')\Delta p/2\hbar\right]}.\end{aligned} \tag{6.38}$$

This implies that $\langle x|x'\rangle = 0$ only when $(x - x') = 2\pi\hbar n/\{(2D+1)\Delta p\}$, where n is a non-zero integer. This allows us to select an orthonormal basis $\{|x_m\rangle\}$, where

$$x_m = \frac{2\pi m\hbar}{(2D+1)\Delta p} \quad (m = -D, ..., 0, ..., D) \tag{6.39}$$

These position eigenvalues are equally-spaced points from x_{-D} to x_D with a spacing of $\Delta x = 2\pi\hbar/\{(2D+1)\Delta p\}$. We note that by orthonormality and completeness, the basis vectors $|x_m\rangle$ and $|p_j\rangle$ satisfy

$$\langle x_m|x_n\rangle = \delta_{mn}, \qquad \langle p_j|p_k\rangle = \delta_{jk}, \tag{6.40a}$$

$$\sum_{m=-D}^{+D} |x_m\rangle\langle x_m| = 1, \qquad \sum_{j=-D}^{+D} |p_j\rangle\langle p_j| = 1. \tag{6.40b}$$

Using equations (6.37) and (6.39), we find that the basis vectors have the form

$$|x_m\rangle = \frac{1}{\sqrt{2D+1}} \sum_{j=-D}^{+D} e^{-i2\pi mj/(2D+1)} |p_j\rangle, \tag{6.41a}$$

$$|p_j\rangle = \frac{1}{\sqrt{2D+1}} \sum_{m=-D}^{+D} e^{+i2\pi mj/(2D+1)} |x_m\rangle. \tag{6.41b}$$

We have derived a finite-dimensional proper representation for position and momentum. For clarity, we depict the representation in Figure 2. In order to prove that it is a physically consistent representation, we must now show that the commutator $[\hat{x}, \hat{p}]$ in this representation is physically indistinguishable from the improper commutation relation $[\hat{x}, \hat{p}] = i\hbar$. To that end, we note that the operators $\hat{x}$ and $\hat{p}$ can

be represented as

$$\hat{x} = \sum_{m=-D}^{+D} x_m |x_m\rangle\langle x_m| \,, \tag{6.42a}$$

$$\hat{p} = \sum_{j=-D}^{+D} p_j |p_j\rangle\langle p_j|. \tag{6.42b}$$

Using the above equations, we find that the commutator $[\hat{x}, \hat{p}]$ has the following matrix elements in the position and momentum bases:

$$\langle x_m|[\hat{x},\hat{p}]|x_n\rangle = \frac{2\pi\hbar(m-n)}{(2D+1)^2} \sum_{j=-D}^{+D} j\, e^{i2\pi(m-n)j/(2D+1)}, \tag{6.43a}$$

$$\langle p_j|[\hat{x},\hat{p}]|p_k\rangle = \frac{2\pi\hbar(k-j)}{(2D+1)^2} \sum_{m=-D}^{+D} m\, e^{-i2\pi(j-k)m/(2D+1)}. \tag{6.43b}$$

We note that the diagonal elements $\langle x_m|[\hat{x},\hat{p}]|x_m\rangle$ and $\langle p_j|[\hat{x},\hat{p}]|p_j\rangle$ are all zero. As a result, the trace of $[\hat{x}, \hat{p}]$ is zero, as expected for any commutator of finite-dimensional operators. We can evaluate the above equations (6.43) in the limit $D \to \infty$ using Mathematica [217] to obtain the effective forms

$$[\hat{x},\hat{p}] = i\hbar\Big[1 - \sum_{m,n} \cos\{(m-n)\pi\}|x_m\rangle\langle x_n|\Big], \tag{6.44a}$$

$$[\hat{x},\hat{p}] = i\hbar\Big[1 - \sum_{j,k} \cos\{(j-k)\pi\}|p_j\rangle\langle p_k|\Big]. \tag{6.44b}$$

Using $\cos\{(m-n)\pi\} = \{e^{+i(m-n)\pi} + e^{-i(m-n)\pi}\}/2$ and equations (6.41), it can be shown that Equations (6.44) are equivalent to

$$[\hat{x},\hat{p}] = \lim_{D\to\infty} i\hbar\Big[1 - (2D+1)|x_{(D+\frac{1}{2})}\rangle\langle x_{(D+\frac{1}{2})}|\Big], \tag{6.45a}$$

$$[\hat{x},\hat{p}] = \lim_{D\to\infty} i\hbar\Big[1 - (2D+1)|p_{(D+\frac{1}{2})}\rangle\langle p_{(D+\frac{1}{2})}|\Big]. \tag{6.45b}$$

Now we note that any physical state will be localized to a finite region in both position and momentum space. As a result, when the expectation value of $[\hat{x}, \hat{p}]$ is evaluated for such a state, the contributions from the second term in the above

expressions will vanish. In this limit, we recover the usual commutator $[\hat{x}, \hat{p}] = i\hbar$ for infinite-dimensional operators. Thus, we have constructed a consistent proper finite-dimensional representation for position and momentum.

6.3.3 Derivation of the expression for P_∞

Following the Pegg-Barnett procedure, the state ρ from Equation (6.31) can be written in the proper position representation as

$$\rho = \lim_{D\Delta x\to\infty} \lim_{\Delta x\to 0} \sum_{m=-D}^{+D} \sum_{n=-D}^{+D} \bar{G}_{x_m x_n} |x_m\rangle\langle x_n|. \tag{6.46}$$

Similarly, ρ can be written in the momentum proper representation as

$$\rho = \lim_{D\Delta p\to\infty} \lim_{\Delta p\to 0} \sum_{j=-D}^{+D} \sum_{k=-D}^{+D} \bar{\Gamma}_{p_j p_k} |p_j\rangle\langle p_k|, \tag{6.47}$$

where using equations (6.40) and (6.46), we find

$$\bar{\Gamma}_{p_j p_k} = \frac{1}{2D+1} \sum_{m=-D}^{+D} \sum_{n=-D}^{+D} \bar{G}_{x_m x_n} e^{-i2\pi(jm-kn)/(2D+1)}. \tag{6.48}$$

As ρ is normalized, we have $\sum_{m=-D}^{+D} \bar{G}_{x_m x_m} = \sum_{j=-D}^{+D} \bar{\Gamma}_{p_j,p_j} = 1$. We shall now compute P_∞ for ρ by first computing P_{2D+1} in terms of $\bar{G}_{x_m x_n}$ and $\bar{\Gamma}_{p_j p_k}$, and then evaluating its limiting value as $D \to \infty$ and $p_{\max} \to \infty$, subject to the constraint $D/p_{\max} \to \infty$. These limits together ensure that $\Delta x \to 0$ and $\Delta p \to 0$, such that $D\Delta x \to \infty$ and $D\Delta p \to \infty$. Thus, we can compute P_∞ in terms of $\bar{G}_{x_m x_n}$ as

$$P_\infty = \lim_{D\Delta x\to\infty} \lim_{\Delta x\to 0} \sqrt{\frac{2D+1}{2D}\Big[\sum_{m,n} |\bar{G}_{x_m x_n}|^2 - \frac{1}{2D+1}\Big]}. \tag{6.49}$$

Similarly in terms of $\bar{\Gamma}_{p_j p_k}$, we have

$$P_\infty = \lim_{D\Delta p\to\infty} \lim_{\Delta p\to 0} \sqrt{\frac{2D+1}{2D}\Big[\sum_{j,k} |\bar{\Gamma}_{p_j p_k}|^2 - \frac{1}{2D+1}\Big]}. \tag{6.50}$$

Now for physical states P_∞ can be quantified in terms of the functions $G(x, x')$ and $\Gamma(p, p')$ of Equations (6.31) and (6.32). To that end, we must now obtain the relation between $G(x, x')$ and $\Gamma(p, p')$ and their finite-dimensional counterparts $\bar{G}_{x_m x_n}$ and $\bar{\Gamma}_{p_j p_k}$, respectively. Using a line of reasoning similar to the one used previously for arriving at Equation (6.22), one can show that

$$G(x_m, x_n) = \lim_{D\Delta x\to\infty} \lim_{\Delta x\to 0} \bar{G}_{x_m x_n}/\Delta x, \tag{6.51a}$$

$$\Gamma(p_j, p_k) = \lim_{D\Delta p\to\infty} \lim_{\Delta p\to 0} \bar{\Gamma}_{p_j p_k}/\Delta p. \tag{6.51b}$$

Upon substituting Equation (6.51a) in Equation (6.49), and Equation (6.51b) in Equation (6.50) and simplifying, we obtain

$$P_\infty = \lim_{D\Delta x\to\infty} \lim_{\Delta x\to 0} \sqrt{\sum_{m,n=-D}^{+D} |G(m\Delta x, n\Delta x)|^2 \, \Delta x \, \Delta x},$$

$$P_\infty = \lim_{D\Delta p\to\infty} \lim_{\Delta p\to 0} \sqrt{\sum_{j,k=-D}^{+D} |\Gamma(j\Delta p, k\Delta p)|^2 \, \Delta p \, \Delta p}.$$

We now note that any physical state must have a finite extent in position and momentum space. This implies that $G(m\Delta x, n\Delta x) = 0$ for $m\Delta x, n\Delta x$ that lie outside a finite region, say $[-\zeta, \zeta]$ in position space, and $\Gamma(j\Delta p, k\Delta p) = 0$ for $j\Delta p, k\Delta p$ that lie outside a finite region, say $[-\eta, \eta]$ in momentum space. As $D\Delta x$ and $D\Delta p$ can always be chosen to be larger than ζ and η, respectively, the above equations for P_∞ can be expressed in integral form as [1]

$$P_\infty = \sqrt{\iint_{-\infty}^{+\infty} |G(x, x')|^2 \, \mathrm{d}x \, \mathrm{d}x'} = \sqrt{\mathrm{Tr}(\rho^2)}, \tag{6.52a}$$

$$P_\infty = \sqrt{\iint_{-\infty}^{+\infty} |\Gamma(p, p')|^2 \, \mathrm{d}p \, \mathrm{d}p'} = \sqrt{\mathrm{Tr}(\rho^2)}, \tag{6.52b}$$

[1] The Riemann integral is strictly defined only for bounded intervals. Therefore, the summation $\lim_{N\to\infty} \lim_{\Delta x\to 0} \sum_{n=-N}^{+N} f(n\Delta x)\Delta x$, where $N\Delta x \to \infty$, is first identified with the Cauchy principal value $\lim_{a\to\infty} \int_{-a}^{a} f(x)\,\mathrm{d}x$, which is then identified with the improper integral $\int_{-\infty}^{+\infty} f(x)\,\mathrm{d}x$.

where ρ is normalized such that $\mathrm{Tr}(\rho) = \int_{-\infty}^{+\infty} G(x,x)\,\mathrm{d}x = \int_{-\infty}^{+\infty} \Gamma(p,p)\,\mathrm{d}p = 1$. Thus, using equations (6.52), we can compute P_∞ for physical states in the position and momentum representations.

Another representation of states that is widely employed in continuous-variable quantum information [203, 204, 205] and optical state tomography [218] is the phase-space representation in terms of the Wigner function $W(x,p)$, which is given by [219]

$$W(x,p) = \frac{1}{2\pi\hbar}\int_{-\infty}^{+\infty} \langle x + \frac{y}{2}|\hat{\rho}|x - \frac{y}{2}\rangle e^{-ipy/\hbar}\,\mathrm{d}y, \tag{6.53}$$

where $\int_{-\infty}^{+\infty}\int_{-\infty}^{+\infty} W(x,p)\,\mathrm{d}x\,\mathrm{d}p = 1$. Using Equation (6.52a) and Equation (6.53), one can show that P_∞ can be expressed in terms of $W(x,p)$ as

$$P_\infty = \sqrt{2\pi\hbar \iint_{-\infty}^{+\infty} W^2(x,p)\,\mathrm{d}x\,\mathrm{d}p} = \sqrt{\mathrm{Tr}(\rho^2)}. \tag{6.54}$$

Thus, the intrinsic coherence P_∞ of a physical state ρ can be computed using equations (6.52) or (6.54), which are all equal to $\sqrt{\mathrm{Tr}(\rho^2)}$.

Example: Gaussian-Schell field

As an illustrative example, we now compute P_∞ for a light field whose transverse spatial profile is described by the two-dimensional version of the Gaussian-Schell model [220]. Such a field can be represented in the transverse spatial representation using the state

$$\rho = \int\int G(\boldsymbol{\rho}_1, \boldsymbol{\rho}_2)|\boldsymbol{\rho}_1\rangle\langle\boldsymbol{\rho}_2|\,\mathrm{d}\boldsymbol{\rho}_1\,\mathrm{d}\boldsymbol{\rho}_2, \tag{6.55}$$

where the spatial cross-correlation function $G(\boldsymbol{\rho}_1, \boldsymbol{\rho}_2)$ is given by

$$G(\boldsymbol{\rho}_1, \boldsymbol{\rho}_2) = \frac{1}{2\pi\sigma_s^2}\exp\Big\{-\frac{({\boldsymbol{\rho}_1}^2 + {\boldsymbol{\rho}_2}^2)}{4\sigma_s^2}\Big\}\exp\Big\{-\frac{|\boldsymbol{\rho}_1 - \boldsymbol{\rho}_2|^2}{2\sigma_g^2}\Big\}. \tag{6.56}$$

Here we have denoted $\boldsymbol{\rho}_1 \equiv (x_1, y_1)$ and $\boldsymbol{\rho}_2 \equiv (x_2, y_2)$. The quantities σ_s and σ_g are the rms spatial width and rms spatial coherence width of the beam, respectively. We have normalized ρ so that $\mathrm{Tr}(\rho) = \int G(\boldsymbol{\rho},\boldsymbol{\rho})\,\mathrm{d}\boldsymbol{\rho} = 1$. The intrinsic coherence

P_∞ of ρ is simply the two-dimensional generalization of Equation (6.52a) given by

$$P_\infty = \sqrt{\mathrm{Tr}(\rho^2)} = \sqrt{\int\int |G(\boldsymbol{\rho}_1, \boldsymbol{\rho}_2)|^2 \, \mathrm{d}\boldsymbol{\rho}_1 \, \mathrm{d}\boldsymbol{\rho}_2}. \tag{6.57}$$

Substituting Equation (6.56) into the above equation and evaluating the integrals, we obtain

$$P_\infty = \frac{1}{\sqrt{1 + 4\sigma_s^2/\sigma_g^2}} = \frac{1}{\sqrt{1 + 4/q^2}}. \tag{6.58}$$

The parameter $q \equiv \sigma_g/\sigma_s$ is often referred to as the degree of global coherence of the field (see Section 5.6.4 of Ref. [3]). Here we notice that in the limit $q \to \infty$ corresponding to a perfectly spatially coherent field, we have $P_\infty = 1$, whereas in the limit $q \to 0$, we have $P_\infty = 0$.

6.4 Summary

We have extended the intrinsic coherence measure P_N, defined for N-dimensional states, to the $N \to \infty$ limit to obtain the corresponding measure P_∞ for infinite-dimensional states. For states in the OAM-angle and photon number representations, we used the existing Pegg-Barnett formalisms for this purpose, whereas for states in the position and momentum representations, we explicitly developed a Pegg-Barnett-type formalism. We have shown that for any normalized physical state ρ in these representations, the measure P_∞ can be computed as $P_\infty = \sqrt{\mathrm{Tr}(\rho^2)}$.

We now note that an equivalent measure, termed as the "overall degree of coherence", had been defined in the context of classical light fields by Bastiaans in a series of papers in the 1980s [221, 222, 223, 224, 225]. In addition, the closely related quantity $\mathrm{Tr}(\rho^2)$, which is often referred to as purity, has also been used extensively in the field of quantum information [16]. Indeed, studies have discussed the close relationship between the notions of purity of quantum states and coherence of partially coherent fields [226, 227].

We expect P_∞ to have wide applicability in the fields of optics and quantum in-

formation. In optical communication protocols that employ superpositions of OAM states, it would now be possible to quantify the degradation of coherence in long distance transmission in a basis-invariant manner [202, 112]. In the photon number representation, P_∞ can be relevant for studies on squeezed states [228, 229, 230, 231] and general Gaussian states [203, 204, 205] for continuous-variable protocols. In the position and momentum representations, P_∞ can be useful for quantifying the effects of turbulence on the intrinsic spatial coherence of light [206, 207, 208]. In addition, P_∞ can be used to quantify decoherence in open quantum systems [209, 210, 211].

Chapter 7

Conclusions and Discussions

In this thesis, we have presented some experimental and theoretical studies on the characterization of the correlations of the signal-idler photons produced from parametric down-conversion (PDC) and their relationship to the intrinsic correlations of the pump photon in the angular, polarization, and temporal degrees of freedom.

We first considered the orbital angular momentum (OAM) or angular degree of freedom of photons. The OAM basis of photons – by virtue of being discrete and infinite-dimensional – provides a natural platform for preparing and manipulating high-dimensional quantum states. We focused on the problem of measuring the OAM spectrum of a beam of photons that is described as an incoherent mixture of different OAM-carrying modes. The previously existing techniques for measuring the OAM spectrum suffered from issues such as poor scaling with spectral width, stringent stability requirements, and too much loss. Furthermore, most techniques measured only a post-selected part of the true spectrum. We demonstrated that a Mach-Zender interferometer with the simple-yet-crucial feature of having an odd and even number of mirrors in the two arms results in the angular coherence function of the input field being directly encoded in the output interferogram. As a result, the OAM spectrum of the input field can be obtained directly through an inverse Fourier transform of the angular coherence function. By performing proof-of-concept demonstrations with laboratory-synthesized fields with known spectra, we showed that the interferometer provides a robust and efficient technique for measuring the

true OAM spectrum of a field in a single-shot acquisition. In the absence of noise, a single-shot acquisition is sufficient, whereas in the presence of noise, two shots are required for the purpose.

We then reported our experimental and theoretical characterization of the angular Schmidt spectrum of the entangled two-photon state produced from PDC of a Gaussian pump. The angular Schmidt spectrum completely characterizes the angular correlations between the signal and idler photons. The existing theoretical procedures for computing the spectrum were computationally cumbersome and suffered from convergence problems. Also, experimental measurements of the Schmidt spectrum measured only a post-selected part of the true spectrum or required coincidence detections with stringent alignment conditions or both. We first derived an analytic formula that is computationally efficient and yields the true Schmidt spectrum without any convergence problems. Next, by exploiting the fact that the OAM spectrum of the one-photon field comprising the signal and idler photons is identical to the angular Schmidt spectrum, we used the single-shot technique to experimentally measure the true angular Schmidt spectrum without the need for coincidence detections. We presented a complete characterization of the true Schmidt spectrum of the signal-idler photons from collinear to non-collinear emission regimes with excellent agreement with theoretical predictions. In the non-collinear regime, we have measured the widest-ever spectrum measured so far with an angular Schmidt number of 233.

We then theoretically investigated how the intrinsic correlations of the pump photon are transferred through the process of PDC to eventually manifest as entanglement in the polarization and temporal degrees of freedom. In the polarization degree of freedom, we demonstrated that independent of the details of the generation scheme, the degree of polarization of the pump photon predetermines the maximum achievable polarization entanglement of two-qubit signal-idler states. In the temporal degree of freedom, following up on previous studies that considered the specific cases of a continuous-wave pump and a transform-limited pulsed pump, we

theoretically demonstrated that even for a completely general pump, the temporal correlations of the pump photon are entirely transferred to the signal-idler photons. We further showed that the energy-time entanglement of two-qubit signal-idler states as quantified by concurrence is bounded by the degree of temporal coherence of the pump photon.

Lastly, we presented our theoretical formulation of a basis-invariant measure of coherence for infinite-dimensional states. For two-dimensional states, the degree of polarization P_2 is a well-accepted basis-invariant measure of coherence. Until recently, although some measures had been proposed, no unique measure that possesses all the interpretations of P_2 was established for higher-dimensional states. As a result, it was not possible to study the intrinsic correlations of the pump and signal-idler photons in PDC in the OAM, photon number, position and momentum degree of freedoms in a basis-invariant manner. Recently, a study demonstrated an analogous measure P_N for finite-N-dimensional states to possess all the interpretations of the two-dimensional counterpart P_2. We used the Pegg-Barnett procedure to generalize this measure to the $N \to \infty$ limit to quantify the intrinsic coherence of infinite-dimensional states. For states in the OAM and photon number representations, we used the existing Pegg-Barnett formalisms, whereas for states in the position and momentum representations, we explicitly constructed a Pegg-Barnett-type formalism. We showed that for any normalized physical state ρ in these representations, the intrinsic degree of coherence P_∞ of a state ρ is given by $P_\infty = \sqrt{\mathrm{Tr}(\rho^2)}$.

We will now briefly discuss the future outlook of the work presented in this thesis. Firstly, we expect that the single-shot OAM spectrum measurement technique – which applies only to states that are diagonal in the OAM basis – may be generalized to measure pure and arbitrary mixed states of photons in the OAM basis. In other words, this work could potentially lead to efficient schemes for high-dimensional quantum state tomography in the OAM basis. Also, the idea of co-ordinate inversion exploited in the single-shot technique is quite general, and can be adapted to

measure correlations in other degrees of freedom as well. For instance, a recent study employed such a co-ordinate inversion to measure the transverse spatial coherence of photons [123].

Next, we expect our experimental and theoretical characterizations of the angular Schmidt spectrum from PDC to be relevant for information processing protocols that employ OAM-entangled states produced from PDC. Our studies could enable a precise tuning of the dimensionality of the entangled state by varying the different physical parameters of the pump field and the crystal medium. Moreover, as demonstrated by our studies, the single-shot technique can be used to efficiently and accurately measure such states.

Finally, our work on the propagation of correlations in PDC and the quantification of the intrinsic coherence of infinite-dimensional states also opens up interesting avenues for future research. Our studies on the transfer of correlations in PDC in the polarization and temporal degrees of freedom contribute to an existing program that attempts to understand how the intrinsic correlations of the pump photon are transferred to eventually manifest as nonlocal correlations in PDC. This program could eventually lead to a physically intuitive picture of entanglement. In addition, our work on the quantification of intrinsic coherence of infinite-dimensional states could now enable studies on the transfer of correlations in the OAM-angle, photon-number and position-momentum degrees of freedom.

Appendix A

Theory of asymmetric OAM spectrum measurement

In this appendix, we present the theoretical analysis of single-shot technique for the case of an asymmetric OAM spectrum, i.e, when $S_l \neq S_{-l}$. We will describe two distinct ways in which an asymmetric OAM spectrum can be measured: one requires two acquisitions for $\delta = \delta_c$ and $\delta = \delta_d$, such that $\delta_c + \delta_d = \pi/2$; and the other requires four acquisitions corresponding to $\delta = 0, \pi/2, \pi$ and $3\pi/2$.

Just as in the case of symmetric spectrum, let us assume that the measured azimuthal intensity $\bar{I}^{\delta}_{\text{out}}(\phi)$ at the output contains the noise term $I^{\delta}_{\text{n}}(\phi)$ in addition to the signal $I_{\text{out}}(\phi)$. Thus

$$\begin{aligned}\bar{I}^{\delta}_{\text{out}}(\phi) &= I^{\delta}_{\text{n}}(\phi) + I_{\text{out}}(\phi) \\ &= I^{\delta}_{\text{n}}(\phi) + \frac{k_1 + k_2}{2\pi} + \gamma\sqrt{k_1 k_2}[W(2\phi)e^{-i\delta} + \text{c.c.}]. \end{aligned} \tag{A.1}$$

A.1 Two-shot method

Now, suppose we have two interferogram measured at two different values of δ, say at δ_c and δ_d. The difference $\Delta\bar{I}_{\text{out}}(\phi)$ in the intensities of the two interferogram is

then given by

$$\begin{aligned}\Delta\bar{I}_{\rm out}(\phi) &= \bar{I}^{\delta_c}_{\rm out}(\phi) - \bar{I}^{\delta_d}_{\rm out}(\phi) \\ &= \Delta I_{\rm n}(\phi) + \gamma\sqrt{k_1 k_2}[W(2\phi)e^{-i\delta_c} + W^*(2\phi)e^{i\delta_c} \\ &\qquad - W(2\phi)e^{-i\delta_d} - W^*(2\phi)e^{i\delta_d}], \end{aligned} \tag{A.2}$$

where $\Delta I_{\rm n}(\phi) = I^{\delta_c}_{\rm n}(\phi) - I^{\delta_d}_{\rm n}(\phi)$ is the difference in the noise intensities. Unlike in the case of symmetric spectrum, $\Delta\bar{I}_{\rm out}(\phi)$ is not proportional to the angular coherence function $W(2\phi)$. Multiplying each side of Equation (A.2) by $e^{i2l\phi}$ and using the angular Wiener-Khintchine relation $S_l = \int_{-\pi}^{\pi} W(2\phi)e^{i2l\phi}d(2\phi)$, we obtain

$$\begin{aligned}\int_{-\pi}^{\pi}\Delta\bar{I}_{\rm out}(\phi)e^{i2l\phi}d(2\phi) &= \int_{-\pi}^{\pi}\Delta I_{\rm n}(\phi)(\phi)e^{i2l\phi}d(2\phi) \\ + \gamma\sqrt{k_1 k_2}[S_l e^{-i\delta_c} + S_{-l}e^{i\delta_c} - S_l e^{-i\delta_d} - S_{-l}e^{i\delta_d}]. \end{aligned} \tag{A.3}$$

Now, multiplying each side of Equation (A.2) by $e^{-i2l\phi}$ and using the angular Wiener-Khintchine relation $S_l = \int_{-\pi}^{\pi} W(2\phi)e^{i2l\phi}d(2\phi)$, we obtain

$$\begin{aligned}\int_{-\pi}^{\pi}\Delta\bar{I}_{\rm out}(\phi)e^{-i2l\phi}d(2\phi) &= \int_{-\pi}^{\pi}\Delta I_{\rm n}(\phi)(\phi)e^{-i2l\phi}d(2\phi) \\ + \gamma\sqrt{k_1 k_2}[S_{-l} e^{-i\delta_c} + S_l e^{i\delta_c} - S_{-l} e^{-i\delta_d} - S_l e^{i\delta_d}]. \end{aligned} \tag{A.4}$$

Adding Equations (A.3) and (A.4), we get

$$\begin{aligned}\int_{-\pi}^{\pi}\Delta\bar{I}_{\rm out}(\phi)\cos(2l\phi)d(2\phi) &= \int_{-\pi}^{\pi}\Delta I_{\rm n}(\phi)\cos(2l\phi)d(2\phi) \\ &\quad + \gamma\sqrt{k_1 k_2}(S_l + S_{-l})(\cos\delta_c - \cos\delta_d). \end{aligned} \tag{A.5}$$

Subtracting Equation (A.4) from Equation (A.3), we get

$$\begin{aligned}\int_{-\pi}^{\pi}\Delta\bar{I}_{\rm out}(\phi)\sin(2l\phi)d(2\phi) &= \int_{-\pi}^{\pi}\Delta I_{\rm n}(\phi)\sin(2l\phi)d(2\phi) \\ &\quad - \gamma\sqrt{k_1 k_2}(S_l - S_{-l})(\sin\delta_c - \sin\delta_d). \end{aligned} \tag{A.6}$$

Now the question is how should one define the spectrum so that the defined spectrum becomes proportional to the true spectrum. Upon inspection we find that for the non-symmetric case it is not possible to define the spectrum the way we did it in the case of symmetric spectrum. Nevertheless, in the special situation in which $\delta_c + \delta_d = \pi/2$, it is possible to define the measured spectrum just like we did it in the symmetric case. Let us consider the situation when $\delta_c = \theta$ and $\delta_d = \pi/2 - \theta$ such that $\delta_c + \delta_d = \pi/2$. Equations (A.5) and (A.6) for this situation can be written as

$$\int_{-\pi}^{\pi} \Delta\bar{I}_{\rm out}(\phi)\cos(2l\phi)d(2\phi) = \int_{-\pi}^{\pi} \Delta I_{\rm n}(\phi)\cos(2l\phi)d(2\phi) + \gamma\sqrt{k_1k_2}(S_l + S_{-l})(\cos\theta - \sin\theta). \tag{A.7}$$

and

$$\int_{-\pi}^{\pi} \Delta\bar{I}_{\rm out}(\phi)\sin(2l\phi)d(2\phi) = \int_{-\pi}^{\pi} \Delta I_{\rm n}(\phi)\sin(2l\phi)d(2\phi) + \gamma\sqrt{k_1k_2}(S_l - S_{-l})(\cos\theta - \sin\theta). \tag{A.8}$$

Adding Equations (A.7) and (A.8), we get

$$\begin{aligned}&\int_{-\pi}^{\pi} \Delta\bar{I}_{\rm out}(\phi)\left[\cos(2l\phi) + \sin(2l\phi)\right]d(2\phi)\\ &= \int_{-\pi}^{\pi} \Delta I_{\rm n}(\phi)\left[\cos(2l\phi) + \sin(2l\phi)\right]d(2\phi)\\ &\qquad + 2\gamma\sqrt{k_1k_2}(\cos\theta - \sin\theta)S_l.\end{aligned} \tag{A.9}$$

So, now if we define the measured spectrum $\bar{S}_l$ to be

$$\bar{S}_l \equiv \int_{-\pi}^{\pi} \Delta\bar{I}_{\rm out}(\phi)\left[\cos(2l\phi) + \sin(2l\phi)\right]d(2\phi)$$

we get,

$$\bar{S}_l = \int_{-\pi}^{\pi} \Delta I_{\rm n}(\phi) \left[\cos(2l\phi) + \sin(2l\phi)\right] d\phi + 2\gamma\sqrt{k_1 k_2}(\cos\theta - \sin\theta) S_l. \tag{A.10}$$

In situations in which the noise neither has any explicit functional dependence on δ nor has any shot-to-shot variation, we have $\Delta I_{\rm n}(\phi) = 0$. Thus the defined spectrum $\bar{S}_l$ becomes proportional to the true spectrum S_l. We see that just as in the case of symmetric spectrum, one does not have to know the exact values of k_1, k_2, γ and θ. The only thing different in this case is that one has to take the two shots such $\delta_c + \delta_d = \pi/2$.

A.2 Four-shot method

Note that equation (A.1) can equivalently be written as

$$\begin{aligned} \bar{I}^{\delta}_{\rm out}(\phi) &= I^{\delta}_{\rm n}(\phi) + I_{\rm out}(\phi) \\ &= I^{\delta}_{\rm n}(\phi) + \frac{k_1 + k_2}{2\pi} + 2\gamma\sqrt{k_1 k_2}{\rm Re}\left[W(2\phi)e^{-i\delta}\right]. \end{aligned} \tag{A.11}$$

Consider two interferograms measured at two different values of δ, say at $\delta = 0$ and $\delta = \pi$. The difference $\Delta\bar{I}^{(r)}_{\rm out}(\phi)$ between the intensities of the two interferograms is given by

$$\begin{aligned} \Delta\bar{I}^{(r)}_{\rm out}(\phi) &= \bar{I}^{0}_{\rm out}(\phi) - \bar{I}^{\pi}_{\rm out}(\phi) \\ &= \Delta I^{(r)}_{\rm n}(\phi) + 4\gamma\sqrt{k_1 k_2}{\rm Re}\left[W(2\phi)\right], \end{aligned} \tag{A.12}$$

where $\Delta I^{(r)}_{\rm n}(\phi)$ is the difference between the noise intensities $I^{0}_{\rm n}(\phi)$ and $I^{\pi}_{\rm n}(\phi)$ for the two shots.

Similarly, consider two interferograms measured for $\delta = \pi/2$ and $\delta = 3\pi/2$. The difference $\Delta\bar{I}^{(i)}_{\rm out}(\phi)$ between the intensities of the two interferograms is given by

$$\begin{aligned}\Delta\bar{I}^{(i)}_{\rm out}(\phi) &= \bar{I}^{\pi/2}_{\rm out}(\phi) - \bar{I}^{3\pi/2}_{\rm out}(\phi) \\ &= \Delta I^{(i)}_{\rm n}(\phi) - 4\gamma\sqrt{k_1 k_2}\,{\rm Im}\left[W(2\phi)\right], \end{aligned} \tag{A.13}$$

where $\Delta I^{(i)}_{\rm n}(\phi)$ is the difference between noise intensities $I^{\pi/2}_{\rm n}(\phi)$ and $I^{3\pi/2}_{\rm n}(\phi)$ for the two shots. If both the difference noise intensities, namely $\Delta\bar{I}^{(r)}_{\rm n}(\phi)$ and $\Delta\bar{I}^{(i)}_{\rm n}(\phi)$ are identically zero, then using Equation (A.12) and Equation (A.13) we obtain

$$\Delta\bar{I}^{(r)}_{\rm out}(\phi) - i\,\Delta\bar{I}^{(i)}_{\rm out}(\phi) = 4\gamma\sqrt{k_1 k_2}\left[W(2\phi)\right]. \tag{A.14}$$

If we now define the measured spectrum $\bar{S}_l$ as

$$\bar{S}_l = \int_{-\pi}^{+\pi} \left[\Delta\bar{I}^{(r)}_{\rm out}(\phi) - i\,\Delta\bar{I}^{(i)}_{\rm out}(\phi)\right] e^{i2l\phi}\,{\rm d}\phi, \tag{A.15}$$

then from Equation(A.14) we find

$$\bar{S}_l = 4\gamma\sqrt{k_1 k_2}S_l, \tag{A.16}$$

i.e, the measured spectrum is the true OAM spectrum of the field upto an overall scaling constant. In this way, we can measure an asymmetric spectrum using the four interferograms corresponding to $\delta = 0, \pi/2, \pi$ and $3\pi/2$. Again, it is not necessary to know the precise values of k_1, k_2 and γ, which makes the technique very robust.

Finally we note that while the two-shot method is more efficient, it is experimentally difficult to acquire two interferograms precisely at δ_c and δ_d such that $\delta_c + \delta_d = \pi/2$. On the other hand, it is easier to acquire interferograms at the four values of δ, namely $0, \pi/2, \pi$, and $3\pi/2$ using precision automated translation stages or through geometric phases using waveplates.

Appendix B

Calculation of pump spectral amplitude at distance d from beam waist

In this appendix, we will derive the expression for the momentum-space pump spectral amplitude at a distance d from the beam waist. The momentum-space spectral amplitude $V(\boldsymbol{q}_p; z = -d)$ of the Gaussian pump field at the beam waist location $z = -d$ takes the form [119],

$$V(\boldsymbol{q}_p, z = -d) = C \exp\left(-\frac{|\boldsymbol{q}_p|^2 w_p^2}{4}\right), \tag{B.1}$$

where C is a constant and w_p is the beam waist size. The position-space transverse spatial amplitude profile $\tilde{V}(\boldsymbol{\rho}; z = -d)$ of the field is given by the Fourier transform relation

$$\tilde{V}(\boldsymbol{\rho}; z = -d) = \iint V(\boldsymbol{q}_p, z = -d)\, e^{-i\boldsymbol{q}_p \cdot \boldsymbol{\rho}}\, \mathrm{d}^2\boldsymbol{q}_p. \tag{B.2}$$

The field propagates in the longitudinal co-ordinate via the Fresnel diffraction integral as [232],

$$\tilde{V}(\boldsymbol{\rho}; z = 0) = \frac{e^{ik_p d}}{i\lambda_p d} \iint \tilde{V}(\boldsymbol{\rho}'; z = -d) \exp\left\{\frac{ik}{2d}|\boldsymbol{\rho} - \boldsymbol{\rho}'|^2\right\} \mathrm{d}^2\boldsymbol{\rho}'$$

If we denote the two-dimensional convolution operation by " $*$ ", then the above equation is equivalent to

$$\tilde{V}(\boldsymbol{\rho}; z=0) = \tilde{V}(\boldsymbol{\rho}; z=-d) * \tilde{h}(\boldsymbol{\rho}; d), \tag{B.3}$$

where

$$\tilde{h}(\boldsymbol{\rho}; d) = \frac{e^{ik_p d}}{i\lambda_p d} \exp\left\{\frac{ik_p|\boldsymbol{\rho}|^2}{2d}\right\}$$

Using the convolution theorem for Fourier transforms [233], it follows that

$$V(\boldsymbol{q}_p, z=0) = V(\boldsymbol{q}_p, z=-d) \times h(\boldsymbol{q}_p; d), \tag{B.4}$$

where $h(\boldsymbol{q}_p; d)$ is the Fourier transform of $\tilde{h}(\boldsymbol{\rho}; d)$, i.e,

$$\begin{aligned} h(\boldsymbol{q}_p; d) &= \iint h(\boldsymbol{\rho}; d)\, e^{i\boldsymbol{q}_p\cdot\boldsymbol{\rho}}\, \mathrm{d}^2\boldsymbol{\rho} \\ &= \frac{e^{ik_p d}}{i\lambda_p d} \iint e^{\frac{ik|\boldsymbol{\rho}|^2}{2d}}\, e^{i\boldsymbol{q}_p\cdot\boldsymbol{\rho}}\, \mathrm{d}^2\boldsymbol{\rho} \\ &= \frac{e^{ik_p d}}{i\lambda_p d} \frac{2\pi i d}{k_p} e^{-\frac{id|\boldsymbol{q}_p|^2}{2k_p}} \\ &= \frac{2\pi}{k_p\lambda_p} e^{i\left(k_p - \frac{|\boldsymbol{q}_p|^2}{2k_p}\right)d} \end{aligned} \tag{B.5}$$

Now note that using the paraxial condition $|\boldsymbol{q}_p| \ll k_p$ on $k_{pz} = \sqrt{k_p^2 - |\boldsymbol{q}_p|^2}$, we get $k_{pz} = k_p - \frac{|\boldsymbol{q}_p|^2}{2k_p}$. Using this in Equation (B.5), we get

$$h(\boldsymbol{q}_p; d) = \frac{2\pi}{k_p\lambda_p} e^{ik_{pz}d}. \tag{B.6}$$

Substituting equations (B.1) and (B.6) into Equation (B.4) and absorbing constants into C, we finally obtain

$$V(\boldsymbol{q}_p, z=0) = C \exp\left(-\frac{|\boldsymbol{q}_p|^2 w_p^2}{4}\right) e^{ik_{pz}d}. \tag{B.7}$$

Bibliography

[1] Frederik Zernike. The concept of degree of coherence and its application to optical problems. *Physica*, 5(8):785–795, 1938.

[2] M. Born and E. Wolf. *Principles of Optics*. Cambridge University Press, Cambridge, 7th expanded edition, 1999.

[3] L. Mandel and E. Wolf. *Optical Coherence and Quantum Optics*. Cambridge university press, New York, 1995.

[4] Roy J. Glauber. The quantum theory of optical coherence. *Phys. Rev.*, 130(6):2529–2539, Jun 1963.

[5] Roy J. Glauber. Coherent and incoherent states of the radiation field. *Phys. Rev.*, 131(6):2766–2788, Sep 1963.

[6] E. C. G. Sudarshan. Equivalence of semiclassical and quantum mechanical descriptions of statistical light beams. *Phys. Rev. Lett.*, 10(7):277–279, Apr 1963.

[7] E. Schrödinger. Die gegenwärtige situation in der quantenmechanik. *Naturewiss*, 23:807, 1935.

[8] A. Einstein, B. Podolsky, and N. Rosen. Can quantum-mechanical description of physical reality be considered complete? *Phys. Rev.*, 47(10):777–780, May 1935.

[9] N. Bohr. Can quantum-mechanical description of physical reality be considered complete? *Phys. Rev.*, 48:696–702, Oct 1935.

[10] Alain Aspect, Philippe Grangier, and Gérard Roger. Experimental tests of realistic local theories via Bell's theorem. *Phys. Rev. Lett.*, 47(7):460–463, Aug 1981.

[11] Alain Aspect, Philippe Grangier, and Gérard Roger. Experimental realization of Einstein-Podolsky-Rosen-Bohm gedankenexperiment: A new violation of Bell's inequalities. *Phys. Rev. Lett.*, 49(2):91–94, Jul 1982.

[12] J. S. Bell. On the Einstein Podolsky Rosen paradox. *Physics*, 1:195, 1964.

[13] Charles H. Bennett and Stephen J. Wiesner. Communication via one- and two-particle operators on Einstein-Podolsky-Rosen states. *Phys. Rev. Lett.*, 69(20):2881–2884, Nov 1992.

[14] Charles H. Bennett, Gilles Brassard, Claude Crépeau, Richard Jozsa, Asher Peres, and William K. Wootters. Teleporting an unknown quantum state via dual classical and Einstein-Podolsky-Rosen channels. *Phys. Rev. Lett.*, 70(13):1895–1899, Mar 1993.

[15] Peter W Shor. Algorithms for quantum computation: Discrete logarithms and factoring. In *Foundations of Computer Science, 1994 Proceedings., 35th Annual Symposium on*, pages 124–134. Ieee, 1994.

[16] Michael A Nielsen and Isaac L Chuang. *Quantum computation and quantum information*. Cambridge university press, New York, 2010.

[17] Charles H Bennett, David P DiVincenzo, John A Smolin, and William K Wootters. Mixed-state entanglement and quantum error correction. *Physical Review A*, 54(5):3824, 1996.

[18] William K. Wootters. Entanglement of formation of an arbitrary state of two qubits. *Phys. Rev. Lett.*, 80(10):2245–2248, Mar 1998.

[19] Guifré Vidal and Rolf Tarrach. Robustness of entanglement. *Phys. Rev. A*, 59(1):141–155, Jan 1999.

[20] Ryszard Horodecki, Pawel Horodecki, Michal Horodecki, and Karol Horodecki. Quantum entanglement. *Reviews of Modern Physics*, 81(2):865, 2009.

[21] Robert W. Boyd. *Nonlinear Optics, Third Edition*. Academic Press, 3rd edition, 2008.

[22] C. K. Hong and L. Mandel. Theory of parametric frequency down conversion of light. *Phys. Rev. A*, 31(4):2409–2418, Apr 1985.

[23] Morton H. Rubin. Transverse correlation in optical spontaneous parametric down-conversion. *Phys. Rev. A*, 54(6):5349–5360, Dec 1996.

[24] W. P. Grice and I. A. Walmsley. Spectral information and distinguishability in type-II down-conversion with a broadband pump. *Phys. Rev. A*, 56(2):1627–1634, Aug 1997.

[25] Timothy E. Keller and Morton H. Rubin. Theory of two-photon entanglement for spontaneous parametric down-conversion driven by a narrow pump pulse. *Phys. Rev. A*, 56(2):1534–1541, Aug 1997.

[26] C. H. Monken, P. H. Souto Ribeiro, and S. Padua. Transfer of angular spectrum and image formation in spontaneous parametric down-conversion. *Physical Review A*, 57:3123, 1998.

[27] E. J. S. Fonseca, C. H. Monken, S. Pádua, and G. A. Barbosa. Transverse coherence length of down-converted light in the two-photon state. *Phys. Rev. A*, 59(2):1608–1614, Feb 1999.

[28] A. K. Jha, Malcolm N. O'Sullivan, Kam Wai Clifford Chan, and Robert W. Boyd. Temporal coherence and indistinguishability in two-photon interference effects. *Phys. Rev. A*, 77(2):021801(R), 2008.

[29] Anand Kumar Jha. *Coherence properties of the entangled two-photon field produced by parametric down-conversion*. Institute of Optics, University of Rochester, 2009.

[30] Anand Kumar Jha and Robert W. Boyd. Spatial two-photon coherence of the entangled field produced by down-conversion using a partially spatially coherent pump beam. *Phys. Rev. A*, 81:013828, Jan 2010.

[31] Anand Kumar Jha, Jonathan Leach, Barry Jack, Sonja Franke-Arnold, Stephen M. Barnett, Robert W. Boyd, and Miles J. Padgett. Angular two-photon interference and angular two-qubit states. *Phys. Rev. Lett.*, 104:010501, Jan 2010.

[32] Anand Kumar Jha, Girish S. Agarwal, and Robert W. Boyd. Partial angular coherence and the angular schmidt spectrum of entangled two-photon fields. *Phys. Rev. A*, 84:063847, Dec 2011.

[33] Paul G. Kwiat, Klaus Mattle, Harald Weinfurter, Anton Zeilinger, Alexander V. Sergienko, and Yanhua Shih. New high-intensity source of polarization-entangled photon pairs. *Phys. Rev. Lett.*, 75(24):4337–4341, Dec 1995.

[34] Paul G. Kwiat, Edo Waks, Andrew G. White, Ian Appelbaum, and Philippe H. Eberhard. Ultrabright source of polarization-entangled photons. *Phys. Rev. A*, 60:R773–R776, Aug 1999.

[35] J. Brendel, N. Gisin, W. Tittel, and H. Zbinden. Pulsed energy-time entangled twin-photon source for quantum communication. *Phys. Rev. Lett.*, 82(12):2594–2597, Mar 1999.

[36] A. Mair, A. Vaziri, G. Weihs, and A. Zeilinger. Entanglement of the orbital angular momentum states of photons. *Nature*, 412(6844):313–316, Jul 2001.

[37] H. Di Lorenzo Pires, H. C. B. Florijn, and M. P. van Exter. Measurement of the spiral spectrum of entangled two-photon states. *Phys. Rev. Lett.*, 104:020505, Jan 2010.

[38] P. A. M. Dirac. *The Principles of Quantum Mechanics*. Clarendon Press, Oxford, 3rd edition, 1947.

[39] R. Hanbury Brown and R. Q. Twiss. Correlation between photons in two coherent beams of light rays. *Nature*, 177:27–29, 1956.

[40] R. Hanbury Brown and R. Q. Twiss. The question of correlation between photons in coherent light rays. *Nature*, 178:1447–1448, 1956.

[41] C. K. Hong, Z. Y. Ou, and L. Mandel. Measurement of subpicosecond time intervals between two photons by interference. *Phys. Rev. Lett.*, 59(18):2044–2046, Nov 1987.

[42] J. D. Franson. Bell inequality for position and time. *Phys. Rev. Lett.*, 62(19):2205–2208, May 1989.

[43] Norbert Wiener. Generalized harmonic analysis. *Acta mathematica*, 55(1):117–258, 1930.

[44] S. M. Barnett and D. T. Pegg. Quantum theory of rotation angles. *Phys. Rev. A*, 41:3427–3435, Apr 1990.

[45] Eric Yao, Sonja Franke-Arnold, Johannes Courtial, Stephen Barnett, and Miles Padgett. Fourier relationship between angular position and optical orbital angular momentum. *Opt. Express*, 14(20):9071–9076, Oct 2006.

[46] Roberta Zambrini and Stephen M. Barnett. Quasi-intrinsic angular momentum and the measurement of its spectrum. *Phys. Rev. Lett.*, 96:113901, Mar 2006.

[47] H. Di Lorenzo Pires, J. Woudenberg, and M. P. van Exter. Measurement of the orbital angular momentum spectrum of partially coherent beams. *Opt. Lett.*, 35(6):889–891, Mar 2010.

[48] Niels Bohr. *Discussion with Einstein on epistemological problems in atomic physics*, volume 7. Elsevier, 1996.

[49] Stuart J. Freedman and John F. Clauser. Experimental test of local hidden-variable theories. *Phys. Rev. Lett.*, 28(14):938–941, Apr 1972.

[50] Z. Y. Ou and L. Mandel. Violation of Bell's inequality and classical probability in a two-photon correlation experiment. *Phys. Rev. Lett.*, 61(1):50–53, Jul 1988.

[51] Gregor Weihs, Thomas Jennewein, Christoph Simon, Harald Weinfurter, and Anton Zeilinger. Violation of bell's inequality under strict einstein locality conditions. *Phys. Rev. Lett.*, 81:5039–5043, Dec 1998.

[52] Lynden K. Shalm, Evan Meyer-Scott, Bradley G. Christensen, Peter Bierhorst, Michael A. Wayne, Martin J. Stevens, Thomas Gerrits, Scott Glancy, Deny R. Hamel, Michael S. Allman, Kevin J. Coakley, Shellee D. Dyer, Carson Hodge, Adriana E. Lita, Varun B. Verma, Camilla Lambrocco, Edward Tortorici, Alan L. Migdall, Yanbao Zhang, Daniel R. Kumor, William H. Farr, Francesco Marsili, Matthew D. Shaw, Jeffrey A. Stern, Carlos Abellán, Waldimar Amaya, Valerio Pruneri, Thomas Jennewein, Morgan W. Mitchell, Paul G. Kwiat, Joshua C. Bienfang, Richard P. Mirin, Emanuel Knill, and Sae Woo Nam. Strong loophole-free test of local realism. *Phys. Rev. Lett.*, 115:250402, Dec 2015.

[53] Bas Hensen, Hannes Bernien, Anaïs E Dréau, Andreas Reiserer, Norbert Kalb, Machiel S Blok, Just Ruitenberg, Raymond FL Vermeulen, Raymond N Schouten, Carlos Abellán, et al. Loophole-free bell inequality violation using electron spins separated by 1.3 kilometres. *Nature*, 526(7575):682, 2015.

[54] Dennis Dieks. Communication by epr devices. *Physics Letters A*, 92(6):271–272, 1982.

[55] William K Wootters and Wojciech H Zurek. A single quantum cannot be cloned. *Nature*, 299(5886):802–803, 1982.

[56] Charles H Bennett and Gilles Brassard. Advances in cryptology: Proceedings of crypto84, august 1984. 1984.

[57] Charles H. Bennett. Quantum cryptography using any two nonorthogonal states. *Phys. Rev. Lett.*, 68:3121–3124, May 1992.

[58] Artur K. Ekert. Quantum cryptography based on Bell's theorem. *Phys. Rev. Lett.*, 67(6):661–663, Aug 1991.

[59] Klaus Mattle, Harald Weinfurter, Paul G. Kwiat, and Anton Zeilinger. Dense coding in experimental quantum communication. *Phys. Rev. Lett.*, 76:4656–4659, Jun 1996.

[60] Dik Bouwmeester, Jian-Wei Pan, Klaus Mattle, Manfred Eibl, Harald Weinfurter, and Anton Zeilinger. Experimental quantum teleportation. *Nature*, 390(6660):575–579, 1997.

[61] D. Boschi, S. Branca, F. De Martini, L. Hardy, and S. Popescu. Experimental realization of teleporting an unknown pure quantum state via dual classical and einstein-podolsky-rosen channels. *Phys. Rev. Lett.*, 80:1121–1125, Feb 1998.

[62] Akira Furusawa, Jens Lykke Sørensen, Samuel L Braunstein, Christopher A Fuchs, H Jeff Kimble, and Eugene S Polzik. Unconditional quantum teleportation. *Science*, 282(5389):706–709, 1998.

[63] M. Żukowski, A. Zeilinger, M. A. Horne, and A. K. Ekert. "event-ready-detectors" bell experiment via entanglement swapping. *Phys. Rev. Lett.*, 71:4287–4290, Dec 1993.

[64] Jian-Wei Pan, Dik Bouwmeester, Harald Weinfurter, and Anton Zeilinger. Experimental entanglement swapping: Entangling photons that never interacted. *Phys. Rev. Lett.*, 80:3891–3894, May 1998.

[65] Lieven MK Vandersypen, Matthias Steffen, Gregory Breyta, Costantino S Yannoni, Mark H Sherwood, and Isaac L Chuang. Experimental realization of shor's quantum factoring algorithm using nuclear magnetic resonance. *Nature*, 414(6866):883, 2001.

[66] V Giovannetti. V. giovannetti, s. lloyd, and l. maccone, science 306, 1330 (2004). *Science*, 306:1330, 2004.

[67] Tomohisa Nagata, Ryo Okamoto, Jeremy L O'brien, Keiji Sasaki, and Shigeki Takeuchi. Beating the standard quantum limit with four-entangled photons. *Science*, 316(5825):726–729, 2007.

[68] E. Knill and R. Laflamme. Power of one bit of quantum information. *Phys. Rev. Lett.*, 81:5672–5675, Dec 1998.

[69] B. P. Lanyon, M. Barbieri, M. P. Almeida, and A. G. White. Experimental quantum computing without entanglement. *Phys. Rev. Lett.*, 101:200501, Nov 2008.

[70] Seth Lloyd. Quantum search without entanglement. *Phys. Rev. A*, 61:010301, Dec 1999.

[71] Guo-Ping Guo and Guang-Can Guo. Quantum secret sharing without entanglement. *Physics Letters A*, 310(4):247–251, 2003.

[72] Richard Jozsa and Noah Linden. On the role of entanglement in quantum-computational speed-up. *Proceedings of the Royal Society of London. Series A: Mathematical, Physical and Engineering Sciences*, 459(2036):2011–2032, 2003.

[73] Vittorio Giovannetti, Seth Lloyd, and Lorenzo Maccone. The role of entanglement in dynamical evolution. *EPL (Europhysics Letters)*, 62(5):615, 2003.

[74] Ayman F. Abouraddy, Bahaa E. A. Saleh, Alexander V. Sergienko, and Malvin C. Teich. Role of entanglement in two-photon imaging. *Phys. Rev. Lett.*, 87:123602, Aug 2001.

[75] Animesh Datta and Guifre Vidal. Role of entanglement and correlations in mixed-state quantum computation. *Phys. Rev. A*, 75:042310, Apr 2007.

[76] Mark Howard, Joel Wallman, Victor Veitch, and Joseph Emerson. Contextuality supplies the 'magic'for quantum computation. *Nature*, 510(7505):351, 2014.

[77] J. P. Torres, A. Alexandrescu, and Lluis Torner. Quantum spiral bandwidth of entangled two-photon states. *Phys. Rev. A*, 68(5):050301, Nov 2003.

[78] E Wolf. Coherence properties of partially polarized electromagnetic radiation. *Il Nuovo Cimento*, 13:1165–1181, 1959.

[79] Richard Barakat. Degree of polarization and the principal idempotents of the coherency matrix. *Optics Communications*, 23(2):147 – 150, 1977.

[80] Richard Barakat. n-fold polarization measures and associated thermodynamic entropy of n partially coherent pencils of radiation. *Optica Acta: International Journal of Optics*, 30(8):1171–1182, 1983.

[81] JC Samson and JV Olson. Some comments on the descriptions of the polarization states of waves. *Geophysical Journal International*, 61(1):115–129, 1980.

[82] T. Setala, A. Shevchenko, M. Kaivola, and A. T. Friberg. Degree of polarization for optical near fields. *Physical Review E*, 66(016615), 2002.

[83] T. Setala, M. Kaivola, and A. T. Friberg. Degree of polarization in near fields of thermal sources: Effects of surface waves. *Physical Review Letters*, 88(123902), 2002.

[84] A Luis. Degree of coherence for vectorial electromagnetic fields as the distance between correlation matrices. *J Opt Soc Am A Opt Image Sci Vis*, 24(4), 2007.

[85] Yao Yao, G. H. Dong, Xing Xiao, and C. P. Sun. Frobenius norm based measures of quantum coherence and asymmetry. *Nature, Scientific Reports*, 6(32010), 2016.

[86] Abu Saleh Musa Patoary, Girish Kulkarni, and Anand K. Jha. Intrinsic measure of coherence for high-dimensional systems. *arXiv:quant-ph/1712.03475*, 2017.

[87] Asher Peres. Separability criterion for density matrices. *Phys. Rev. Lett.*, 77:1413–1415, Aug 1996.

[88] G. Vidal and R. F. Werner. Computable measure of entanglement. *Phys. Rev. A*, 65:032314, Feb 2002.

[89] William K Wootters. Entanglement of formation and concurrence. *Quantum Information & Computation*, 1(1):27–44, 2001.

[90] Rodney Loudon. *The quantum theory of light*. Oxford University Press, 2000.

[91] Enno Giese, Robert Fickler, Wuhong Zhang, Lixiang Chen, and Robert W Boyd. Influence of pump coherence on the quantum properties of spontaneous parametric down-conversion. *Physica Scripta*, 93(8):084001, 2018.

[92] C. K. Law and J. H. Eberly. Analysis and interpretation of high transverse entanglement in optical parametric down conversion. *Phys. Rev. Lett.*, 92:127903, Mar 2004.

[93] Jonathan Leach, Barry Jack, Jacqui Romero, Anand K Jha, Alison M Yao, Sonja Franke-Arnold, David G Ireland, Robert W Boyd, Stephen M Barnett, and Miles J Padgett. Quantum correlations in optical angle–orbital angular momentum variables. *Science*, 329(5992):662–665, 2010.

[94] L. Allen, M. W. Beijersbergen, R. J. C. Spreeuw, and J. P. Woerdman. Orbital angular momentum of light and the transformation of laguerre-gaussian laser modes. *Phys. Rev. A*, 45:8185–8189, Jun 1992.

[95] H Jeff Kimble. The quantum internet. *Nature*, 453(7198):1023–1030, 2008.

[96] Manuel Erhard, Robert Fickler, Mario Krenn, and Anton Zeilinger. Twisted photons: new quantum perspectives in high dimensions. *Light: Science & Applications*, 7(3):17146, 2018.

[97] B. Jack, MJ Padgett, and S. Franke-Arnold. Angular diffraction. *New Journal of Physics*, 10(103013):103013, 2008.

[98] Artur K. Ekert. Quantum cryptography based on bell's theorem. *Phys. Rev. Lett.*, 67:661–663, Aug 1991.

[99] Vahid Karimipour, Alireza Bahraminasab, and Saber Bagherinezhad. Quantum key distribution for d-level systems with generalized bell states. *Phys. Rev. A*, 65:052331, May 2002.

[100] Nicolas J. Cerf, Mohamed Bourennane, Anders Karlsson, and Nicolas Gisin. Security of quantum key distribution using d-level systems. *Phys. Rev. Lett.*, 88(12):127902, Mar 2002.

[101] Georgios M. Nikolopoulos, Kedar S. Ranade, and Gernot Alber. Error tolerance of two-basis quantum-key-distribution protocols using qudits and two-way classical communication. *Phys. Rev. A*, 73:032325, Mar 2006.

[102] Mikio Fujiwara, Masahiro Takeoka, Jun Mizuno, and Masahide Sasaki. Exceeding the classical capacity limit in a quantum optical channel. *Phys. Rev. Lett.*, 90:167906, Apr 2003.

[103] John Cortese. Holevo-schumacher-westmoreland channel capacity for a class of qudit unital channels. *Phys. Rev. A*, 69:022302, Feb 2004.

[104] T. C. Ralph, K. J. Resch, and A. Gilchrist. Efficient toffoli gates using qudits. *Phys. Rev. A*, 75:022313, Feb 2007.

[105] Benjamin P. Lanyon, Marco Barbieri, Marcelo P. Almeida, Thomas Jennewein, Timothy C. Ralph, Kevin J. Resch, Geoff J. Pryde, Jeremy L. O/'Brien, Alexei Gilchrist, and Andrew G. White. Simplifying quantum logic using higher-dimensional hilbert spaces. *Nat Phys*, 5(2):134–140, Feb 2009.

[106] Anand Kumar Jha, Girish S. Agarwal, and Robert W. Boyd. Supersensitive measurement of angular displacements using entangled photons. *Phys. Rev. A*, 83:053829, May 2011.

[107] Dagomir Kaszlikowski, Piotr Gnaciński, Marek Żukowski, Wieslaw Miklaszewski, and Anton Zeilinger. Violations of local realism by two entangled N-dimensional systems are stronger than for two qubits. *Phys. Rev. Lett.*, 85:4418–4421, Nov 2000.

[108] Daniel Collins, Nicolas Gisin, Noah Linden, Serge Massar, and Sandu Popescu. Bell inequalities for arbitrarily high-dimensional systems. *Phys. Rev. Lett.*, 88(4):040404, Jan 2002.

[109] Tamás Vértesi, Stefano Pironio, and Nicolas Brunner. Closing the detection loophole in bell experiments using qudits. *Phys. Rev. Lett.*, 104:060401, Feb 2010.

[110] J. Leach, B. Jack, J. Romero, M. Ritsch-Marte, R. W. Boyd, A. K. Jha, S. M. Barnett, S. Franke-Arnold, and M. J. Padgett. Violation of a Bell inequality in two-dimensional orbital angular momentum state-spaces. *Opt. Express*, 17(10):8287–8293, 2009.

[111] Jian Wang, Jeng-Yuan Yang, Irfan M Fazal, Nisar Ahmed, Yan Yan, Hao Huang, Yongxiong Ren, Yang Yue, Samuel Dolinar, Moshe Tur, et al. Terabit free-space data transmission employing orbital angular momentum multiplexing. *Nature Photonics*, 6(7):488, 2012.

[112] Nenad Bozinovic, Yang Yue, Yongxiong Ren, Moshe Tur, Poul Kristensen, Hao Huang, Alan E. Willner, and Siddharth Ramachandran. Terabit-scale orbital angular momentum mode division multiplexing in fibers. *Science*, 340(6140):1545–1548, 2013.

[113] Yan Yan, Guodong Xie, Martin P. J. Lavery, Hao Huang, Nisar Ahmed, Changjing Bao, Yongxiong Ren, Yinwen Cao, Long Li, Zhe Zhao, Andreas F. Molisch, Moshe Tur, Miles J. Padgett, and Alan E. Willner. High-capacity millimetre-wave communications with orbital angular momentum multiplexing. *Nature Communications*, 5:4876 EP –, Sep 2014. Article.

[114] Mehul Malik, Sangeeta Murugkar, Jonathan Leach, and Robert W. Boyd. Measurement of the orbital-angular-momentum spectrum of fields with partial angular coherence using double-angular-slit interference. *Phys. Rev. A*, 86:063806, Dec 2012.

[115] Girish Kulkarni, Rishabh Sahu, Omar S Magaña-Loaiza, Robert W Boyd, and Anand K Jha. Single-shot measurement of the orbital-angular-momentum spectrum of light. *Nature Communications*, 8(1):1054, 2017.

[116] CV Raman and S Bhagavantam. Experimental proof of the spin of the photon. *Indian Journal of Physics*.

[117] CV Raman and S Bhagavantam. Experimental proof of the spin of the photon. *Nature*, 129:22–23, 1931.

[118] Richard A. Beth. Mechanical detection and measurement of the angular momentum of light. *Phys. Rev.*, 50(2):115–125, Jul 1936.

[119] Peter W Milonni and Joseph H Eberly. Laser physics, 2010.

[120] L. Mandel and E. Wolf. *Optical Coherence and Quantum Optics*. Cambridge University Press, 1995.

[121] Hammam Qassim, Filippo M. Miatto, Juan P. Torres, Miles J. Padgett, Ebrahim Karimi, and Robert W. Boyd. Limitations to the determination of a laguerre-gauss spectrum via projective, phase-flattening measurement. *J. Opt. Soc. Am. B*, 31(6):A20–A23, Jun 2014.

[122] Victor Arrizón, Ulises Ruiz, Rosibel Carrada, and Luis A. González. Pixelated phase computer holograms for the accurate encoding of scalar complex fields. *J. Opt. Soc. Am. A*, 24(11):3500–3507, Nov 2007.

[123] Abhinandan Bhattacharjee, Shaurya Aarav, and Anand K. Jha. Two-shot measurement of spatial coherence. *Applied Physics Letters*, 113(5):051102, 2018.

[124] Filippo M. Miatto, Alison M. Yao, and Stephen M. Barnett. Full characterization of the quantum spiral bandwidth of entangled biphotons. *Phys. Rev. A*, 83:033816, Mar 2011.

[125] Alison M Yao. Angular momentum decomposition of entangled photons with an arbitrary pump. *New Journal of Physics*, 13(5):053048, 2011.

[126] F. M. Miatto, H. Di Lorenzo Pires, S. M. Barnett, and M. P. van Exter. Spatial schmidt modes generated in parametric down-conversion. *The European Physical Journal D*, 66(10):263, Oct 2012.

[127] Yingwen Zhang and Filippus S. Roux. Modal spectrum in spontaneous parametric down-conversion with noncollinear phase matching. *Phys. Rev. A*, 89:063802, Jun 2014.

[128] J. B. Pors, S. S. R. Oemrawsingh, A. Aiello, M. P. van Exter, E. R. Eliel, G. W. 't Hooft, and J. P. Woerdman. Shannon dimensionality of quantum channels and its application to photon entanglement. *Phys. Rev. Lett.*, 101:120502, Sep 2008.

[129] WH Peeters, EJK Verstegen, and MP Van Exter. Orbital angular momentum analysis of high-dimensional entanglement. *Physical Review A*, 76(4):042302, 2007.

[130] D Giovannini, F M Miatto, J Romero, S M Barnett, J P Woerdman, and M J Padgett. Determining the dimensionality of bipartite orbital-angular-momentum entanglement using multi-sector phase masks. *New Journal of Physics*, 14(7):073046, 2012.

[131] Girish Kulkarni, Lavanya Taneja, Shaurya Aarav, and Anand K. Jha. Angular schmidt spectrum of entangled photons: Derivation of an exact formula and experimental characterization for noncollinear phase matching. *Phys. Rev. A*, 97:063846, Jun 2018.

[132] S.P. Walborn, C.H. Monken, S. Pádua, and P.H. Souto Ribeiro. Spatial correlations in parametric down-conversion. *Physics Reports*, 495(4):87 – 139, 2010.

[133] Agata M Brańczyk, Thomas M Stace, and TC Ralph. Time ordering in spontaneous parametric down-conversion. In *AIP Conference Proceedings*, volume 1363, pages 335–338. AIP, 2011.

[134] Z. Y. Ou, L. J. Wang, and L. Mandel. Vacuum effects on interference in two-photon down conversion. *Phys. Rev. A*, 40(3):1428–1435, Aug 1989.

[135] Suman Karan, Shaurya Aarav, Homanga Bharadhwaj, Lavanya Taneja, Girish Kulkarni, and Anand K Jha. Phase matching in spontaneous parametric down conversion. *arXiv preprint arXiv:1810.01184*, 2018.

[136] D. Eimerl, L. Davis, S. Velsko, E. K. Graham, and A. Zalkin. Optical, mechanical, and thermal properties of barium borate. *Journal of Applied Physics*, 62(5):1968–1983, 1987.

[137] Bart-Jan Pors, Filippo Miatto, G W 't Hooft, E R Eliel, and J P Woerdman. High-dimensional entanglement with orbital-angular-momentum states of light. *Journal of Optics*, 13(6):064008, 2011.

[138] David C. Burnham and Donald L. Weinberg. Observation of simultaneity in parametric production of optical photon pairs. *Phys. Rev. Lett.*, 25:84–87, Jul 1970.

[139] Emil Wolf. *Introduction to the Theory of Coherence and Polarization of Light*. Cambridge University Press, New York, 2007.

[140] Charles H. Bennett, Herbert J. Bernstein, Sandu Popescu, and Benjamin Schumacher. Concentrating partial entanglement by local operations. *Phys. Rev. A*, 53:2046–2052, Apr 1996.

[141] Charles H. Bennett, Gilles Brassard, Sandu Popescu, Benjamin Schumacher, John A. Smolin, and William K. Wootters. Purification of noisy entanglement and faithful teleportation via noisy channels. *Phys. Rev. Lett.*, 76:722–725, Jan 1996.

[142] Sandu Popescu and Daniel Rohrlich. Thermodynamics and the measure of entanglement. *Phys. Rev. A*, 56:R3319–R3321, Nov 1997.

[143] Scott Hill and William K. Wootters. Entanglement of a pair of quantum bits. *Phys. Rev. Lett.*, 78(26):5022–5025, Jun 1997.

[144] M. A. Nielsen. Conditions for a class of entanglement transformations. *Phys. Rev. Lett.*, 83:436–439, Jul 1999.

[145] Christopher E. Kuklewicz, Marco Fiorentino, Gaétan Messin, Franco N. C. Wong, and Jeffrey H. Shapiro. High-flux source of polarization-entangled photons from a periodically poled ktiopo parametric down-converter. *Phys. Rev. A*, 69:013807, Jan 2004.

[146] Thomas Jennewein, Christoph Simon, Gregor Weihs, Harald Weinfurter, and Anton Zeilinger. Quantum cryptography with entangled photons. *Phys. Rev. Lett.*, 84(20):4729–4732, May 2000.

[147] Rupert Ursin, F Tiefenbacher, T Schmitt-Manderbach, H Weier, Thomas Scheidl, M Lindenthal, B Blauensteiner, T Jennewein, J Perdigues, P Trojek, B Omer, M Furst, M Meyunburg, J Rarity, Z Sodnik, C Barbieri, H Weinfurter, and A Zeilinger. Entanglement-based quantum communication over 144 km. *Nature physics*, 3(7):481–486, 2007.

[148] Sonja Franke-Arnold Miguel Angel Olvera. Two photon amplitude of partially coherent partially entangled electromagnetic fields. *arXiv:1507.08623v1*, 2015.

[149] Girish Kulkarni, V Subrahmanyam, and Anand K Jha. Intrinsic upper bound on two-qubit polarization entanglement predetermined by pump polarization correlations in parametric down-conversion. *Physical Review A*, 93(6):063842, 2016.

[150] R Bhatia. *Matrix Analysis*. Springer Science ans Business Media, 2013.

[151] E. C. G. Sudarshan, P. M. Mathews, and Jayaseetha Rau. Stochastic dynamics of quantum-mechanical systems. *Phys. Rev.*, 121:920–924, Feb 1961.

[152] Thomas F Jordan and ECG Sudarshan. Dynamical mappings of density operators in quantum mechanics. *Journal of Mathematical Physics*, 2(6):772–775, 1961.

[153] Karl Kraus. General state changes in quantum theory. *Annals of Physics*, 64(2):311–335, 1971.

[154] Michael A Nielsen. An introduction to majorization and its applications to quantum mechanics. *Lecture Notes, Department of Physics, University of Queensland, Australia*, 2002.

[155] Satoshi Ishizaka and Tohya Hiroshima. Maximally entangled mixed states under nonlocal unitary operations in two qubits. *Phys. Rev. A*, 62:022310, Jul 2000.

[156] Frank Verstraete, Koenraad Audenaert, and Bart De Moor. Maximally entangled mixed states of two qubits. *Phys. Rev. A*, 64:012316, Jun 2001.

[157] S. Ramelow, A. Fedrizzi, A. Poppe, N. K. Langford, and A. Zeilinger. Polarization-entanglement-conserving frequency conversion of photons. *Phys. Rev. A*, 85:013845, Jan 2012.

[158] M Titov, B Trauzettel, B Michaelis, and C W J Beenakker. Transfer of entanglement from electrons to photons by optical selection rules. *New Journal of Physics*, 7(1):186, 2005.

[159] Veronica Cerletti, Oliver Gywat, and Daniel Loss. Entanglement transfer from electron spins to photons in spin light-emitting diodes containing quantum dots. *Phys. Rev. B*, 72:115316, Sep 2005.

[160] E Altewischer, MP Van Exter, and JP Woerdman. Plasmon-assisted transmission of entangled photons. *Nature*, 418(6895):304–306, 2002.

[161] A. A. Semenov and W. Vogel. Entanglement transfer through the turbulent atmosphere. *Phys. Rev. A*, 81:023835, Feb 2010.

[162] Deny R Hamel, Lynden K Shalm, Hannes Hübel, Aaron J Miller, Francesco Marsili, Varun B Verma, Richard P Mirin, Sae Woo Nam, Kevin J Resch, and Thomas Jennewein. Direct generation of three-photon polarization entanglement. *Nature Photonics*, 8(10):801–807, 2014.

[163] W. Vogel and J. Sperling. Unified quantification of nonclassicality and entanglement. *Phys. Rev. A*, 89:052302, May 2014.

[164] T. Baumgratz, M. Cramer, and M. B. Plenio. Quantifying coherence. *Phys. Rev. Lett.*, 113:140401, Sep 2014.

[165] Davide Girolami. Observable measure of quantum coherence in finite dimensional systems. *Phys. Rev. Lett.*, 113:170401, Oct 2014.

[166] Eric Chitambar and Min-Hsiu Hsieh. Relating the resource theories of entanglement and quantum coherence. *Phys. Rev. Lett.*, 117:020402, Jul 2016.

[167] J. Brendel, W. Dultz, and W. Martienssen. Geometric phases in two-photon interference experiments. *Phys. Rev. A*, 52(4):2551–2556, Oct 1995.

[168] X. Y. Zou, L. J. Wang, and L. Mandel. Induced coherence and indistinguishability in optical interference. *Phys. Rev. Lett.*, 67(3):318–321, Jul 1991.

[169] T. J. Herzog, J. G. Rarity, H. Weinfurter, and A. Zeilinger. Frustrated two-photon creation via interference. *Phys. Rev. Lett.*, 72(5):629–632, Jan 1994.

[170] T. B. Pittman, D. V. Strekalov, A. Migdall, M. H. Rubin, A. V. Sergienko, and Y. H. Shih. Can two-photon interference be considered the interference of two photons? *Phys. Rev. Lett.*, 77(10):1917–1920, Sep 1996.

[171] J. Brendel, E. Mohler, and W. Martienssen. Time-resolved dual-beam two-photon interferences with high visibility. *Phys. Rev. Lett.*, 66(9):1142–1145, Mar 1991.

[172] Anand Kumar Jha, Mehul Malik, and Robert W. Boyd. Exploring energy-time entanglement using geometric phase. *Phys. Rev. Lett.*, 101(18):180405, 2008.

[173] R. T. Thew, S. Tanzilli, W. Tittel, H. Zbinden, and N. Gisin. Experimental investigation of the robustness of partially entangled qubits over 11 km. *Phys. Rev. A*, 66(6):062304, Dec 2002.

[174] Leonardo Neves, G. Lima, E. J. S. Fonseca, L. Davidovich, and S. Pádua. Characterizing entanglement in qubits created with spatially correlated twin photons. *Phys. Rev. A*, 76(3):032314, 2007.

[175] Eleonora Nagali, Linda Sansoni, Fabio Sciarrino, Francesco De Martini, Lorenzo Marrucci, Bruno Piccirillo, Ebrahim Karimi, and Enrico Santamato. Optimal quantum cloning of orbital angular momentum photon qubits through hong–ou–mandel coalescence. *Nature Photonics*, 3(12):720–723, 2009.

[176] Adel Joobeur, Bahaa E. A. Saleh, Todd S. Larchuk, and Malvin C. Teich. Coherence properties of entangled light beams generated by parametric down-conversion: Theory and experiment. *Phys. Rev. A*, 53(6):4360–4371, Jun 1996.

[177] P. H. Souto Ribeiro. Partial coherence with twin photons. *Phys. Rev. A*, 56(5):4111–4117, Nov 1997.

[178] Bahaa E. A. Saleh, Malvin C. Teich, and Alexander V. Sergienko. Wolf equations for two-photon light. *Phys. Rev. Lett.*, 94(22):223601, Jun 2005.

[179] S. P. Walborn, A. N. de Oliveira, R. S. Thebaldi, and C. H. Monken. Entanglement and conservation of orbital angular momentum in spontaneous parametric down-conversion. *Phys. Rev. A*, 69(2):023811, Feb 2004.

[180] W. Tittel, J. Brendel, H. Zbinden, and N. Gisin. Quantum cryptography using entangled photons in energy-time bell states. *Phys. Rev. Lett.*, 84:4737–4740, May 2000.

[181] Takahiro Inagaki, Nobuyuki Matsuda, Osamu Tadanaga, Masaki Asobe, and Hiroki Takesue. Entanglement distribution over 300 km of fiber. *Opt. Express*, 21(20):23241–23249, Oct 2013.

[182] Morton H. Rubin, David N. Klyshko, Y. H. Shih, and A. V. Sergienko. Theory of two-photon entanglement in type-II optical parametric down-conversion. *Phys. Rev. A*, 50(6):5122–5133, Dec 1994.

[183] P. W. Milonni, H. Fearn, and A. Zeilinger. Theory of two-photon down-conversion in the presence of mirrors. *Phys. Rev. A*, 53(6):4556–4566, Jun 1996.

[184] Osung Kwon, Young-Sik Ra, and Yoon-Ho Kim. Coherence properties of spontaneous parametric down-conversion pumped by a multi-mode cw diode laser. *Optics express*, 17(15):13059–13069, 2009.

[185] Osung Kwon, Kwang-Kyoon Park, Young-Sik Ra, Yong-Su Kim, and Yoon-Ho Kim. Time-bin entangled photon pairs from spontaneous parametric down-conversion pumped by a cw multi-mode diode laser. *Optics express*, 21(21):25492–25500, 2013.

[186] Pertti Pääkkönen, Jari Turunen, Pasi Vahimaa, Ari T. Friberg, and Frank Wyrowski. Partially coherent Gaussian pulses. *Opt. Comm.*, 204(1-6):53 – 58, 2002.

[187] Girish Kulkarni, Prashant Kumar, and Anand K. Jha. Transfer of temporal coherence in parametric down-conversion. *J. Opt. Soc. Am. B*, 34(8):1637–1643, Aug 2017.

[188] L. J. Wang, X. Y. Zou, and L. Mandel. Induced coherence without induced emission. *Phys. Rev. A*, 44(7):4614–4622, Oct 1991.

[189] I. Marcikic, H. de Riedmatten, W. Tittel, V. Scarani, H. Zbinden, and N. Gisin. Time-bin entangled qubits for quantum communication created by femtosecond pulses. *Phys. Rev. A*, 66:062308, Dec 2002.

[190] Ivan Marcikic, Hugues De Riedmatten, Wolfgang Tittel, Hugo Zbinden, and Nicolas Gisin. Long-distance teleportation of qubits at telecommunication wavelengths. *Nature*, 421(6922):509–513, 2003.

[191] I. Marcikic, H. de Riedmatten, W. Tittel, H. Zbinden, M. Legré, and N. Gisin. Distribution of time-bin entangled qubits over 50 km of optical fiber. *Phys. Rev. Lett.*, 93:180502, Oct 2004.

[192] Anand K. Jha, Glenn A. Tyler, and Robert W. Boyd. Effects of atmospheric turbulence on the entanglement of spatial two-qubit states. *Phys. Rev. A*, 81:053832, May 2010.

[193] D. V. Strekalov, T. B. Pittman, and Y. H. Shih. What we can learn about single photons in a two-photon interference experiment. *Phys. Rev. A*, 57(1):567–570, Jan 1998.

[194] S. Ramelow, L. Ratschbacher, A. Fedrizzi, NK Langford, and A. Zeilinger. Discrete, tunable color entanglement. *Arxiv preprint arXiv:0904.4916*, 2009.

[195] Leonardo Neves, G. Lima, J. G. Aguirre Gómez, C. H. Monken, C. Saavedra, and S. Pádua. Generation of entangled states of qudits using twin photons. *Phys. Rev. Lett.*, 94(10):100501, Mar 2005.

[196] J. G. Rarity and P. R. Tapster. Experimental violation of Bell's inequality based on phase and momentum. *Phys. Rev. Lett.*, 64(21):2495–2498, May 1990.

[197] Alipasha Vaziri, Gregor Weihs, and Anton Zeilinger. Experimental two-photon, three-dimensional entanglement for quantum communication. *Phys. Rev. Lett.*, 89(24):240401, Nov 2002.

[198] N. K. Langford, R. B. Dalton, M. D. Harvey, J. L. O'Brien, G. J. Pryde, A. Gilchrist, S. D. Bartlett, and A. G. White. Measuring entangled qutrits and their use for quantum bit commitment. *Phys. Rev. Lett.*, 93(5):053601, Jul 2004.

[199] Alfredo Luis. Degree of polarization in quantum optics. *Phys. Rev. A*, 66:013806, Jul 2002.

[200] Miguel A. Alonso, Xiao-Feng Qian, and J. H. Eberly. Center-of-mass interpretation for bipartite purity analysis of n-party entanglement. *Phys. Rev. A*, 94:030303, Sep 2016.

[201] A. E. Willner, H. Huang, Y. Yan, Y. Ren, N. Ahmed, G. Xie, C. Bao, L. Li, Y. Cao, Z. Zhao, J. Wang, M. P. J. Lavery, M. Tur, S. Ramachandran, A. F. Molisch, N. Ashrafi, and S. Ashrafi.

[202] Giuseppe Vallone, Vincenzo D'Ambrosio, Anna Sponselli, Sergei Slussarenko, Lorenzo Marrucci, Fabio Sciarrino, and Paolo Villoresi. Free-space quantum key distribution by rotation-invariant twisted photons. *Phys. Rev. Lett.*, 113:060503, Aug 2014.

[203] Matteo G. A. Paris, Fabrizio Illuminati, Alessio Serafini, and Silvio De Siena. Purity of gaussian states: Measurement schemes and time evolution in noisy channels. *Phys. Rev. A*, 68:012314, Jul 2003.

[204] Alessio Serafini, Fabrizio Illuminati, Matteo G. A. Paris, and Silvio De Siena. Entanglement and purity of two-mode gaussian states in noisy channels. *Phys. Rev. A*, 69:022318, Feb 2004.

[205] Gerardo Adesso, Alessio Serafini, and Fabrizio Illuminati. Determination of continuous variable entanglement by purity measurements. *Phys. Rev. Lett.*, 92:087901, Feb 2004.

[206] S. C. H. Wang and M. A. Plonus. Optical beam propagation for a partially coherent source in the turbulent atmosphere. *J. Opt. Soc. Am.*, 69(9):1297–1304, Sep 1979.

[207] Aristide Dogariu and Stefan Amarande. Propagation of partially coherent beams - turbulence-induced degradation. *Opt. Lett.*, 28(1):10–12, Jan 2003.

[208] Tomohiro Shirai, Aristide Dogariu, and Emil Wolf. Mode analysis of spreading of partially coherent beams propagating through atmospheric turbulence. *J. Opt. Soc. Am. A*, 20(6):1094–1102, 2003.

[209] Juan Pablo Paz, Salman Habib, and Wojciech H. Zurek. Reduction of the wave packet: Preferred observable and decoherence time scale. *Phys. Rev. D*, 47:488–501, Jan 1993.

[210] Wojciech H. Zurek, Salman Habib, and Juan Pablo Paz. Coherent states via decoherence. *Phys. Rev. Lett.*, 70:1187–1190, Mar 1993.

[211] A. Isar, A. Sandulescu, and W. Scheid. Purity and decoherence in the theory of a damped harmonic oscillator. *Phys. Rev. E*, 60:6371–6381, Dec 1999.

[212] E. Merzbacher. *Quantum Mechanics*. Wiley International, Cambridge, 3rd edition edition, 1998.

[213] Peter Woit. *Quantum Theory, Groups and Representations*. Springer, 2017.

[214] D. T. Pegg and S. M. Barnett. Phase properties of the quantized single-mode electromagnetic field. *Phys. Rev. A*, 39:1665–1675, Feb 1989.

[215] D. T. Pegg and S. M. Barnett. Unitary phase operator in quantum mechanics. *EPL (Europhysics Letters)*, 6(6):483, 1988.

[216] G. S. Agarwal. *Quantum Optics*. Cambridge University Press, 2012.

[217] Wolfram Research Inc. Mathematica, version 8.0. Champaign, IL, 2010.

[218] DT Smithey, M Beck, Michael G Raymer, and A Faridani. Measurement of the wigner distribution and the density matrix of a light mode using optical homodyne tomography: Application to squeezed states and the vacuum. *Physical review letters*, 70(9):1244, 1993.

[219] E. Wigner. On the quantum correction for thermodynamic equilibrium. *Phys. Rev.*, 40:749–759, Jun 1932.

[220] E. Collett and E. Wolf. Is complete spatial coherence necessary for the generation of highly directional light beams? *Opt. Lett.*, 2(2):27–29, Feb 1978.

[221] Martin J Bastiaans. Uncertainty principle for spatially quasi-stationary, partially coherent light. *JOSA*, 72(10):1441–1443, 1982.

[222] Martin J Bastiaans. Uncertainty principle for partially coherent light. *JOSA*, 73(3):251–255, 1983.

[223] Martin J Bastiaans. Lower bound in the uncertainty principle for partially coherent light. *JOSA*, 73(10):1320–1324, 1983.

[224] Martin J Bastiaans. New class of uncertainty relations for partially coherent light. *JOSA A*, 1(7):711–715, 1984.

[225] Martin J Bastiaans. Uncertainty principle and informational entropy for partially coherent light. *JOSA A*, 3(8):1243–1246, 1986.

[226] Omar Gamel and Daniel F. V. James. Measures of quantum state purity and classical degree of polarization. *Phys. Rev. A*, 86:033830, Sep 2012.

[227] M Alonso, T Setälä, and AT Friberg. Minimum uncertainty solutions for partially coherent fields and quantum mixed states. *New Journal of Physics*, 16(12):123023, 2014.

[228] S. Schiller, G. Breitenbach, S. F. Pereira, T. Müller, and J. Mlynek. Quantum statistics of the squeezed vacuum by measurement of the density matrix in the number state representation. *Phys. Rev. Lett.*, 77:2933–2936, Sep 1996.

[229] G. Breitenbach, S. Schiller, and J. Mlynek. Measurement of the quantum states of squeezed light. *Nature*, 387(6632):471–475, 1997.

[230] M. Avenhaus, H. B. Coldenstrodt-Ronge, K. Laiho, W. Mauerer, I. A. Walmsley, and C. Silberhorn. Photon number statistics of multimode parametric down-conversion. *Phys. Rev. Lett.*, 101:053601, Aug 2008.

[231] Moritz Mehmet, Henning Vahlbruch, Nico Lastzka, Karsten Danzmann, and Roman Schnabel. Observation of squeezed states with strong photon-number oscillations. *Phys. Rev. A*, 81:013814, Jan 2010.

[232] J.W. Goodman. *Introduction to Fourier Optics*. McGraw Hill, New York, 2nd edition, 1996.

[233] E Oran Brigham. *The fast Fourier transform and its applications*, volume 448. prentice Hall Englewood Cliffs, NJ, 1988.